Artificial Intelligence Backed Automation for Detecting Cracks in Solar Cells

Sharmarke Hassan

Doctor of Philosophy

University of York

School of Physics, Engineering and Technology

November 2025

Abstract

The reliability and performance of photovoltaic (PV) systems are strongly influenced by manufacturing and operational defects that accelerate degradation and reduce energy yield. Conventional inspection methods are often time-consuming and ineffective for detecting early-stage or micro-scale defects. This research presents an automated PV defect detection framework that integrates electroluminescence (EL) imaging with deep learning techniques to improve inspection accuracy and efficiency.

The thesis is structured around five peer-reviewed publications covering key aspects of intelligent PV quality assessment. The early chapters review existing EL-based inspection methods and convolutional neural network (CNN) architectures, identifying limitations that motivate the need for automation. Subsequent chapters propose novel CNN-based models, including a Dual Spin Max-Pooling network and an ensemble architecture designed to enhance classification robustness and feature extraction.

Experimental results demonstrate validation accuracies exceeding 98% in distinguishing healthy and defective PV cells under varying imaging conditions. In addition to cell-level defect classification, the research develops a hybrid inspection framework combining cell-level and module-level analysis to support PV acceptance testing and quality assurance.

The proposed methods are validated using large-scale datasets obtained through in-house EL imaging of commercial PV modules, supported by photoluminescence and thermal measurements. Overall, the research contributes a scalable and data-driven methodology for automated PV defect detection and provides a foundation for integrating artificial intelligence-based inspection technologies into industrial PV manufacturing and maintenance processes.

Author’s Declaration

I declare that this thesis is a presentation of my original work and that I am the sole author. This work has not previously been submitted for any degree or other qualification at this or any other university. All sources of information have been duly acknowledged through references.

Publications Arising from This Research

The following peer-reviewed journal articles were published as part of this PhD research. Each publication corresponds to one or more chapters of this thesis.

1. **Hassan, S.**, & Dhimish, M. (2022). *Review of Current State-of-the-Art Research on Photovoltaic Soiling, Anti-Reflective Coating, and Solar Roads Deployment Supported by a Pilot Experiment on a PV Road.* **Energies**, 15(24), 9620. https://doi.org/10.3390/en15249620

2. **Hassan, S.**, & Dhimish, M. (2023). *A Survey of CNN-Based Approaches for Crack Detection in Solar PV Modules: Current Trends and Future Directions.* **Solar**, 3(4), 663–683. https://doi.org/10.3390/solar3040036

3. **Hassan, S.**, & Dhimish, M. (2023). *Dual Spin Max-Pooling Convolutional Neural Network for Solar Cell Crack Detection.* **Scientific Reports**, 13, 11099. https://doi.org/10.1038/s41598-023-38177-8

4. **Hassan, S.**, & Dhimish, M. (2023). *Enhancing Solar Photovoltaic Modules Quality Assurance through Convolutional Neural Network-Aided Automated Defect Detection.* **Renewable Energy**, 219, 119389. https://doi.org/10.1016/j.renene.2023.119389

5. **Hassan, S.**, & Dhimish, M. (2024). *Broad-Scale Electroluminescence Analysis of 5 million+ Photovoltaic Cells for Defect Detection and Degradation Assessment.* **Renewable Energy**, Elsevier. https://doi.org/10.1016/j.renene.2023.119389

Conference Presentations and Contributions

The following conferences and exhibitions were attended as part of this PhD research. These events provided valuable opportunities to present, discuss, and further develop the findings of this work, while also fostering academic and industrial collaborations.

1. **Hassan, S.** (2023). *Automated Defect Detection in Photovoltaic Modules Using Electroluminescence Imaging and Deep Learning.* Poster presentation at **PVSAT-19 (Photovoltaic Science, Applications and Technology Conference)**, London, UK.

2. **Hassan, S.** (2024). *Large-Scale PV Quality Assessment Using Convolutional Neural Networks.* Poster presentation at **PVSAT-20**, Glasgow, UK.

3. **Hassan, S.** (2025). Participation in the **Middle East Solar Exhibition**, Dubai, UAE — established industrial partnerships and explored collaborative opportunities related to AI-based PV quality inspection.

Acknowledgements

This research would not have been possible without the support, guidance and encouragement of several individuals and institutions.

First and foremost, I would like to express my sincere gratitude to **Dr. Mahmoud Dhimish**, whose supervision, advice and expertise were instrumental during the initial stages of my PhD. His insightful discussions and constructive feedback helped shape the early direction of my research and provided a strong foundation for this work.

I would also like to extend my heartfelt appreciation to **Dr. Xing Zhao**, who took over supervision in the later stages of the project. His continuous support, technical guidance, and critical input were invaluable in bringing this research to completion.

Special thanks go to the **School of Physics, Engineering and Technology, University of York**, for providing an excellent research environment and access to laboratory facilities. I am also grateful to my colleagues and fellow researchers in the **Photovoltaics Laboratory** for their collaboration, encouragement, and friendship throughout my research journey.

Finally, I would like to express my deepest gratitude to my family and friends for their unwavering support, patience and understanding, which gave me strength and motivation during the most challenging stages of this PhD.

Contents

List of Figures

List of Tables

List of Abbreviations

Acronym	**Full Form**
BB	Busbar
CCD	Charge-Coupled Device
CNN	Convolutional Neural Network
DSMP	Dual Spin Max-Pooling
EL	Electroluminescence
ER	Enhanced Recombination
EVA	Ethylene-Vinyl Acetate
FIA	Filter-Induced Augmentation
FPN	Feature Pyramid Network
GPU	Graphics Processing Unit
HP	Hybrid Convolutional Pooling
I–V	Current–Voltage
LAA	Loss of Active Area
MATLAB	Matrix Laboratory
PET	Polyethylene Terephthalate

PID	Potential-Induced Degradation
PL	Photoluminescence
PP	Polypropylene
PV	Photovoltaic
STC	Standard Test Condition
UK	United Kingdom
VGG	Visual Geometry Group
XFEM	Extended Finite Element Method

Nomenclature

Symbol	**Description**
Voc	Open-circuit voltage of photovoltaic module
Isc	Short-circuit current
η	PV conversion efficiency
LR	Learning rate used in CNN training
E	Number of training epochs
B	Mini-batch size
F	Number of convolutional filters
K	Kernel (filter) size
l_s	Image input size
A	Classification accuracy
L	Loss function value
TP	True positive classification
TN	True negative classification
FP	False positive classification
FN	False negative classification

Chapter 1 Introduction

1.1 Background and Motivation

PV has become a major contributor to the world's response efforts to mitigate carbon emissions and develop an environmentally friendly energy future [1]. The price of PV panels has dropped dramatically over the last 20 years, while their efficiency and lifespan have both increased. PV energy is one of the fastest-growing electricity generating options in international energy reports. Countries from all regions of the economic development spectrum are building not only large PV farms but also small rooftop systems [2]. But the rapid growth in output has presented difficulties to ensuring that PV systems deliver their best output over their natural 20 to 30 years of life.

For long-term energy security and economic value of PV systems, the overall reliability is important. Stakeholders: Relying on modules to perform to their nameplate and limit degradation over time, stakeholders including investors, utilities operators, end-users among others. Small annual losses if realised when production is measured in GW can mean lots of lost energy and money [3]. Thus, it is important to detect and correct module malfunctions immediately to maintain the expected energy production as well as confidence in PV power technology.

PV modules are subject to different types of defects that occur throughout their lifecycle[4]. During manufacturing, defects such as minicracks or soldering anomalies can be introduced

through mechanical handling or process inconsistencies [5]. Transportation and installation can cause further mechanical stresses, sometimes leading to edge ribbon cracks or hidden fractures [6]. After being installed in the field, PV modules experience various types of environmental stress, including humidity, temperature fluctuations, high voltages and mechanical loads from wind or snow. All these factors can accelerate processes of degradation, such as potential-induced degradation (PID), separation and fatigue [7]. Combined, these disadvantages can make conduction less smooth, internal resistance nearer to the edge of positive return, and cast doubt upon reliability over time.

Traditional inspection techniques such as visual inspection, infrared thermography, and current-voltage (IV) curve testing remain widely used in both manufacturing and field operations. However, all these methods have limitations. In terms of cost-effectiveness and efficiency, visual inspection is unbeatable [8]. However, it cannot detect internal defects that are not visible from the outside. Infrared thermography will indicate a hotspot when the heat accumulates significant enough Yet, it lacks the sensitivity to detect minicracks and defects that have not yet accumulated a substantial amount of heat [9].

Despite providing some valid performance data, IV curve testing does not give any indication of where these defects might be located and what they are. As PV farms continue to expand in scale, these methods become increasingly inefficient. As a result, they are unable to provide detailed descriptions of millions of PV cells over a large area.

EL imaging is an effective method for measuring the efficiency of photovoltaic systems. By applying a forward bias to a PV module, silicon emits light that can be captured by cameras, revealing internal structures and defects that were previously hidden from other diagnostic techniques [10]. With EL imaging, cracks, shunts, and various types of hidden defects can be

clearly visible, enabling a direct assessment of whether cells remain intact. However, the largescale implementation of this technique in multi-megawatt PV systems generates a great deal of data, making manual inspection both inefficient and unreliable.

This thesis is motivated by the urgent need to combine the diagnostic power of EL imaging with automated analysis tools. Convolutional neural networks (CNN), a type of deep learning model specialised in image recognition, offer a strong solution. CNN can learn complex features directly from data and classify defects with high accuracy. By integrating CNN with EL imaging, this research aims to provide a scalable, automated method for detecting defects in PV modules, reducing reliance on manual inspection and improving the long-term performance of PV systems.

1.2 The Research Problem

The central problem addressed in this thesis is the lack of scalable and accurate methods for automated defect detection in PV systems. While EL imaging can reveal critical information about cell health, the main barrier is the analysis of the massive number of images generated. A utility-scale PV installation may include hundreds of thousands of modules, producing millions of EL images during inspection campaigns. Manually classifying such datasets is unrealistic and prone to human error.

There are several ways in which this matter affects photovoltaic PV performance. As a result of the propagation of these defects during manufacturing, modules are shipped to the market with mini-level errors. As a result, warranty costs are incurred, customer confidence is undermined, and the defective modules are returned to the manufacturer. During operation, more defects can emerge than are detected, resulting in greater failures and power losses if

not detected early. Additionally, on the long-term system scale, accurate defect data is needed for the degradation models and the performance prediction. Despite technological advancements, the PV industry faces significant challenges in maintaining system reliability as assets age, due to the lack of accessible and automated diagnostic tools.

1.2 Research Rationale and Novelty

The rationale for this research is founded on the need for reliable, scalable, and automated methodologies for PV defect detection capable of addressing emerging industrial inspection challenges. While EL imaging provides high sensitivity for detecting micro-level structural defects within PV cells, the interpretation of large volumes of EL data remains a significant technical challenge. Traditional inspection methods rely heavily on manual assessment or conventional machine learning approaches, which are often limited in scalability, robustness, and generalisation capability.

This thesis aims to address several key scientific and engineering challenges. The first challenge relates to the development of deep learning architectures capable of accurately distinguishing subtle defect patterns from normal structural variations in EL imagery. Photovoltaic defects such as microcracks, PID, and shading artefacts often exhibit complex spatial characteristics, making reliable feature extraction and classification a non-trivial task.

A second major challenge concerns the extension of defect detection methodologies from the cell level to the module level. While cell-level analysis enables precise identification of localised defects, module-level inspection introduces additional complexities, including spatial defect aggregation, imaging variability, segmentation uncertainty, and the need to translate defect classification results

into practical industrial decision-making criteria such as module acceptance, repair prioritisation, or replacement strategies.

Furthermore, the large-scale deployment of PV systems generates extensive datasets characterised by environmental variability, ageing effects, and installation-specific operational conditions. Developing computational frameworks capable of handling such high-dimensional datasets while maintaining classification accuracy and computational efficiency represents another critical research challenge addressed in this work.

The novelty of this thesis therefore lies in the integration of EL imaging and optimised convolutional neural network architectures within a unified multi-scale diagnostic framework. First, the research develops CNN models that achieve high classification accuracy for defect detection at the solar cell level. Second, it extends the analytical approach to module-level assessment by incorporating practical decision rules aligned with industrial quality assurance requirements. Third, the methodology is validated using one of the largest EL datasets reported in the literature, comprising approximately 85,000 modules and over 5.5 million individual cells. This comprehensive, data-driven investigation provides new insights into defect propagation mechanisms, power loss correlations, and long-term degradation behaviour in photovoltaic systems.

1.4 Research Aim and Objectives

This thesis aims to develop and validate EL imaging techniques for detecting and classifying PV module defects using CNNs. Additionally, use these techniques to assess how defects affect PV systems' performance and degradation.

The specific objectives are:

1. To design and evaluate CNN architectures for classifying EL images of PV cells as healthy or defective.
2. To extend the approach to module-level analysis, introducing acceptance and rejection thresholds based on defect prevalence.
3. To apply the methodology to a large dataset of 85,000 modules and 5.6 million cells, analysing defect distributions and performance impacts.
4. To study correlations between defect types, power loss, and long-term degradation rates.
5. To compare results with existing inspection methods and industry benchmarks to validate the accuracy of the approach.
6. To provide insights and recommendations for manufacturers, operators, and policymakers on the use of automated diagnostics for improving PV reliability.

1.5 Research Contributions

This thesis makes the following contributions:

- Cell-level CNN architectures: Four different CNN networks were proposed and evaluated, achieving a best validation accuracy of 98.07% in the classification of cracks, soldering defects and PID
- Module-level framework: The method was further scaled up to account for the classification of entire modules, introducing a criterion not to discard modules that present more than 20% of defective cells.

- Large-scale dataset analysis: One of the most extensive EL datasets was analysed, covering 167 PV installations and more than 5.5 million cells, enabling statistical insights not available in smaller studies.
- Emerging defect trends: The study identified a sharp increase in edge ribbon cracks for installation carried out after 2022, highlighting an emerging challenge to module manufacturing and installation.
- Correlation with performance: Regression models showed a clear link between the number of defective cells and measurable reductions in power output, providing predictive capability.
- Degradation forecasting: Long-term projections demonstrated that PV systems are likely to retain about 82 percent of their rated capacity after 25 years, in line with industry warranties, supporting the economic case for PV energy.

1.6 Structure of the Thesis

This thesis is organised into seven chapters.

- Chapter 1 – Introduction presents the background, problem statement, rationale, aims, objectives, contributions and thesis structure.
- Chapter 2 – Literature Review reviews PV defects, inspection methods, EL imaging, and CNN applications, identifying gaps in current knowledge.
- Chapter 3 – Automated PV Defect Detection at the Cell Level describes the design and validation of CNN architectures for detecting defects in EL images of cells.
- Chapter 4 – CNN for Module-Level Defect Classification extends the analysis to full modules, establishing acceptance and rejection criteria.

- Chapter 5 – Large-Scale EL Analysis of PV Systems applies the methodology to 85,000 modules, investigating defect patterns, correlations with power loss, and degradation trends.
- Chapter 6 – Discussion and Synthesis of Findings integrate the results, discussing strengths, limitations, implications, and contributions to knowledge.

Chapter 2: Literature Review

2.1 Introduction

PV systems are key to the global shift toward clean energy, but their long-term reliability remains a challenge due to recurring issues such as cell cracks, PID, and soldering faults. Performance stability over time requires early detection of degradation and effective management of its effects. This chapter examines the current state of knowledge about PV module defects, placing a special focus on crack formation and its direct consequences for energy output.

The review begins by surveying conventional diagnostic tools used to detect defects, such as EL, PL, thermal imaging, and current-voltage (I-V) analysis. These techniques form the foundation for existing practices. In addition, this chapter explores recent developments in methodology, such as the use of CNN for automating defect classification and improving accuracy.

In addition, this chapter touches on degradation patterns observed over time and how specific types of cracks contribute to performance loss. These longitudinal studies using EL imaging provide an invaluable view of how modules degrade in real-world situations. Together, these studies provide a greater understanding of where the field stands and what obstacles still exist.

This review also lays the groundwork for addressing gaps in the current state of knowledge. A few of these gaps are limited datasets, the interpretability of machine learning models, and

the difficulty in identifying minor or compound crack patterns. These challenges define the foundation behind the research presented here.

2.2 PV Module Defects

Cracks are one of the most common and damaging defects in PV cells. Such fractures are generated by the combined effects of thermal cycling, mechanical loading, and material fatigue (either minicracks or macroscopic structural failures) [11]. The magnitude of these cracks depends not only on size and number, but also on the physical characteristics of the materials used to manufacture PV cells.

Cracks also result from multiple external causes. The environmental fluctuations, mechanical stresses during handling and mounting, and internal stresses occurring in the process of lamination and encapsulation are all critical to defect formation [12], [13], [14].

Once initiated, cracks become stress raisers that influence PV cell degradation through several mechanisms. It can result in resistance to electron flow, reduction of the effective active area, and the creation of leaks that tend to reduce the efficiency. Small minicracks can develop over time into significant failures, especially when subjected to moisture and thermal stress.

These cracks can allow moisture to penetrate portions of the PV cells, which in turn may cause localised heat abnormalities appearing as high temperature spots, also known as hotspots. Such thermal anomalies aggravate the damage due to accelerated material degradation and cause the activation of bypass diodes [15], [16].

In-depth modelling work has shown that crack-induced performance loss is exacerbated by the accumulation of heat within the crack itself [17]. The high temperatures caused by defects

contribute not only to power degradation but also to thermal expansion, which can worsen existing cracks or causing new cracks to initiate.

In addition to cell-level concerns, interconnect reliability is a critical factor. Ribbon cracks and interfacial delamination at solder joints can be extended under mechanical stress or during high-temperature operation. An XFEM simulation was used to determine crack initiation and propagation along interconnect ribbons under thermal and mechanical loading, which provided predictions about the long-term reliability of the interconnects [18]. XFEM-based simulations show that careful control of geometry and lamination pressure can effectively suppress the risk of these possible failure modes.

At a more microscopic scale, one study used an equivalent single-diode model and parameter optimization to assess how minicracks influence I–V curves [19]. It demonstrated that early stage minicracks may not visibly affect module output but can distort electrical characteristics, which accumulate over time.

The electrical modelling shows that small cracks in the system affect the current-voltage relationship which demands precise detection techniques for prompt intervention. The selection of materials together with module construction methods determines how cracks will spread through the system [20]. The combination of Zebra-EVA encapsulants with tiling ribbon mono-crystalline PV modules during lamination resulted in a 3.6% decrease of minicracks and better thermal performance.

The results from Zebra-EVA encapsulated modules during lamination and load tests demonstrate that optimised composite materials enhance cracking resistance. The research on C-ER (enhanced recombination) and C-LAA (loss of active area) crack types showed distinct

thermal and electrical behaviour patterns. The multiple maximum power points that occur because of local heating in C-LAA cracks make it difficult to predict module performance. The electro-thermal model uses crack type analysis to identify their effects on power point stability and temperature distribution [21].

Research on back sheet materials indicates that co-extruded polypropylene (PP) types outperform laminated PET variants in terms of crack and discoloration resistance [22]. However, results depend on the specific formulations used by manufacturers. Material tests demonstrate that PP back sheets demonstrate better resistance to cracking than standard PET based layers which makes them suitable for future standardisation.

Researchers have developed an effective method to identify PV cell cracks through four distinct classification categories. The first classification stage shows no cracks, while the second stage indicates that small minicracks exist. The third category of PV cell damage results from partial fractures, which create shading zones, while the fourth category represents total structural failure [23].

The power loss from PV cells becomes more than 60% when cracks expand in size and complexity according to the classification framework. The data presented in Figure 1 demonstrates that prompt identification and exact classification of defects play a vital role in minimising energy loss.

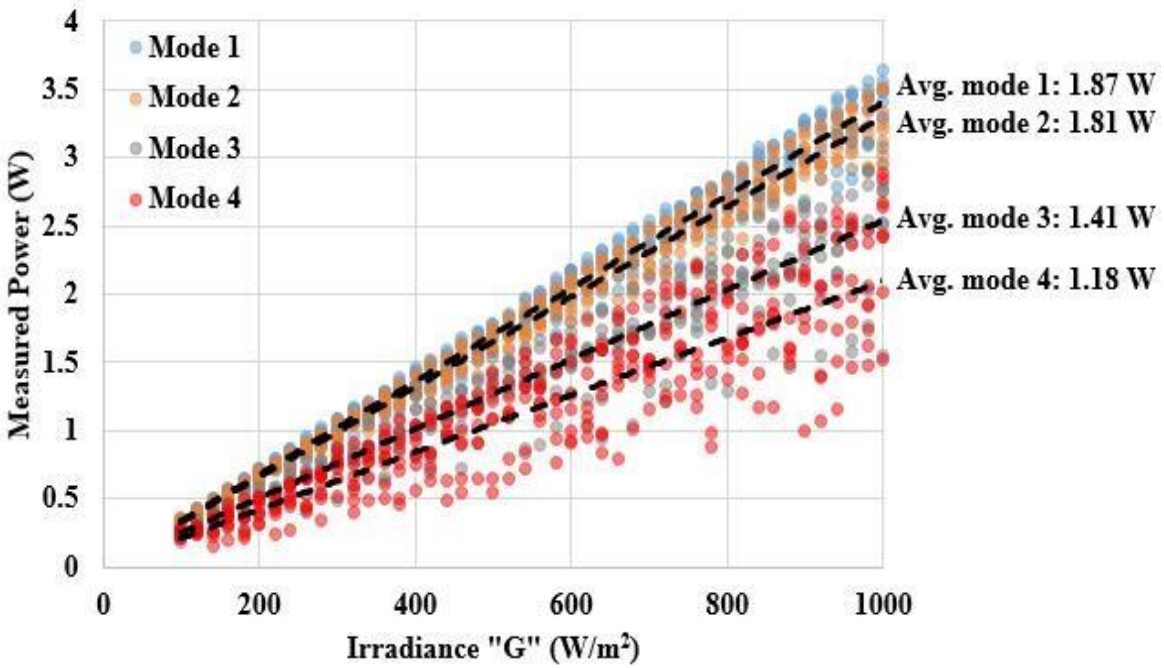

Figure 1. Measured electrical power plotted against PV irradiance for the examined PV cells, illustrating the performance behaviour of the modules under varying illumination conditions [23].

The inability to determine fault locations in PV installations results in substantial delays during inspection procedures [24]. To address this issue, we conducted a pilot study focused on identifying crack formation in PV panels embedded in two PV roads, as illustrated in Figure 2(a).

For this investigation, both electrical performance (I–V and P–V characteristics) and EL imaging of the PV panels were captured under real "road" conditions. The I–V curves were measured using the Seaward PV200 device, with a precision of ±2%. EL images were obtained using a dedicated EL imaging setup, Figure 2(b), which included a digital camera with a 6k × 4k resolution and an 18–55 mm zoom lens. The PV panel was connected to a biased power supply and operated under short-circuit conditions to stimulate luminescence in the cells.

The PV modules displayed equal EL intensity patterns when first examined but no cracks were detectable, as shown in Figure 3(a). The PV cells developed major cracks across their surfaces during their first thirty days of outdoor exposure, which caused substantial power loss. The performance measurements conducted on day 1 and day 30 under the same environmental conditions (760 W/m² irradiance and 16°C temperature) showed a detectable performance decrease.

(a)

(**b**)

Figure 2. PV modules installed along a public walkway at the University of York. (a) General view of the installed panels; (b) electroluminescence (EL) imaging setup used for inspection [24].

The open-circuit voltage (Voc) of PV Module #1 dropped by 29.5%, and the short-circuit current (Isc) fell by 3.2%, resulting in a power output reduction from 1.94 W to 1.58 W and an 18.5% power loss. The power output of PV Module #2 suffered from greater degradation than PV Module #1 because its Voc decreased by 36.1% and Isc decreased by 11.36% which resulted in a total power loss of 51.3% as shown in Figure 3(b).

The current PV technologies deployed for PV road applications demonstrate insufficient durability according to the obtained results. The study highlights the need for developing more durable PV cells and incorporating anti-resistance materials to enhance reliability under mechanical and environmental stress.

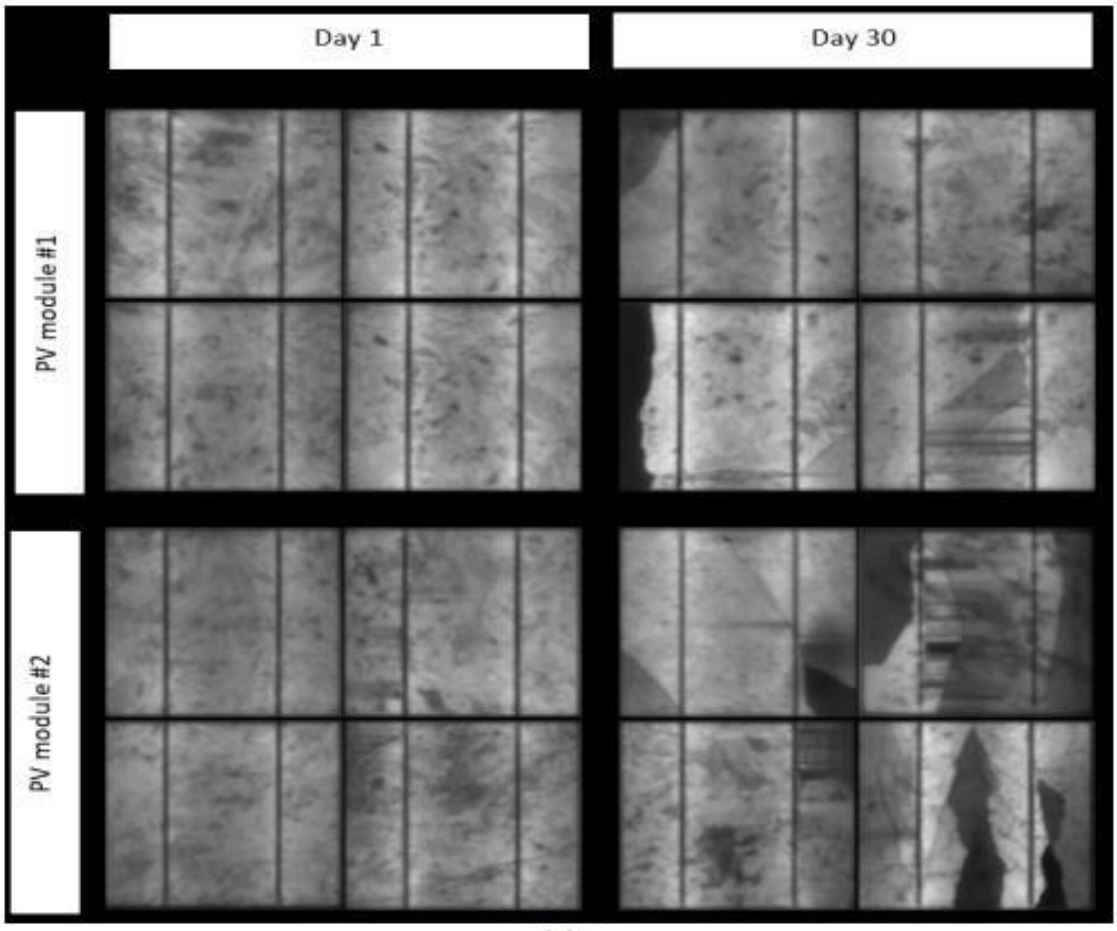

(a)

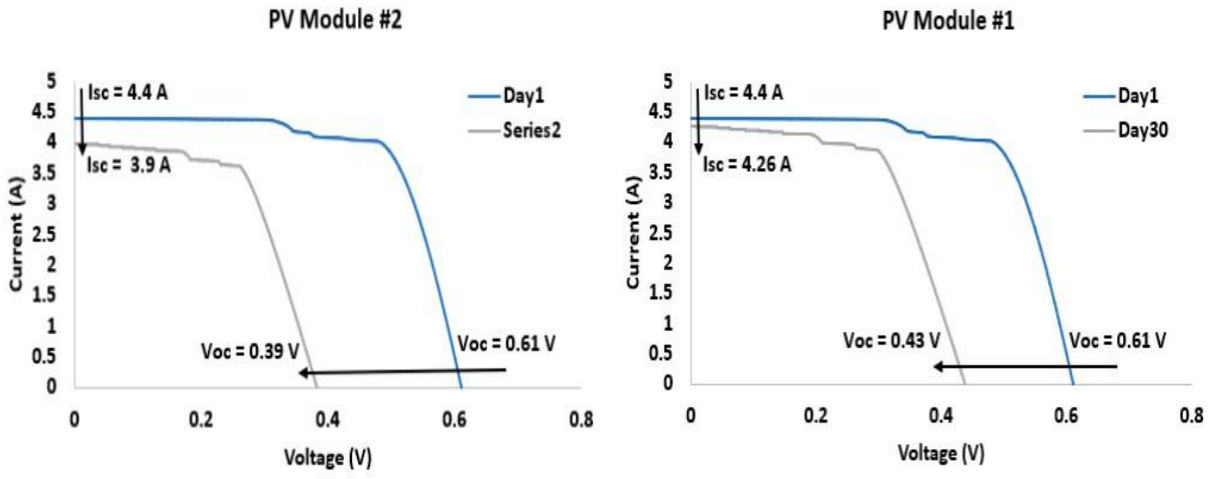

(b)

Figure 3. PV panels on the path.: (**a**) EL images of the PV panels on day 1 and after 30 days of installation. The EL images were taken during night-time at short-circuit conditions, and the irradiance level at 0 W/m^2 and the temperature at 16.3 °C, (b) I–V curve of the two PV modules [24].

2.3 Crack Classification in Photovoltaic Modules

Different types of cracks and defects can severely damage PV modules throughout their lifecycle starting from manufacturing until installation and continuing through operational exposure. The precise identification of defect types requires immediate attention since it determines both the extent of damage and the selection of appropriate corrective actions. The following classification receives additional support from Figure 4 which presents a complete visualisation of the defect categories

1. Line Cracks (Fig. 4(a)): The defects appear as straight or slightly curved breaks that run across the PV cell surface because of external mechanical stress during handling and shipping, and internal stress from thermal cycling [25]. The extent of linear crack penetration through the cell determines whether it affects the entire module or only particular sections of the conductive paths which results in reduced module performance [26].

2. Solder Anomalies (Fig. 4(b)): Soldering contains defects, which derive from imperfect execution. The dark and irregularly shaped zones that appear in EL images are known as anomalies [27]. The presence of these defects indicates poor soldering techniques and insufficient material bonding and mechanical damage at joints which disrupts electrical flow and reduces module performance [28].

3. Compound or Complex Cracks (Fig. 4(c)): The category contains multiple crack patterns such as intersecting lines, branching fractures and star-shaped formations that appear in a single cell. The formation of these patterns results from multiple stress factors that

include mechanical and thermal elements. The complex nature of these patterns leads to complete electrical separation between the affected area and its surrounding regions, which speeds up power system deterioration.

4. Edge Ribbon Cracks (Fig. 4(d)): Cracks appear at the outer edges of PV cells where soldered ribbon connections are located due to assembly stress, thermal expansion differences, and mechanical forces [29]. The cracks at cell edges block current flow which results in higher series resistance and significant power loss [30].

5. Potential-Induced Degradation (PID) (Fig. 4(e)): PID is a voltage-driven degradation phenomenon that typically develops due to high potential differences between photovoltaic cells and grounded module components, particularly under conditions of elevated temperature, humidity, and prolonged system operation. This mechanism leads to the gradual breakdown of cell surface passivation layers and anti-reflective coatings, thereby facilitating the formation of leakage current pathways and localised shunting effects within the p–n junction structure [31].

   Consequently, PID results in a reduction in shunt resistance and an associated decline in electrical performance, including decreased open-circuit voltage and reduced power output at the module level. In EL imaging, PID-affected regions typically appear as diffuse, large-area darkening patterns that extend across multiple cells rather than being confined to localised structural defects such as microcracks. This spatially distributed degradation behaviour can significantly impair overall module efficiency and long-term system reliability.

Furthermore, the severity of PID is influenced by installation configuration, grounding practices, environmental stress exposure, and inverter topology. Early detection and accurate classification of PID using automated image-based diagnostic techniques are therefore essential for supporting preventive maintenance strategies and ensuring sustained photovoltaic system performance.

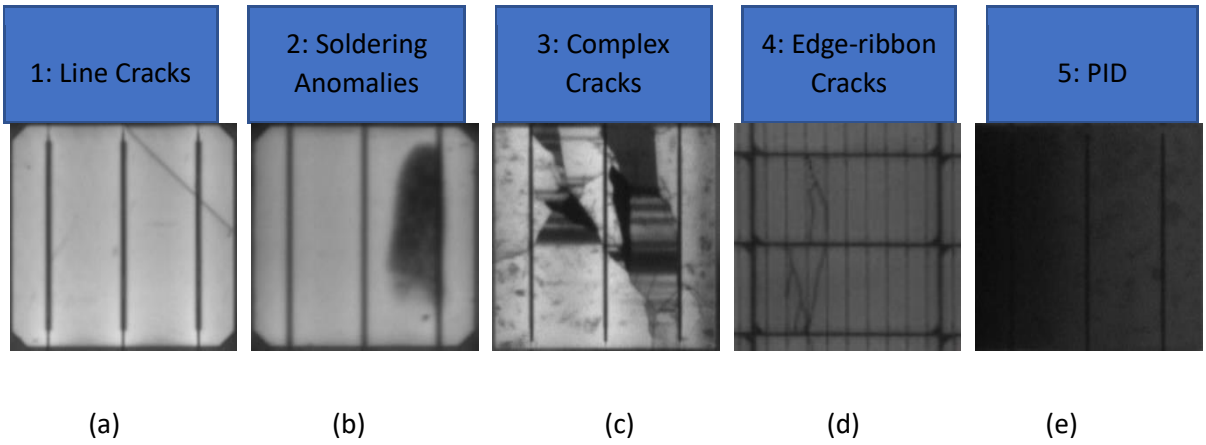

Figure 4. examples of PV defect categories identified in this study: (a) Line cracks; (b) Soldering anomalies; (c) Complex cracks; (d) Edge ribbon cracks; (e) PID [33].

2.4Lifecycle Stages of PV Module Defect Generation

PV module defects occur at various stages in the module lifecycle, including manufacturing, transportation, installation and operational phases. Different stages of module production create stress factors that threaten both structural and electrical module performance unless proper management exists. For manufacturers to improve their quality control systems and maintenance techniques, they need to identify the origins and types of defects at different stages of the process.

The manufacturing stage represents the first step of the process where defects emerge because of material issues and production mistakes. The combination of improper material selection, inadequate production temperature control and rough handling during lamination and soldering operations creates minicracks and weakens cell structures. The initial defects that appear during manufacturing operations become visible only after stress exposure leads to development, which results in reduced system reliability.

The second stage of PV module processing involves transportation, where modules face mechanical stress from vibrations, shocks, and environmental variations. The combination of poor stacking methods, insufficient cushioning, and extended humidity exposure during extended transportation leads to delamination, glass breakage, and stress fracture development. The defects that occur during transportation remain hidden until the module reaches its installation site for load testing.

The installation process becomes problematic when modules receive excessive mechanical stresses due to incorrect mounting methods. The combination of incorrect bolt tightening and improper panel alignment with inappropriate mounting systems leads to the development of cracks while making the existing ones more severe. Improper grounding and connection of modules during installation can result in future electrical problems and unbalanced current flow.

The operational phase represents the last stage were environmental exposure and poor maintenance result in equipment performance deterioration. Thermal fluctuations and wind pressure cause minicracks to grow larger. Typically, degradation is caused by dust accumulation, bird droppings, and pollution exposure. Inadequate maintenance routines

allow minor issues to escalate into significant system failures; extended voltage stress combined with inadequate insulation systems leads to PID.

2.5 Crack Detection Methods

The presence of cracks of any size causes significant damage to the PV cells which affects the operational performance and lifespan [34]. Early detection of these defects becomes vital for both performance maintenance and system failure prevention and costly repairs [35]. EL imaging stands as a leading and reliable method for crack detection among various inspection techniques [36]. This technique enables non-destructive and high-sensitivity inspection of PV cells and modules to detect hidden defects that standard visual examination cannot detect [37]. This chapter examines the fundamental concepts and operational steps of EL imaging for PV cell crack detection while demonstrating its essential function in PV industry operations.

EL imaging operates by applying a forward bias current to a PV cell or module, causing electrons to be excited within the cell's conduction band, as shown in figure 5. As these electrons react with holes, they emit infrared radiation, producing EL waves with wavelengths typically ranging from 950 to 1250 nm [38]. This emitted light generates an EL image, as illustrated in Figure 6, that clearly displays cracks and other defects on the surface of PV cell [39].

The system operates through a simple yet efficient method that enables fast and precise examination of complete PV cells and module surfaces. EL imaging serves as a non-destructive testing method that maintains cell integrity so that it can be used multiple times for manufacturing, quality control, and field inspection applications [40].

A controlled environment must be set up for EL imaging to achieve precise results. The PV cell or module needs forward bias conditions to produce electron excitation through a stable current source which generates EL emission. The faint infrared emissions from the cell surface become visible through high-sensitivity cooled charge-coupled device (CCD) cameras which produce detailed images of the cell's surface [41]. The EL wave detection process needs to happen either in complete darkness or during nighttime to eliminate external light interference [42], [43]. The absence of external light sources enables the detection of EL light emissions, which produce detailed images that reveal all minicracks.

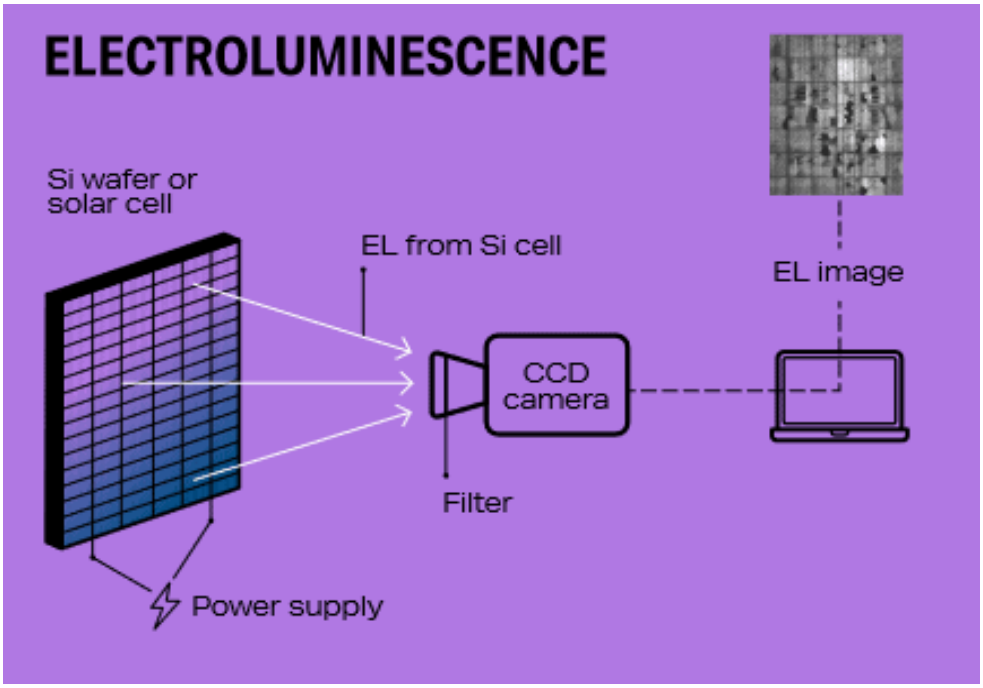

Figure 5. EL image setup.

EL imaging proves effective because it reveals defects that standard visual inspection methods fail to detect. The technique uses an induced current to make PV cells emit light, which reveals hidden cracks and defects that might affect their performance [44]. High sensitivity of EL imaging technology enables effective inspection of small PV cells and big PV modules, serving

various PV industry needs [45]. Furthermore, high-resolution images of EL imaging produce clear images that help detect surface damage and cracks on the module with great precision. This method operates as an effective defect detection system since it uses an efficient and precise operation method [46].

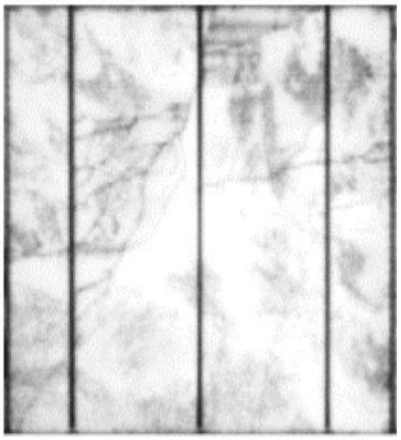

Figure 6. Example of an EL image highlighting intensity variations across individual PV cells within a PV module [24].

EL imaging provides non-destructive inspection capabilities that enable complete system examination without damaging PV cells or module structures. The manufacturing process benefits from this method because it detects defective cells before they become integrated into complete modules. This inspection method helps technicians inspect installed PV systems to detect damage from environmental factors, mechanical stress and aging effects. Moreover, it enables prompt maintenance activities, which increase system operational duration [47]. EL imaging allows researchers to investigate the impact of cracks and other defects on PV cell performance, thereby informing the development of improved materials and designs.

EL imaging can be enhanced by combining photoluminescence (PL) imaging and thermal imaging for a comprehensive assessment of PV cell performance. These additional methods enable the detection of defects and performance issues that EL imaging failed to identify in

full. The combination of different testing methods allows researchers and manufacturers to understand PV cell integrity better and, therefore, results in improved PV energy system performance and a longer lifespan.

Through PL imaging as a complementary method to EL imaging [48]. PL imaging operates contactless because it uses light to create luminescence, while EL imaging needs electrical excitation for its operation. The PV cell absorbs photons from light sources, including lasers, which generate additional carriers that return to equilibrium and produce light emissions. This emitted light, known as photoluminescence, as shown in Figure 7, can be captured to provide an image that reveals cracks and other defects [48], [49]. PL imaging provides contactless inspection that enables simple implementation for fast PV cell assessment based on material quality and defect detection [50]. The detailed analysis of power degradation issues through PL imaging such as bypass diode failure, PID and series resistance effects, makes PL an effective method for PV inspection [51].

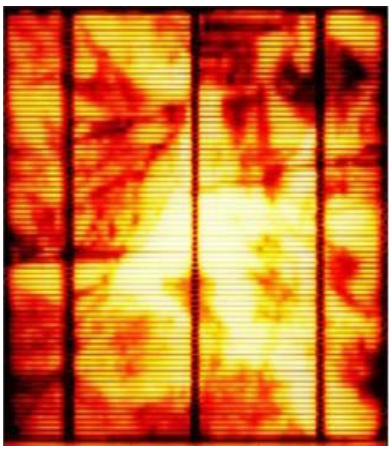

Figure 7. PL image of the examined PV module, revealing structural and material inhomogeneities [24].

The ability of PL imaging to pinpoint the precise location of cracks is one of its key advantages. PL imaging detects defects with high precision since it captures the light that appears during the luminescence process, which helps identify hidden cracks that standard methods cannot detect. The system operates at high resolution, enabling quality control inspections in manufacturing and detailed PV module inspections after installation. PL imaging provides several advantages for quality control but also has limitations. The method requires expensive detection cameras, which increase implementation costs [52], [53]. Also, the PV cells face potential damage from the irradiation light that activates carriers during the imaging procedures [54], [55]. Another challenge is that PL imaging is less effective for materials with high reflectivity, as the emitted light may be difficult to detect accurately in such cases [56]. The limitations of PL imaging limit its flexibility for specific applications, although its noncontact functionality and detailed defect inspection abilities make it a vital supplementary tool.

The Inspection of Large-scale PV systems, which contain numerous modules, can be challenging, but drone thermal imaging technology offers an efficient way to identify cracks and hotspots [57]. This technique employs drones carrying thermal cameras to detect temperature irregularities to help identify PV array malfunctions, as demonstrated in Figure 8. This method works best for utility-scale PV farms since manual inspections become impractical in such large installations.

The thermal imaging system uses an intelligent drone equipped with thermal imaging technology to detect hotspots from PV installation faults and cracks as shown in Figure 9[58]. The system stores these images for future analysis to help engineers detect faulty areas, find solutions quickly and maintain peak system performance [59]. This method enables quick

coverage of large PV arrays, resulting in reduced inspection time and superior safety performance compared to traditional manual inspection methods.

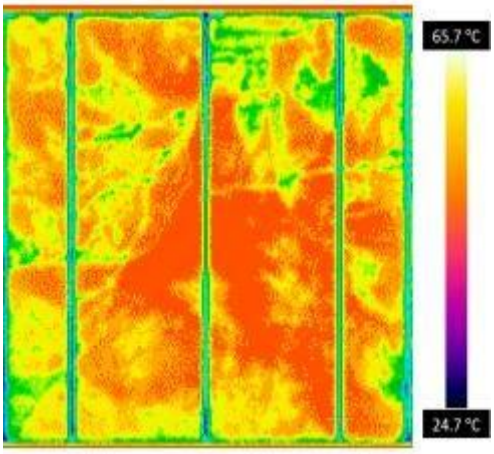

Figure 8. Thermal image of the module surface showing temperature variations and localised hot spots [24].

The primary advantage of drone-based thermal imaging technology lies in its capability to perform fast inspections of large PV systems for detecting potential defects. As a result, the system allows for immediate maintenance activities, which reduce power usage and extend the overall system lifespan [60]. The process requires significant work, as it necessitates drone operators with experience to operate the flights and experts to analyse the gathered information. The process of fault location becomes challenging, which leads to delayed repairs while specialized equipment adds to the overall cost [61].

This method is widely used for maintenance and quality assurance in large-scale PV systems, detecting defects caused by environmental or mechanical stresses but it is less suited to individual PV cells [62]. However, drone-based thermal imaging is a valuable tool for maintaining large PV installations, offering rapid and accurate defect detection despite challenges with labour and cost [63]. As PV energy grows, this method will remain crucial to ensuring system reliability.

Figure 9. Thermal inspection of PV modules performed using an aerial drone equipped with an infrared camera [64].

2.6 CNN-Based Defect Detection

The rapid growth of PV module manufacturing and installation over the last decade necessitates the immediate implementation of automated defect detection systems to achieve optimal performance and extend the system lifespan [65]. PV module inspection requires precise techniques to detect cracks, as it significantly reduces the power output. The PV industry now employs CNN as a deep learning algorithm to detect cracks and serves as an effective tool for inspection processes. The algorithms improve both speed and accuracy of crack detection and classification, which leads to prompt maintenance activities for better energy output.

CNN are designed to process grid-like data, such as images, making them highly effective for analysing PV module visuals. CNN detect cracks in images since these networks use multiple

interconnected nodes to extract features such as edges and textures which results in precise crack detection. In PV inspection, CNN architectures are trained on datasets of module images to identify crack patterns and distinguish them from other defects or normal surface variations {R6}. The automated system provides superior results to human inspectors who conduct manual checks due to their lengthy process and unreliable results.

The detection of cracks through CNNs requires images acquired using EL or thermal imaging technology. The CNN processes these images through convolutional layers to identify crack related features, followed by classification layers to determine the presence and severity of defects. This method provides fast analysis of numerous PV modules, making it suitable for industrial quality control operations and field maintenance activities. The CNNs demonstrate flexibility through their ability to work with multiple module types and different imaging environments, making them suitable for various PV applications [66].

2.6.1 Fundamentals of Convolutional Neural Networks (CNN)

The CNN technology has transformed various sectors through its ability to improve medical imaging diagnostics in healthcare and provide reliable object detection for autonomous driving systems [67], [68], [69]. The PV sector employs CNNs to analyse images acquired through electroluminescence and thermal imaging methods for accurate crack detection. The ability of CNNs to identify patterns in these images enables them to differentiate between cracks and other surface features, which improves manufacturing quality control and PV array maintenance operations [70]. The automated system reduces human involvement in manual inspections and leads to better operational efficiency and standardized inspection results.

The effectiveness of CNNs depends on their ability to detect significant image features such as edges and textures through an integrated multi-layered processing system. The model shows reduced performance when training images contain different levels of degradation than validation images due to the loss of low-level features in early layers [71]. Additionally, CNN models require large amounts of high-quality data and powerful computing equipment, which drives up expenses. Despite these challenges, the precision and adaptability of CNNs make them a transformative technology for PV inspections. {R6}.

CNN architecture development is a critical aspect of the application. CNNs can be optimized by both human expertise and automated techniques, such as genetic CNNs and hierarchical approaches. Specialized knowledge is needed to achieve better results with these designs than with fully automated systems [72]. The implementation of fully automated designs allows users without CNN expertise to build models quickly and easily, which makes these tools more accessible to a broader audience [73], [74], [75]. The Hypotheses-CNN Pooling (HCP) innovation enables CNNs to process multiple object segments through max pooling output aggregation, which provides noise resistance without requiring detailed training data labels [76]. Such advancements have made CNN versatile, suitable for PV crack detection and multiple other complicated applications.

CNN depends on multiple fundamental layers that work together to build a system that performs tasks precisely. CNN operates on these essential layers to function properly. The main layers of the model are described in Table 1 with their corresponding functions.

Layer name	**Function**	**References**
Input layer	Defines the size parameters of the input image or volume, detailing its height, width, and the number of colour channels it contains	[77]
Convolutional layer	Comprises the set of filters learned during the processing stage, each being smaller in size than the original input image	[78], [79]
Normalization layer	Helps preserve model regularity and prevent overfitting, while also enhancing the computational efficiency of the CNN.	[80], [81]
Rectified Linear Unit (ReLU)	Removes all negative values and replaces them with zeros to ensure non-negative activations within the data.	[82], [83]
pooling layer	Extracts representative values from specific image regions defined by the boundaries of the applied kernels.	[82], [84]

A fully connected layer	Transforms input vectors through linear operations using weight matrices, enabling the network to address and solve complex computational tasks.	[85], [86]
SoftMax function Layer	Used to estimate the probability distribution across multiple classes in a classification task.	[87], [88]
Classification layer	Applies a defined set of decision rules to assign inputs to their appropriate categories.	[89], [90]

Table 1. Main layers of CNN's architecture [91].

2.6.2 CNN Crack Detection Based

The growing demand for PV modules in production and installation necessitates automated inspection systems to detect cracks, as these defects reduce both system performance and operational life expectancy [92]. The demand for PV inspection requires CNN technology as a fundamental solution, which utilises various architectures to enhance inspection speed and precision. Two of the most common types of CNN architectures are custom-built models, which are built from scratch and transfer learning models, which are pre-trained for a specific application [93], [94]. The development of custom architectures for complex detection problems requires substantial computational power and large amounts of training data. The PV industry relies on transfer learning architectures that use pre-trained models to speed up

the development process while reducing resource needs and data requirements. Although transfer learning offers efficiency and speed, custom architectures are superior at tackling complex problems that require specialised design [95]. This dual approach fulfils different inspection requirements, which enable quality control in PV manufacturing and operational maintenance.

The PV-Crack Net model from Hussein and his team demonstrates a recent development that uses a lightweight CNN architecture to detect minicracks in PV modules, as shown in Figure 10 [96]. Addressing the challenge of limited representative data due to varying PV cell appearances, the study introduced a filter-induced augmentation flow (FAI) strategy, shown in Figure11. The method uses multiple filters on PV images to create a training dataset that represents various lighting and environmental scenarios. PV-Crack Net achieved a remarkable 97.42% accuracy level, outperforming all other top-performing architectures in terms of recall and precision.

A different research team created a lightweight CNN structure, which achieved 93.02% accuracy using minimal training data while operating without costly GPU systems [97]. The model used data augmentation methods to address data scarcity through image rotation at 90, 180 and 270 degrees and contrast flipping. The new techniques expand the dataset diversity by 6%. This allows the model to understand different image interpretations and detect defects in 8 milliseconds per image. However, research showed that expanding the dataset with defect classification would improve accuracy because the extra information enabled the model to detect multiple PV module defects better [97]. The lightweight CNN methods show promise for fast and precise crack detection for better quality control and maintenance in the growing PV industry.

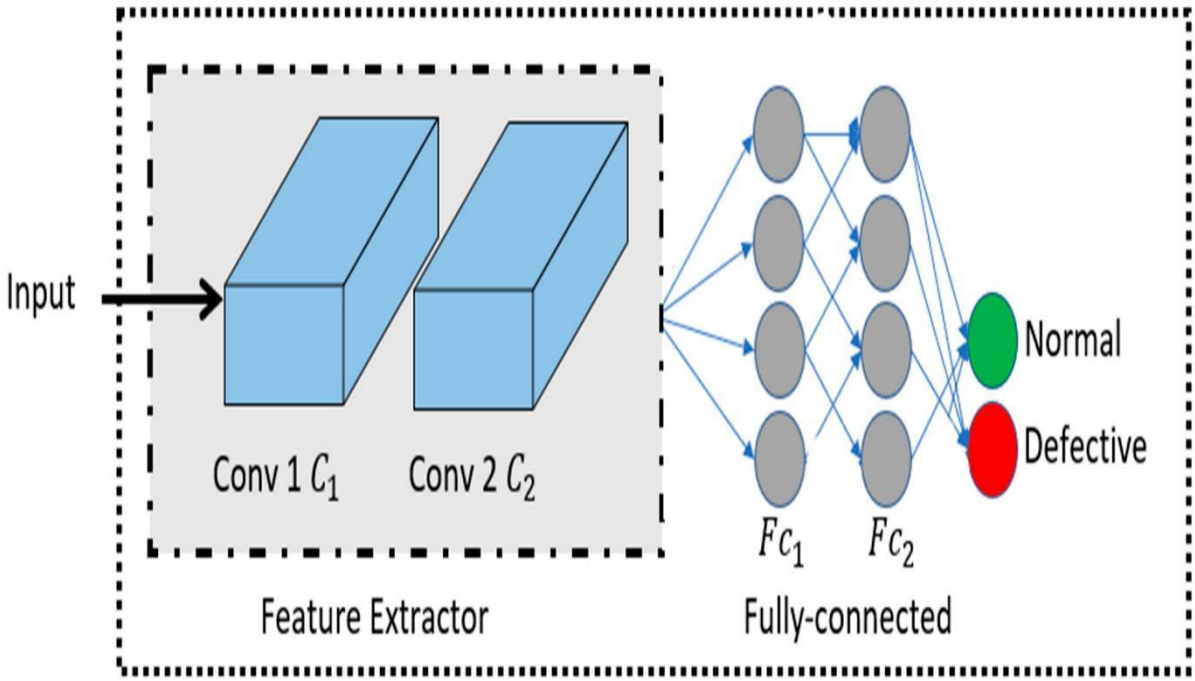

Figure 10. Proposed CNN PV-cracknet architecture [96].

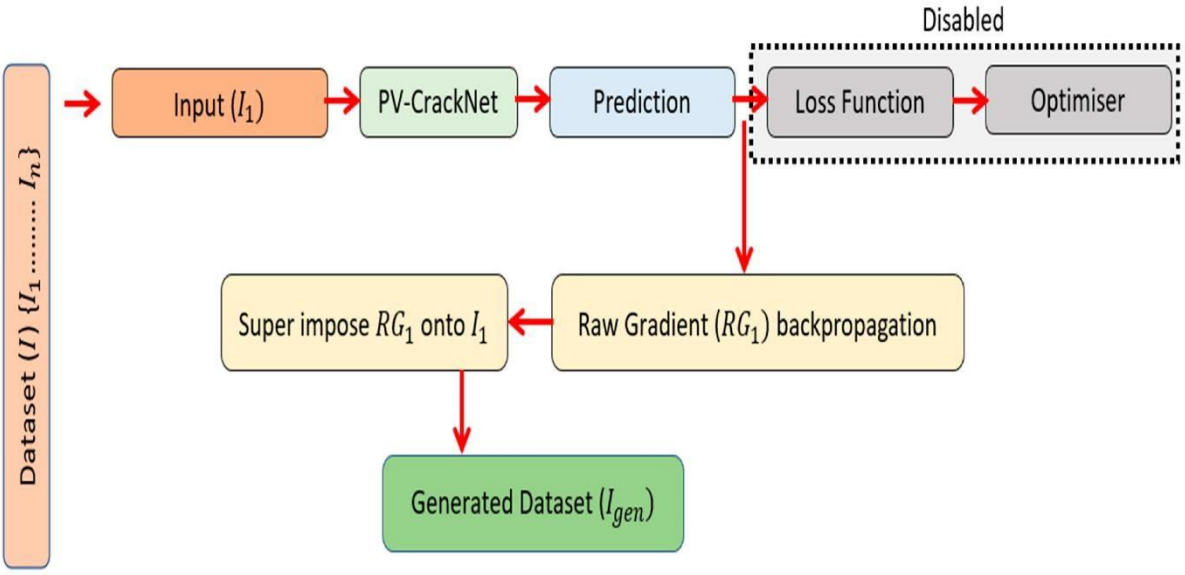

Figure 11. Filter- induced augmentation flow (FIA) [96].

A recent study employed AlexNet as a pre-trained CNN model to detect PV module cracks since this model was initially trained for object classification of more than 1,000 items, as shown in Figure 12 [98]. The researchers adapted AlexNet to classify PV modules into two groups of

defective or non-defective based on a training dataset of 392 images. The modified model reached an accuracy level of 85.2% [98]. The model's performance was limited because of the limited training data availability. The research applied high-performance computing systems to handle big data through enhanced training methods and data improvement techniques. The combination of expanded data and improved training methods in AlexNet led to better results since larger datasets and advanced computing power enhance model performance for PV module defect detection. The method demonstrates how AlexNet can perform efficient automated inspections in the PV industry.

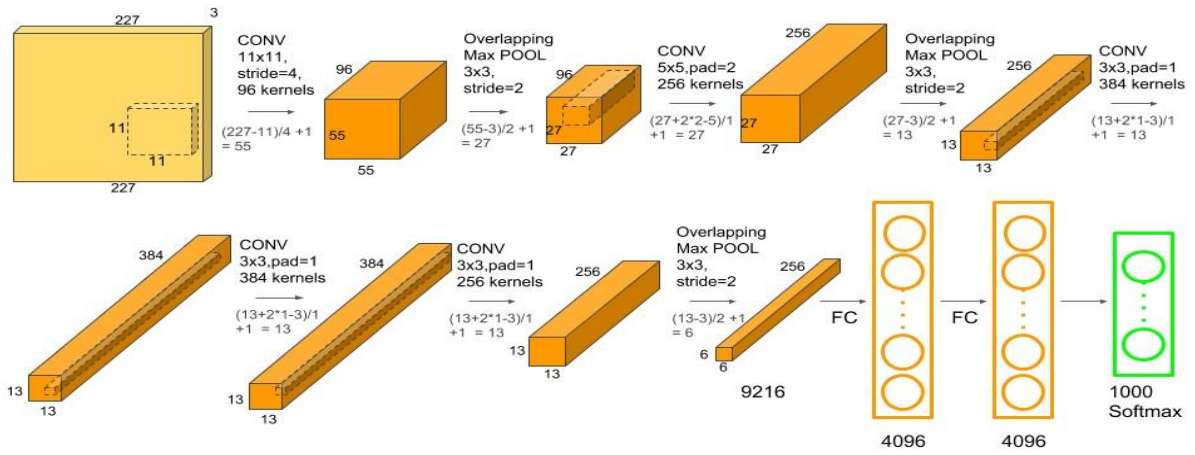

Figure 12. Pre-trained AlexNet CNN architecture [98].

A study by Rahman and colleagues explored six advanced transfer learning architectures VGG16, VGG-19, Inception-V3, ResNet50-V2, ResNetV2, and Exception for identifying minicracks in PV modules using EL images [99]. The approach involved analysing 2,624 EL images, augmented with 90- and 270-degree horizontal flip rotations to enhance dataset diversity. Each architecture was evaluated individually, but the study proposed an ensemble method that combined these pre-trained networks into a single model, aggregating their outputs for improved accuracy, as shown in Figure 13.

The ensemble method employed soft weighting to average predicted probabilities before threshold application which reduced error variance and produced excellent results with complex models. The ensemble method achieved high accuracy, as indicated in Table 2, with 96.97% accuracy for monocrystalline and 97.06% accuracy for polycrystalline panels, exceeding the performance of individual architectures, which range from 90.91% to 96.97% for monocrystalline and from 85.29% to 94.12% for polycrystalline panels [99]. However, the study highlights how ensemble-based transfer learning methods achieve effective minicrack detection, which provides a reliable method for PV quality inspection and maintenance operations.

Architecture	**Evaluation of the accuracy of pretrained networks and ensemble learning methods applied to monocrystalline PV panel analysis.**	**Evaluation of the accuracy of pretrained networks and ensemble learning methods applied to polycrystalline PV panel analysis.**
VGG-16	90.9%	91.2%
VGG-19	96.9%	88.2%
Inception-v2	96.9%	88.2%
ResNet50-v2	90.9%	88.2%
ResNet-v2	96.9%	94.1%
Xception	93.9%	85.3%
Ensemble	96.9%	97.1%

Table 2. Accuracy of pre-trained networks and ensemble learning for monocrystalline and polycrystalline PV panels [99].

Another study introduced an enhanced version of the Faster R-CNN model, a CNN architecture, to improve crack detection in PV cells [100]. The standard Faster R-CNN model showed low accuracy but achieved better results after adding a Feature Pyramid Network (FPN) and guided anchoring Region Proposal Networks (RPNs). The FPN extracted specific features from PV images through edge, corner and texture detection, which resulted in better model performance. The guided anchoring of RPNs allows the model to detect cracks with high precision.

The modified model reached 94.62% accuracy after training on 5,000 images with different brightness levels, resulting in an 11% improvement over the original Fast R-CNN. Additionally, the system achieved a faster crack detection speed through the improvement, reducing the time needed to process each image from 0.91 seconds to 0.19 seconds. As a result, the model provided better performance than traditional methods because of its enhanced feature representation and precise localisation abilities and it could achieve better results with more extensive training data [100].

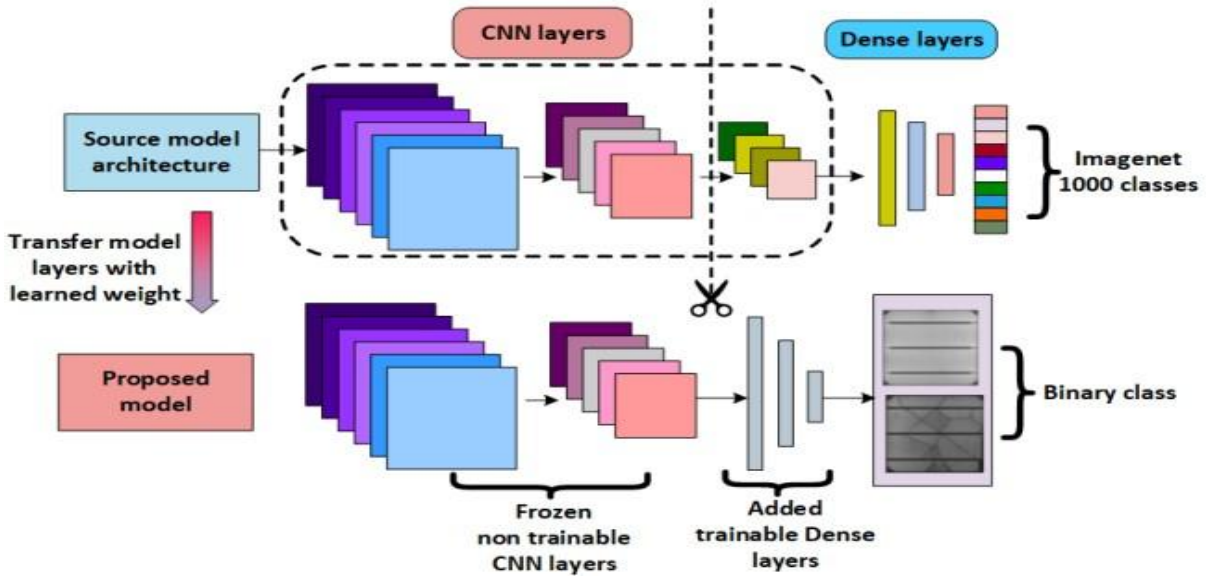

Figure 13. Proposed ensemble learning architecture [99].

Table 3 presents multiple CNN algorithms for PV cell image crack detection and corresponding performance characteristics [101]. This evaluation focuses on detection accuracy as its main performance metric, which represents how well the algorithm detects and classifies cracks, with higher values showing better reliability. The detection speed of the algorithm determines its ability to process images quickly enough to enable real-time or near-real-time PV inspection operations. Moreover, the network complexity that arises from a deep and complex architecture design leads to better performance but demands large computational power. Computational speed determines how fast an algorithm generates predictions for efficient analysis.

CNN Algorithm	**Description**	**Suitable for Detecting**	**Detection Accuracy**	**Detection Speed**	**Network Complexity**
GoogLeNet	A deep CNN architecture incorporating inception modules to enhance feature extraction.	Different types of cracks—such as minicracks, corner cracks, and edge cracks—are effectively identified due to the model's capability to capture features across multiple scales.	High	Moderate	Moderate
SqueezeNet	A lightweight CNN architecture that employs fire modules to achieve efficient feature extraction	Detects surface-level cracks and defects with high efficiency, making it well-suited for real-time image processing and large-scale PV system monitoring	Moderate	High	Low

ResNet-50	A deep CNN architecture with residual connections	Identifies complex cracks and defects, with its deep network architecture enabling the extraction of intricate visual patterns and subtle image details.	High	Moderate	High
DarkNet-53	YOLO (You Only Look Once) CNN architecture for object detection	Capable of detecting both micro- and macro-level cracks, offering efficient object detection essential for accurately identifying diverse crack types.	High	Moderate	High
VGG-19	19 layers CNN architecture	Detects macro-level cracks and defects, with its network depth enabling the extraction of key features that characterize larger structural faults.	High	Moderate	High
AlexNet	8 layers CNN architecture	Identifies surface-level cracks and defects with high efficiency, making it suitable for real-time image analysis and large-scale photovoltaic system applications.	Moderate	High	Moderate

Table 3. Comparison of CNN algorithms for PV cell cracks image detection [91].

The results reveal that GoogLeNet, ResNet-50, and Inception-v3 advanced CNN models achieve the best detection results for PV module crack identification. Due to the complex design of these models, they require enormous computing power, making it challenging to run these models on systems with limited processing capabilities. The SqueezeNet and AlexNet models offer an optimal trade-off between accuracy and computational efficiency, making them suitable for applications that require real-time processing or operate with limited hardware resources. These algorithms operate in MATLAB and Python environments to fulfil the different requirements of PV inspection. The evaluation process reveals that CNN models must strike a balance between speed, accuracy and computational resources to be effective in PV industry crack detection applications [101].

A comparative overview of commonly used deep learning architectures is presented to better understand their suitability for automated defect detection in PV EL imaging applications. As shown in the comparison table 4, deeper networks such as VGG and high-depth ResNet variants generally demonstrate strong feature extraction capability due to their increased representational capacity. However, these architectures are typically associated with higher computational burden, increased memory demand, and longer training times, which may limit their practical scalability when analysing very large PV inspection datasets.

On the other hand, lightweight architectures such as MobileNet and SqueezeNet offer significantly reduced model complexity and faster inference performance, making them attractive for real-time monitoring scenarios and embedded inspection systems. Nevertheless, their relatively constrained feature learning depth can reduce sensitivity to subtle defect signatures often observed in EL images, particularly when dealing with micro-scale degradation patterns.

Architectures with moderate depth, including Inception-based networks and lower-depth ResNet configurations, provide a more balanced compromise between classification accuracy and computational efficiency. These models can capture spatial defect characteristics with improved stability while maintaining manageable training requirements.

Considering these factors, the CNN framework proposed in this research was developed specifically for PV EL defect analysis, rather than relying solely on standard pre-trained architectures. This tailored design approach allows the network to achieve strong classification performance while maintaining computational practicality and improved adaptability to large-scale inspection conditions.

Algorithm	**Parameters (M)**	**Model Size (MB)**	**Computational Complexity**	**Feature Extraction Capability**	**Interpretability**
AlexNet	61	240	High	Moderate	Moderate
ResNet-18	11.7	44	Moderate	Strong	Moderate
MobileNetV3	2.5	10	Low	Moderate	High
DenseNet-121	8.0	33	High	Very strong	Low
VGG-16	138.4	528	High	Moderate	Low
InceptionV2	11.2	42	Moderate	Strong	Moderate
ResNet-50	25.6	98	High	Strong	Moderate
SqueezeNet-1.0	1.2	4.6	Low	Moderate	High

Xception	22.9	88	High	Very strong	Moderate
MobileNetV2	3.5	14	Low	Moderate	High
DenseNet-201	20.2	88	High	Very strong	Low
VGG-19	143.7	548	High	Moderate	Low
InceptionV4	41.2	153	High	Strong	Moderate
ResNet-152	60.2	230	High	Strong	Low

Table 4. Comparison of Deep Learning Architectures for Automated Solar Cell Defect Detection.

2.6.3 Limitations

The shift from traditional to automated crack detection methods in PV modules has significantly enhanced accuracy and efficiency, with CNN leading this transformation. These deep learning algorithms have revolutionised defect identification in PV cells, streamlining inspections and boosting reliability [91]. The high precision crack detection ability of CNNs in image processing leads to accelerated quality control and maintenance operations, which reduce PV system energy losses. However, the training datasets face two significant challenges since they contain fewer than 10,000 images and lack diversity, as shown in Table 3. The model exhibits insufficient performance when applied to restricted data, as it lacks the capability to accurately identify various crack types. In order to make the model more robust, researchers should work with industry and research institutions to obtain extensive high-resolution datasets showing different kinds of defects [91].

Models trained on particular datasets demonstrate an inability to identify cracks in PV panels with distinctive features. The model achieves better detection of distinctive features through training with data diversification using different panel types and fine-tuning a pre-trained network on ImageNet for limited datasets [91]. CNN's decision-making process remains challenging to interpret, as its complex black-box structure prevents users from understanding the underlying reasons behind its defective identification. Users develop trust through transparent decision-making because explainable tools that use attention mechanisms and saliency maps reveal which image sections generate predictions.

Real-time detection systems serve as essential components for large PV farms, as they enable rapid fault detection, preventing power loss. PV installations require CNNs to handle enormous data volumes at fast speeds. Lightweight architectures or optimization techniques like quantization and pruning, which reduce model complexity, can enhance inference speed while maintaining accuracy. The PV industry requires CNN models to handle multiple panel designs and diverse environmental conditions; therefore, integrating multiple datasets with pre-trained networks enables CNN to address these challenges, resulting in reliable and efficient crack detection for various PV systems.

2.7 Research Gaps

Although there has been a growing body of research on PV diagnostics, important gaps remain in both methodology and practical application. Much of the existing literature on EL imaging has focused on small-scale laboratory studies, often using datasets of only a few hundred or a few thousand cells. While these studies demonstrate the potential of EL imaging for identifying cracks and other hidden defects, they do not adequately address the practical requirements of utility-scale

PV inspection, where millions of cells may need to be assessed efficiently, consistently, and under variable field conditions. This therefore reveals not only a methodological gap, but also an application gap between laboratory-based proof-of-concept studies and real-world industrial deployment.

Similarly, although CNN and other deep learning approaches have increasingly been applied to PV image analysis, most existing studies remain limited to cell-level classification. Only a small number of studies have attempted to extend these approaches to the module level, and those that do are often constrained by a number of technical challenges. First, module-level EL images contain greater structural complexity, since they include multiple cells, interconnections, non-uniform illumination effects, and spatially aggregated defects. Second, reliable segmentation of modules into meaningful cell-level regions introduces additional uncertainty. Third, even where cell-level defects are successfully detected, translating these outputs into practical module-level decisions requires acceptance and rejection criteria that are aligned with industrial quality assurance standards. These scientific and engineering challenges help explain why module-level studies remain limited in the literature.

Another important gap lies in the lack of integration between defect detection and performance interpretation. Existing studies often stop at identifying whether a defect is present, without linking defect patterns to power loss behaviour, module acceptance criteria, or long-term degradation forecasting. As a result, the broader operational significance of detected defects is often left unexplored. This limits the usefulness of many current diagnostic frameworks for manufacturers, operators, and asset managers who require not only defect recognition but also decision-support information for maintenance, replacement, and reliability assessment.

A further limitation concerns the availability of large and diverse datasets. Many published studies rely on images collected under controlled indoor conditions, which may not capture the full range of defect appearances, module technologies, busbar configurations, ageing effects, and environmental influences encountered in operational PV systems. Consequently, models trained on such datasets may show strong laboratory performance but limited generalisation when applied to field installations. There is also relatively little evidence on how defect distributions are evolving in more recent PV technologies, such as modules incorporating thinner wafers or multi-busbar designs.

In addition, while some earlier studies have proposed CNN-based classification frameworks, the methodological innovation has often remained incremental, for example by applying standard pre-trained architectures directly to small EL datasets without extending the framework toward multi-scale decision-making or large-scale system interpretation. This leaves an important opportunity for more integrated methodological development that combines model optimisation, application scalability, and engineering relevance within a single framework.

This thesis addresses these gaps by developing and validating a multi-scale, data-driven diagnostic framework for photovoltaic defect detection. The research advances beyond cell-level classification by extending CNN-based analysis to the module level, introducing practical decision rules for acceptance and rejection, and applying the methodology to one of the largest EL datasets studied to date, comprising approximately 85,000 modules and over 5.5 million cells. In addition, the work links defect detection to power loss correlations and long-term degradation assessment, thereby addressing both methodological and application-level shortcomings in the existing literature. By doing so, the thesis contributes new understanding of defect evolution, including the recent rise of

edge ribbon cracks, and demonstrates how automated EL-based diagnostics can be applied at scale to support both manufacturing quality assurance and field operation strategies.

The literature review has highlighted the growing importance of deep learning techniques for photovoltaic defect detection, while also revealing limitations in existing CNN-based methodologies related to classification accuracy and generalisation capability. These identified research gaps motivate the development of an optimised convolutional neural network framework specifically tailored for crack detection at the solar cell level. Consequently, the next chapter presents the design, implementation and validation of a novel CNN architecture aimed at improving defect classification performance using electroluminescence imaging data.

Chapter 3: CNN for Crack Detection at Cell-Level

3.1 Introduction

This chapter presents the development and evaluation of CNN architectures for PV crack detection at the solar cell level. Building upon the general research background and identified knowledge gaps discussed in Chapters 1 and 2, this chapter focuses on the design of a data-driven deep learning framework using electroluminescence EL imaging. The objective is to improve defect classification accuracy through systematic optimisation of CNN structural parameters and training configurations. The proposed methodology investigates different architectural configurations and pooling strategies to enhance feature extraction capability and classification robustness. Experimental validation is conducted using EL image datasets to assess the effectiveness of the developed models in distinguishing between healthy and defective PV cells.

3.2 Materials and Methods

A CNN system, integrated with EL imaging, enables automated defect detection in PV cells directly on manufacturing lines, as shown in Figure 14(a). By processing the EL images, the system detects structural defects, such as cracks and minicracks, as well as areas with high resistance and low light absorption. EL imaging applies a high-voltage current to stimulate light emission from PV cells, which is captured by a camera to reveal performance issues, with examples of healthy (defect-free) cells shown in Figure 14(b) and defective cells in Figure 14(c).

The CNN setup enables fast and accurate cell classification between healthy and defective cells for recycling operations. During the training and validation phases, the system was trained and validated using EL images with pixel resolutions ranging from 1000 × 1000 to 2500 × 2500. By having the ability to work with different levels of quality within the image, the system demonstrated its flexibility. Through the use of various resolution methods, the algorithm becomes more robust and performs well under a range of manufacturing conditions.

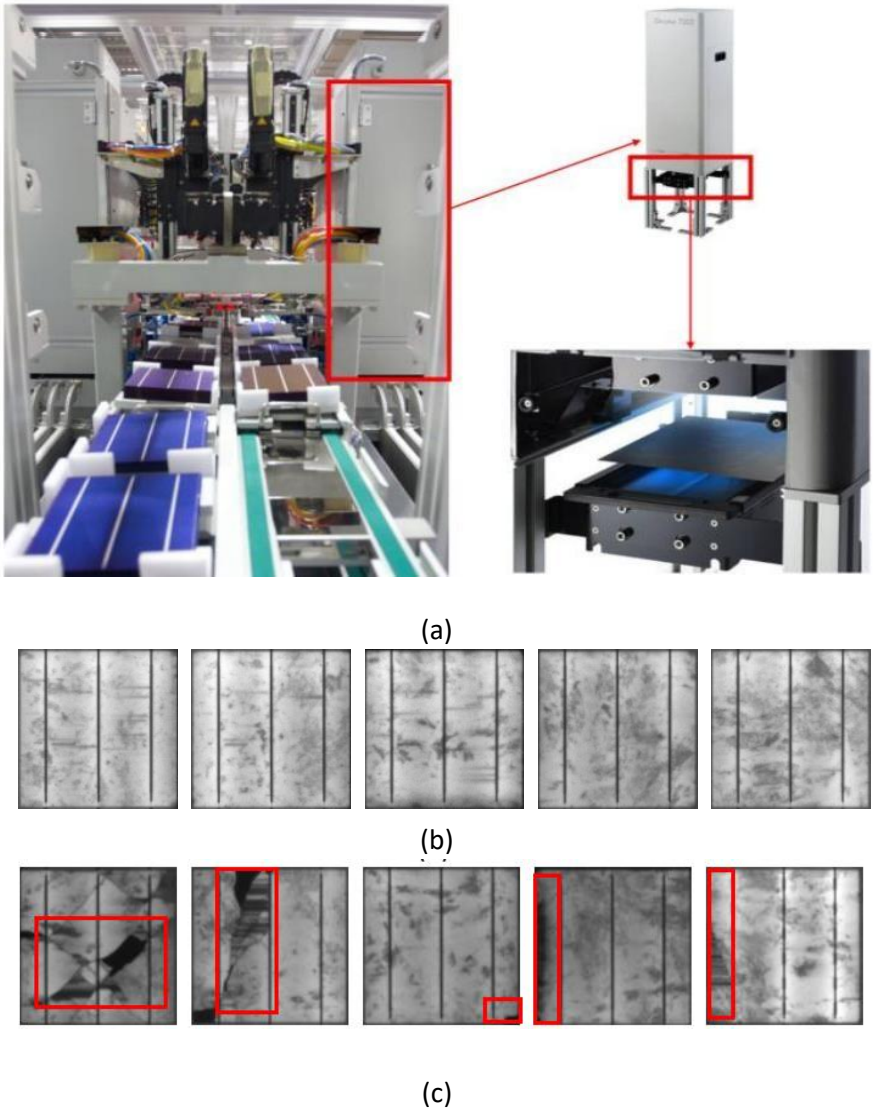

Figure 14. (a) In house EL imaging for PV cell production line(b) Example of PV cells without any cracks “healthy samples”, (c) Example of PV cells with cracks “cracked samples” [102].

The CNN system for PV module defect detection relies on a series of specialised layers to examine EL images, which then determine the cell acceptance or rejection status. Fundamentally, the convolutional layer operates with learnable filters that are smaller than the input image to analyse the EL image and generate activation maps, which detect defect related features. The following layer applies batch normalisation to standardize feature maps, a process that helps prevent overfitting and speeds up training while improving feature extraction accuracy through adjustments to the mean and standard deviation. The Rectified Linear Unit (ReLU) activation function replaces all negative values with zeros, thereby speeding up training while maintaining a linear relationship for positive inputs that exceed a certain threshold.

In the fourth layer, pooling layers reduce spatial dimensions while preserving critical information; max pooling extracts the highest value from a kernel's region, while mean pooling averages values, with the choice determined by training to optimize accuracy. Each layer is connected via linear transformations, ensuring that every input influences each output via weight matrices. SoftMax predicts probability distributions, while the final classification layer categorizes PV cells based on defects, like cracks, to either ""“accept”"" for production or "reject" for recycling. This layered architecture makes it possible to identify defects in PV manufacturing accurately and efficiently.

3.2.1 Developed CNN *Architectures*

Developing a CNN architecture for the detection of cracks in PV modules began with the construction of a training network from scratch, which incorporates multiple stages to process EL images effectively. In the initial architecture, Net1 and Net2, EL images of 227x227x3 pixels

are resized as input, followed by two convolutional layers with 32 filters each to extract defect information. To stabilise training, batch normalization is used and ReLU activation is applied to improve learning speed by nullifying negative values. Pooling layers reduce spatial dimensions while retaining critical information, as shown in Figures 15(a) and Figure 15(b), with mean pooling in Net1 and max pooling in Net2. A final layer of the architecture is connected to the output layers for classifying cells as accepted or rejected. A learning rate of 0.0001 was used in the initial experiments, along with a minibatch size of 16 and a training period of 20 epochs, with key parameters summarised in Table 5.

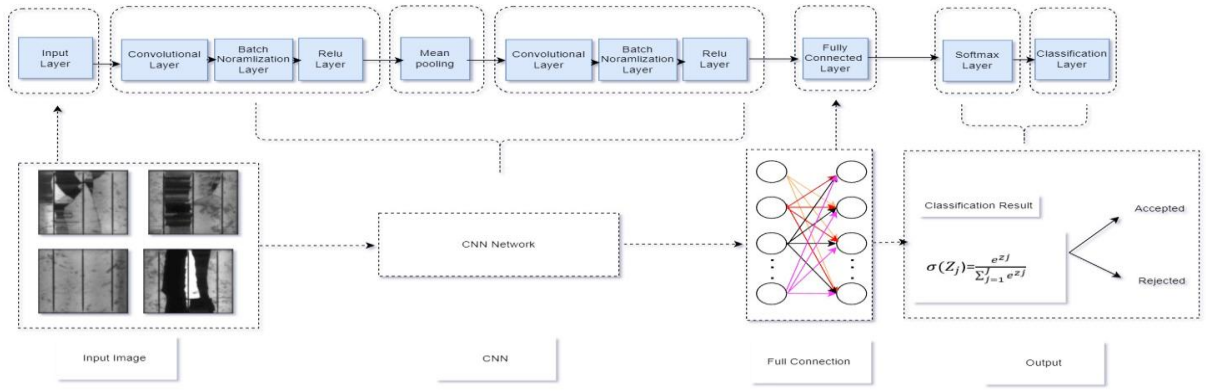

(a)

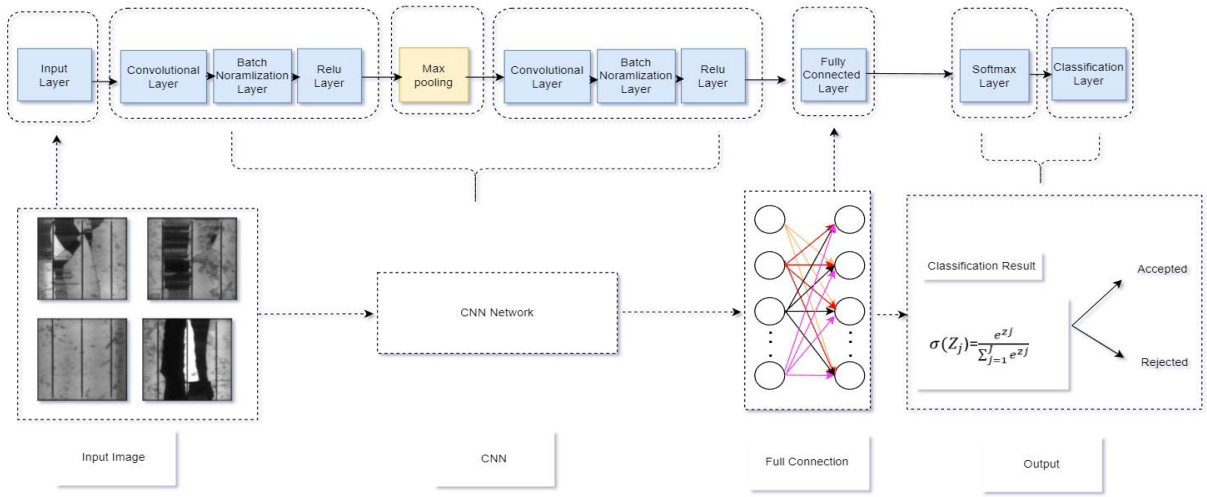

(b)

Figure 15. Developed CNN architectures comprising: (a) two convolutional layers followed by mean pooling, referred to as Net1; and (b) two convolutional layers followed by max pooling, referred to as Net2) [102].

In order to improve validation accuracy with EL images, CNN training networks for PV defect detection were iteratively refined the initial architecture, Net1, employing mean pooling, achieved 81.5% validation accuracy, but fell short of the desired performance. By switching to maximum pooling in Net2, the accuracy improved to 87.5%, a significant improvement; however, further optimisation is still required. As part of an effort to enhance performance, the number of convolutional layers was increased from two to three, and a combination of maximum and average pooling was implemented, as shown in the Figure 16(a), while maintaining the same learning rate of 0.0001 and the same number of epochs as before. As a result of this adjustment, referred to as Net3, 93.75% of validation accuracy was achieved. As a result of this improvement, Net4's pooling strategy was further refined by adopting double max pooling, as shown in Figure 16 (b), while keeping the three convolutional layers. The final configuration achieved 96.97% validation accuracy, demonstrating that Net4, with its optimized max-max pooling approach, is the most efficient architecture.

A sensitivity analysis was conducted to evaluate the influence of the training–validation data split ratio and the number of training epochs on the classification performance of the developed convolutional neural network. Several data partitioning strategies ranging from 50:50 to 80:20 were systematically investigated in combination with training durations between 5 and 30 epochs.

The results indicate that increasing the proportion of training data generally led to improved classification accuracy, highlighting the importance of sufficient feature learning during the optimisation process. In particular, the 70:30 data split ratio demonstrated the most favourable performance, achieving the highest validation accuracy of approximately 96.97%

at 20 training epochs. This finding suggests that the selected ratio provides an effective balance between model learning capacity and validation reliability.

Furthermore, the analysis shows that classification performance improved progressively with increasing training epochs until reaching a convergence region around 20 epochs, after which marginal fluctuations and slight reductions in accuracy were observed. This behaviour is consistent with typical deep learning training dynamics, where extended training may result in diminishing performance gains or potential overfitting effects.

Based on these observations, the final training configuration adopted in this research utilised a 70:30 data split ratio and 20 training epochs, ensuring stable convergence behaviour, high classification accuracy, and improved generalisation capability for photovoltaic defect detection tasks.

Parameter	**Value**	**Parameter**	**Value**
Image Input Size	227x227x3 Pixels	Initial Learn Rate	0.0001
Convolutional Layers	32 Filters	Epochs	20
Filter Size	3,3	Mini Batch Size	16
Learn Rate Drop Factor	0.1	Validation Frequency	16
Random Rotation (Degree)	-90, 90	Solver	SGDM

Table 5. Summary of CNN input parameters for Net4[102].

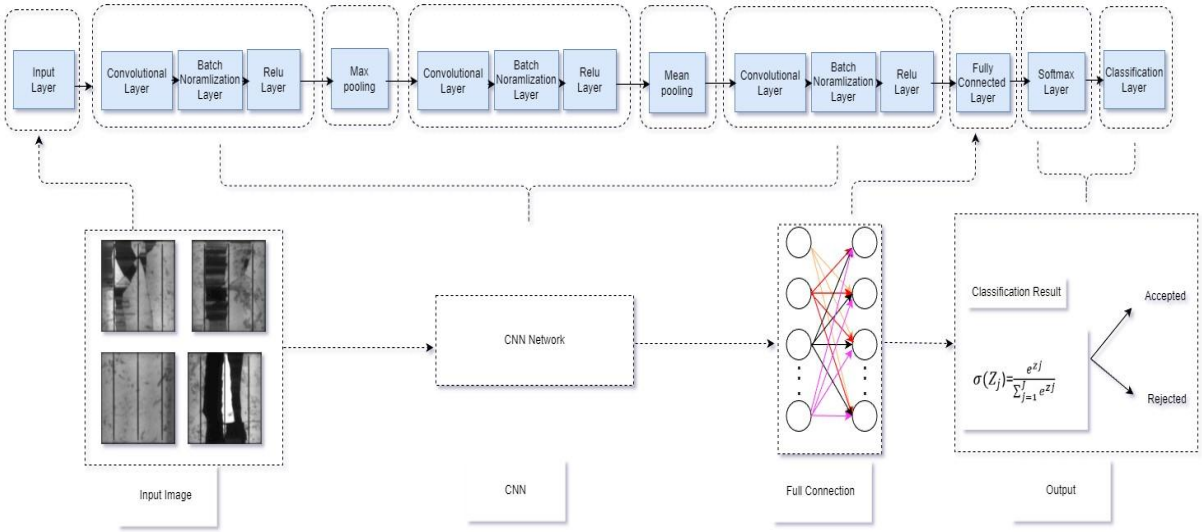

(a)

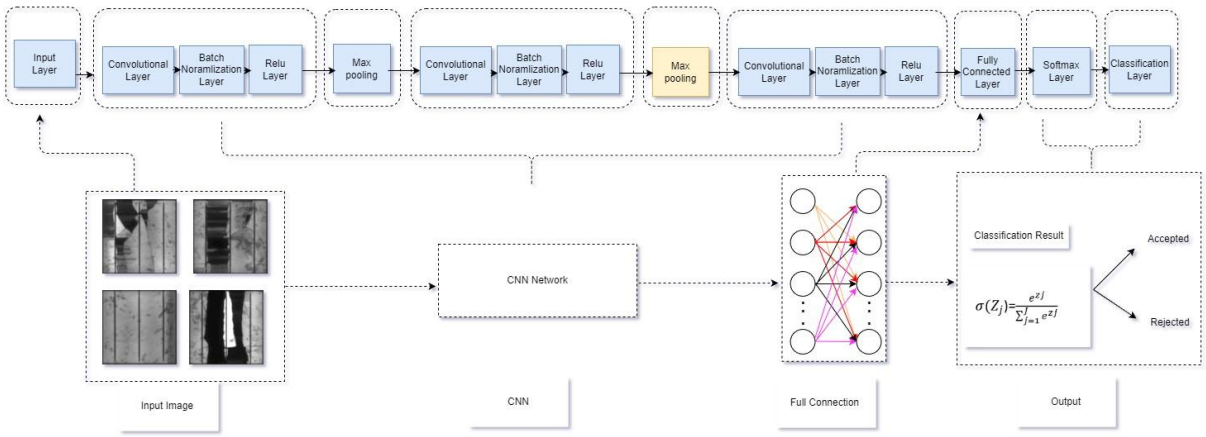

(b)

Figure 16. Enhanced CNN architectures consisting of: (a) three convolutional layers with max–mean pooling, referred to as Net3; and (b) three convolutional layers with max–max pooling, referred to as Net4) [102].

3.2.2 Flow Chart of the Decision-Making Process

According to Figure 17, the inspection flowchart of PV cells begins with the capture of an EL image of the cells just after they are taken off the manufacturing line. The EL imaging process evaluates cell quality by applying an electrical current, which emits light that reveals structural

defects in the cells. The CNN system analyses the acquired EL images to identify patterns that show cracks or defects. The system utilises the CNN network to evaluate cells for PV panel assembly acceptance when no defects are present, However, it recycles them when cracks appear.

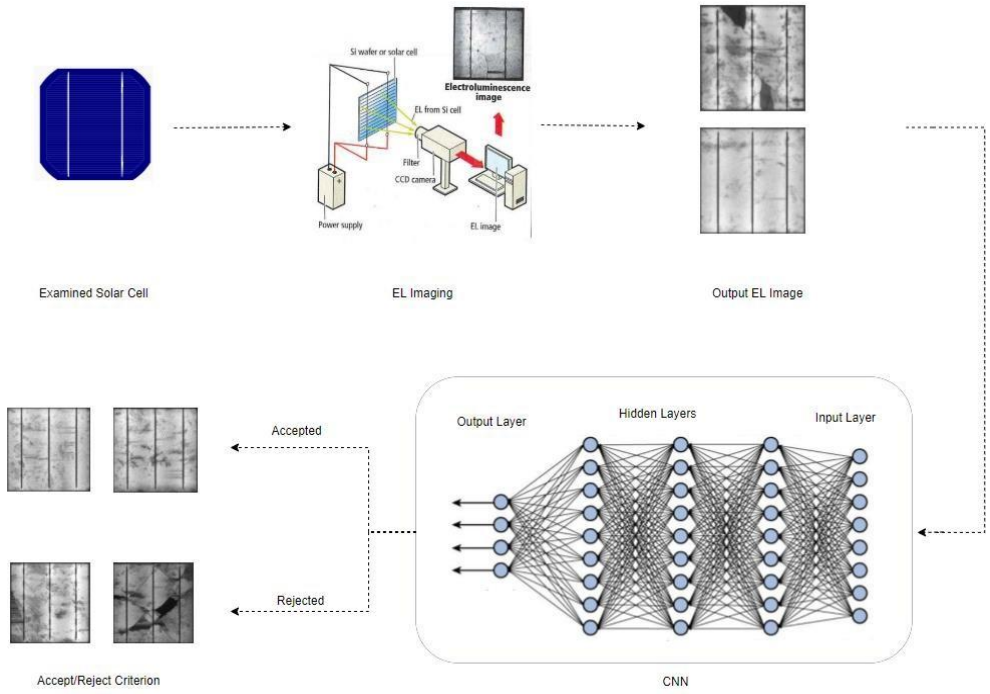

Figure 17. Integration of the CNN model into a decision-making framework for identifying PV cell cracks within an industrial application setting [102].

3.2.3 Validation Accuracy of the Developed CNN *Architectures*

The development of a CNN architecture for PV cell inspection required extensive work to determine the optimal combination of learning rate and number of epochs, as well as validation accuracy, for detecting defects in EL images[103], [104]. Initially, a learning rate of 0.01 and 10 epochs for the Net1 architecture yielded a low validation accuracy of 56%, as shown in Figure 18 (a). The model would reach suboptimal solutions when using high learning

rates, but training would stop when using low learning rates. The learning rate adjustment to 0.01 combined with 20 epochs of training resulted in Net1 achieving 81.5% accuracy.

Several successive time periods produced no progress, so the focus switched to architectural development by replacing mean pooling with max pooling in Net2 raised accuracy to 87.5%, as illustrated in Figure 18 (b). The addition of the third convolutional layer led to the testing of max-mean pooling in Net3, which achieved 93.75% accuracy, and max-max pooling in Net4, which reached 96.97% accuracy, as demonstrated in Figures 18 (c) and 18 (d). Through these improvements, CNN achieved better results by using 20 epochs and a learning rate of 0.0001.

In addition to classification accuracy evaluation, the computational efficiency of the proposed CNN architecture was assessed. The average model training time was approximately 3 hours under the specified hardware and software configuration, while the average testing (inference) time per sample was approximately 0.125 seconds. These results indicate that the developed deep learning framework demonstrates favourable computational performance and is suitable for practical photovoltaic inspection applications where rapid defect identification is required.

Although slightly higher validation accuracy values were observed at intermediate training iterations, the final reported performance corresponds to the convergence stage of the learning process rather than isolated peak values. Selecting intermediate peaks may lead to optimistic performance estimation due to stochastic fluctuations associated with mini-batch gradient updates. Furthermore, extending training beyond the convergence region increases the risk of overfitting, where the model becomes excessively specialised to the training dataset and exhibits reduced generalisation capability. Therefore, a consistent training duration was

maintained across all architectures to ensure fair comparative evaluation and to reflect stable model behaviour rather than transient accuracy variations.

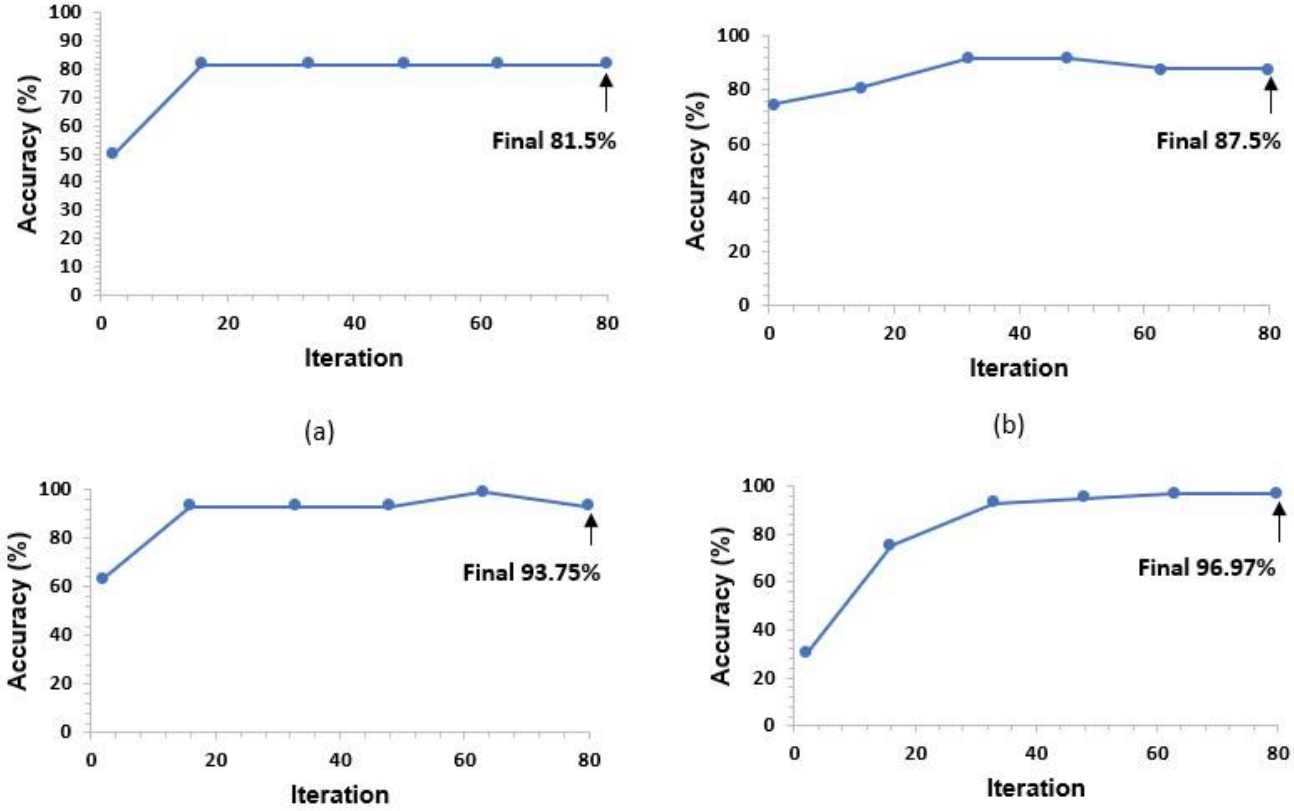

Figure 18. Validation accuracy results of the CNN architectures. (a) Net1, (b) Net2, (c) Net3, (d) Net4 [102].

3.2.4 Loss Function of Net 4

The CNN model requires an appropriate loss function to detect PV defects as it measures output predictions against actual ground truth EL images data to adjust parameters for better performance. A CNN can achieve higher prediction results and improved overall performance by adjusting training parameters that reduce the loss function. The optimal loss graph shows training loss in red and validation loss in blue as both lines converge toward zero indicating a reduction in prediction errors. The Net4 architecture in Figure 19 shows initial training loss values above zero, but through progressive training iterations, both training and validation

losses were reduced to nearly zero. As a result of the Net4 CNN achieving minimal error rates, there is a high degree of accuracy in detecting PV manufacturing defects, including cracks, which is indicative of a high learning rate.

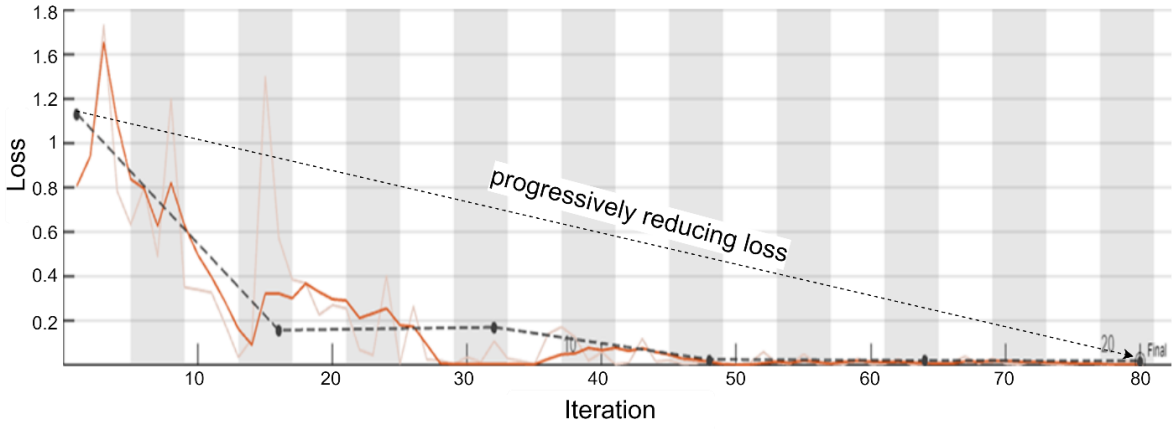

Figure 19. Training loss curve of the Net4 CNN architecture plotted against learning iterations (epochs) [102].

3.2.5 Confusion Matrix of Net 4

The performance of the Net4 CNN model for PV defect detection was evaluated using a confusion matrix, which summarises the accuracy of classifying EL images, as presented in Table 6. Applied to a dataset of 150 images, equally split between 75 healthy and 75 cracked PV cells, the model achieved an accuracy of 93.3%, correctly classifying 93.3% of all samples. The model achieved high accuracy since it successfully identified defective cells from non-defective ones. The precision value of 92.2% shows that the model correctly identified 92.2% of the samples that were cracked cells. The standard formulas used to calculate these metrics demonstrate the Net4 model's success in PV manufacturing quality control based on the accuracy of the reported confusion matrix value.

		Actual No Cracks	Actual Cracks
Predicted Value	Predicted No Cracks	71	4
	Predicted Cracks	6	69

Table 6. Confusion matrix of the developed CNN model "Net4" [102].

$$Accuracy = \frac{TP+TN}{TP+TN+FP+FN} = \frac{71+69}{71+69+6+4} = 93.3\% \quad [1]$$

$$Precision = \frac{TP}{TP+FP} = \frac{71}{71+6} = 92.2\% \quad [2]$$

To systematically evaluate the contribution of key architectural design choices to the overall performance of the proposed CNN framework, an ablation-style experimental analysis was conducted. The study investigated the influence of convolutional depth, pooling strategy, and training configuration on defect classification accuracy using electroluminescence image datasets. Table 7 summarises the comparative performance of the investigated architectures.

The results demonstrate that increasing convolutional depth enhanced the network's capability to extract discriminative spatial features associated with photovoltaic cell defects, leading to progressive improvements in classification performance. In particular, the transition from mean pooling to max pooling mechanisms improved feature preservation and robustness against noise present in electroluminescence imagery. Furthermore, maintaining a consistent training epoch configuration ensured stable convergence behaviour while minimising the risk of overfitting.

Architecture	Convolutional Layers	Pooling Strategy	Training Epochs	Validation Accuracy (%)
Net-1	2	Mean pooling	20	81.50
Net-2	2	Max pooling	20	87.50
Net-3	3	Hybrid pooling	20	93.75
Net-4 (Proposed)	3	Dual max pooling	20	96.97

Table 7. summary of CNN ablation analysis illustrating the impact of architectural refinements on validation accuracy.

.

Comparative evaluation confirms that the proposed Net-4 architecture achieves the most favourable balance between classification accuracy, computational efficiency, and generalisation capability. This ablation analysis therefore provides empirical justification for the selection of the final optimised CNN structure adopted in this research and highlights the importance of systematic architectural refinement in improving photovoltaic defect detection reliability.

3.3 Results and Discussions

3.3.1 Healthy Case

The CNN model for PV defect detection was rigorously tested by analysing EL images of various PV cells to determine their acceptance or rejection status. In the first test case (Case 1), a relatively healthy PV cell with minor black spots, often due to EL camera resolution or calibration, as shown in Figure 20 (a), was evaluated. To ensure consistent analysis, EL images were pre-processed to a uniform resolution range of 1000x1000 to 2500x2500 pixels.

The CNN system predicted that the cell would be accepted at a 98.2% rate while rejecting it at a 1.8% rate, through its analysis of cell dimensions, black spots and distribution against established database parameters. In the second test cell (case 2), the image quality of the EL image was improved and there were fewer black spots, as shown in Figure 20 (b), leading to a 99.5% acceptance rating and a 0.5% rejection rate, showing that the cell is ready for production

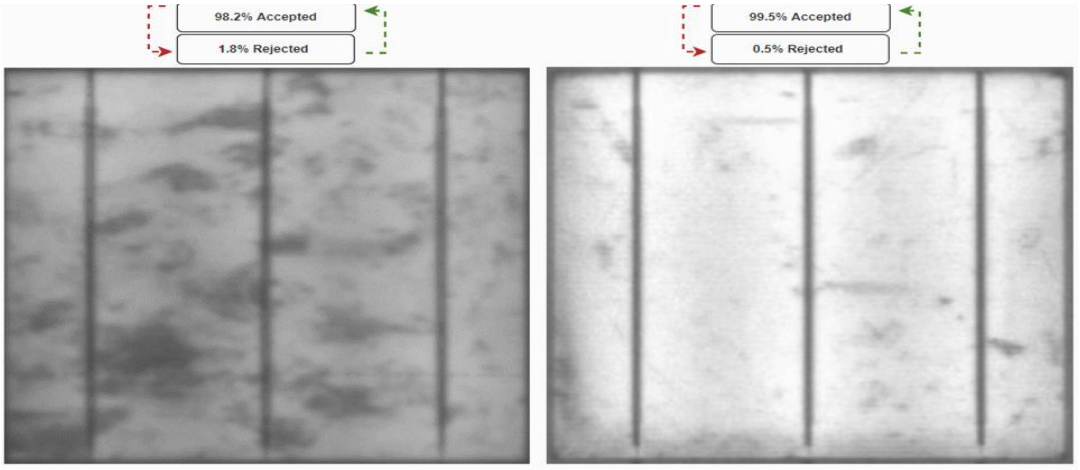

(a) (b)

Figure 20. Analysis of healthy PV cells based on their acceptance and rejection percentage criteria (a) Case 1, (b) Case 2[102].

3.3.2 Cracked Case

The CNN model for PV defect detection was tested on PV cells with significant cracks to evaluate its predictive accuracy using EL images. In Case 3, shown in Figure 21 (a), a PV cell with prominent cracks was analysed, resulting in a 99.1% rejection rate and a 0.9% acceptance rate, accurately reflecting the cell's visible damage. The model's reliability was further tested through Case 4, which examined a cell with minimal cracks as shown in Figure 21(b), and achieved a 98.4% rejection rate which was appropriate prediction for the less severe defect condition. Analysis of these four cases demonstrates the CNN's ability to deliver precise predictions for PV cell quality, though certain complex cases may pose challenges, which are explored in subsequent sections.

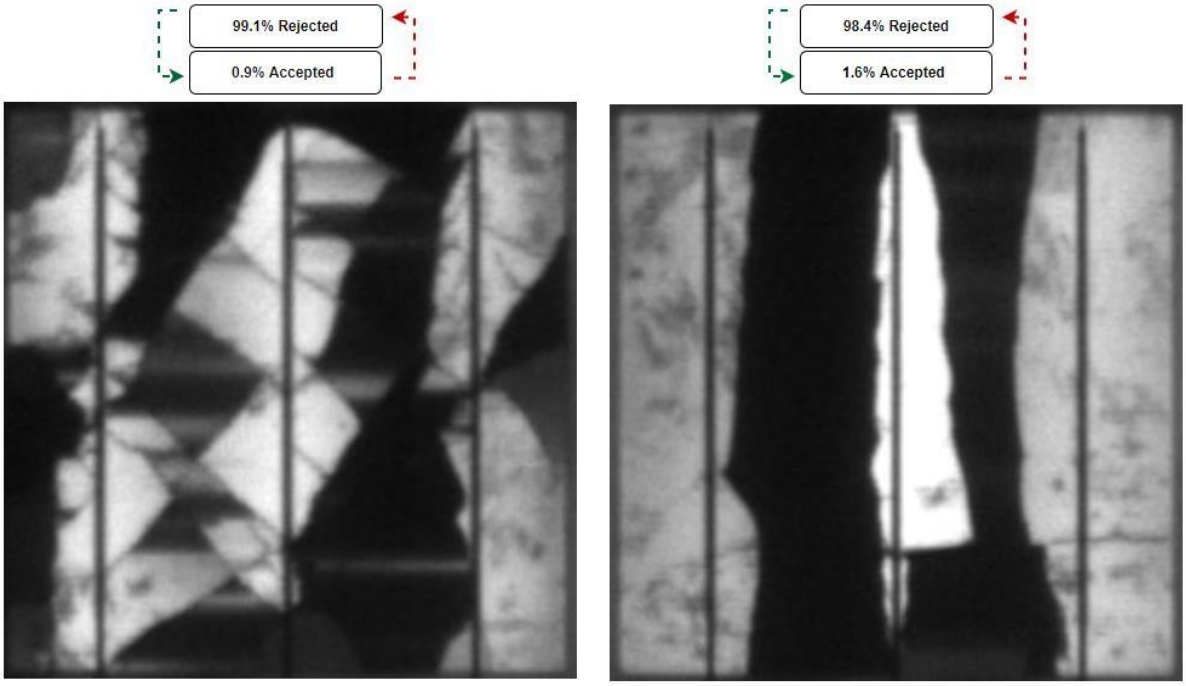

(a) (b)

Figure 21. Examined cracked PV cells with an acceptance/rejection percentage. (a) Case 3, (b) Case 4 [102].

3.3.3 PID Case

A significant challenge in PV cell inspection is accurately predicting PID, a major cause of module degradation driven by high voltage between encapsulants and grounded surfaces. To evaluate the CNN model's capability, EL images of PV cells were tested before and after PID exposure, achieved by applying -1000V for 96 hours. In Case 5, shown in Figure 22 (a), cells before PID achieved a 99.2% acceptance rate, while post-PID cells, exhibiting degradation, were rejected at 98.2%, as depicted in Figure 22 (b). Further validation in Case 6, with more pronounced dimming post-PID, as shown in Figures 23 (a) and 23 (b), resulted in a 99.4% acceptance rate for pre-PID cells and a 99.4% rejection rate for post-PID cells. These precise predictions highlight the CNN's ability to distinguish between healthy and PID-affected cells with high accuracy.

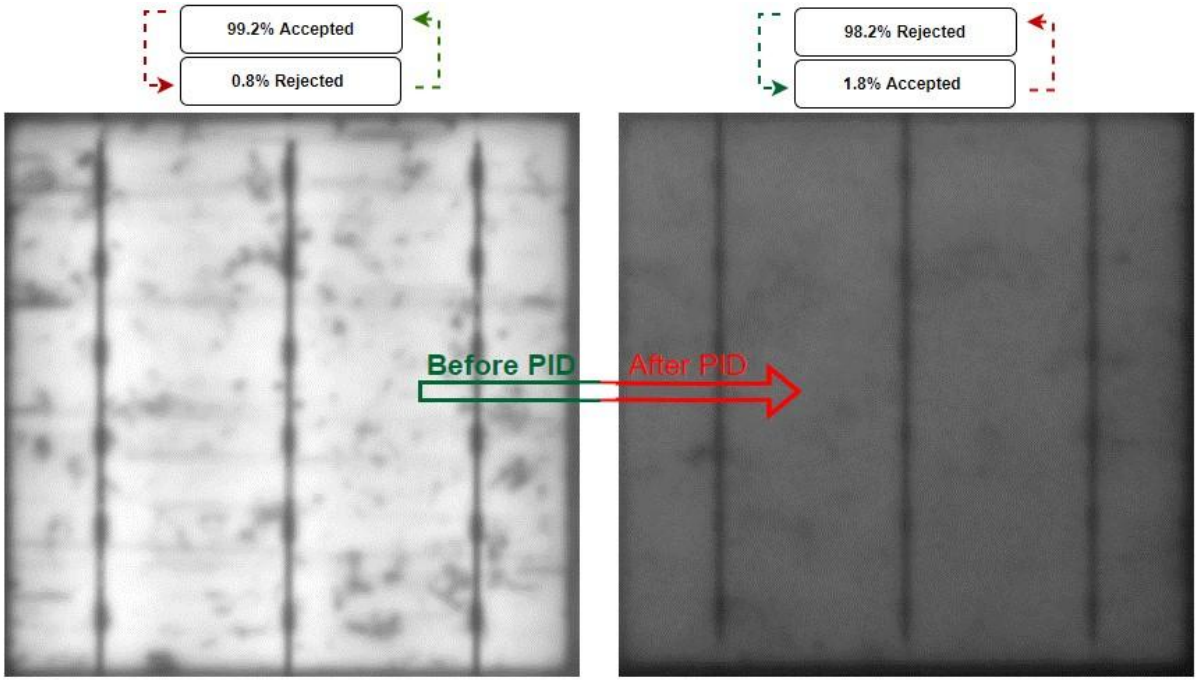

(a) (b)

Figure 22. Examined of PV cells affected by PID (case 5). (a) Before PID, (b) After PID [102].

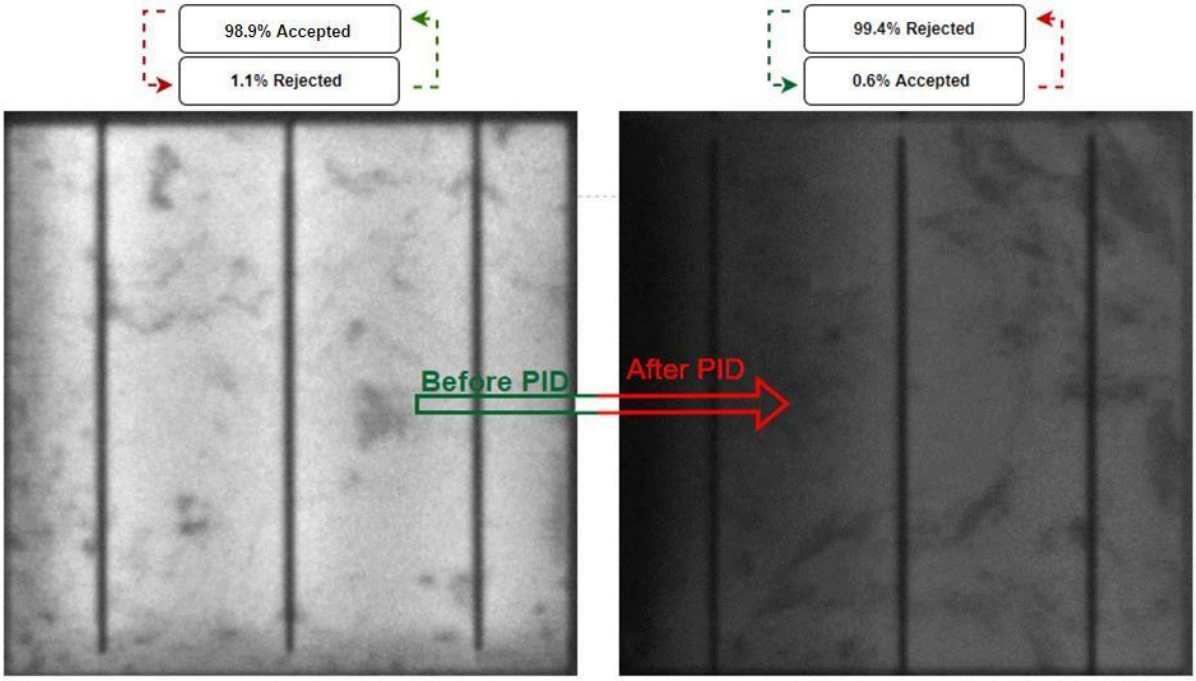

(a) (b)

Figure 23. Examined of PV cells affected by PID (case 6). (a) Before PID, (b) After PID [102].

3.3.4 Shaded area Case

The CNN model developed for PV defect detection underwent rigorous testing to assess its ability to identify shaded areas in silicon-based PV cells, a common defect caused by shunting during the manufacturing process, which manifests as localised dark regions on the cell surface, as highlighted in red dashed circles in Figure 24(a). The process of shunting creates uneven current distribution across busbars which produces stress in the cell structure and elevated temperatures that make it difficult to identify shaded areas from actual cracks. PV manufacturing requires identification of these areas because inaccurate cell identification results in panel defects that reduce both performance and lifespan.

In order to address this issue, two cases composed of PV cells that have shaded areas have been tested, referred to as Cases 7 and 8. The CNN achieved 98.5% rejection accuracy in Case 7 and 98.9% in Case 8 according to Figures 24(a) and 24(b) due to its ability to detect shaded areas as defects. The model achieves high rejection rates which demonstrate its ability to detect PV cells with shaded area.

As part of the standard testing process, the predictions were also formally verified by using a PV simulator of 1000 W/m2 and maintaining a cell temperature of 25°C. According to the results shown in Figures 25(a) and 25(b), the thermal imaging results showed that Case 7 reached 77.6°C and Case 8 reached 57.8°C, respectively. The elevated temperatures proved the existence of shunting defects which caused power loss in both cases as the CNN had previously predicted. The combination of thermal validation with CNN output evaluation leads to better reliability since it provides complete cell condition assessment that extends beyond EL visual inspection.

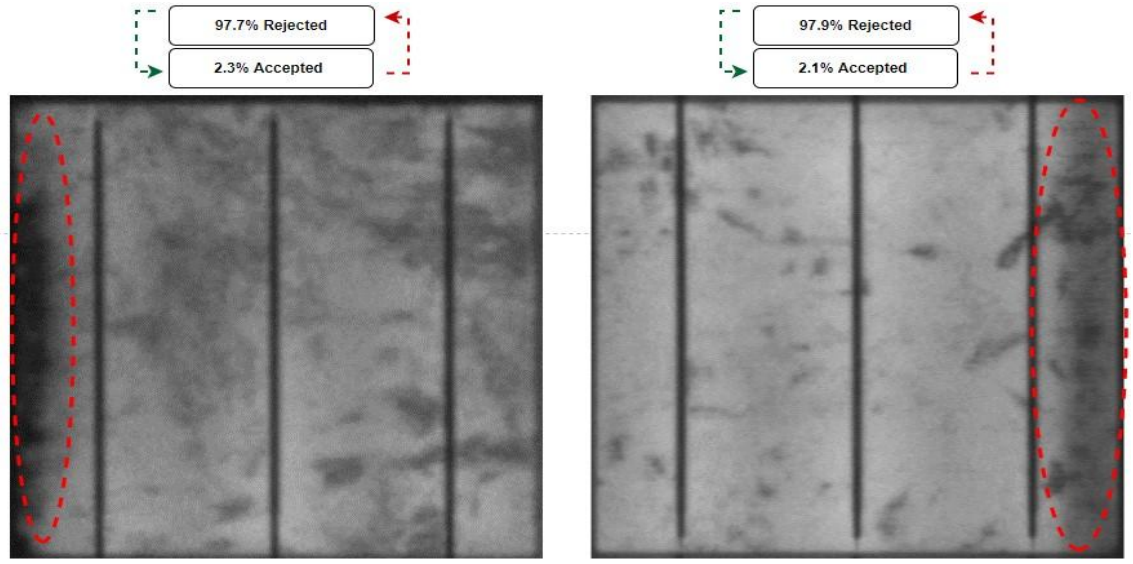

(a) *(b)*

Figure 24. Examined PV cells with shaded area. (a) Case 7, (b) Case 8 [102].

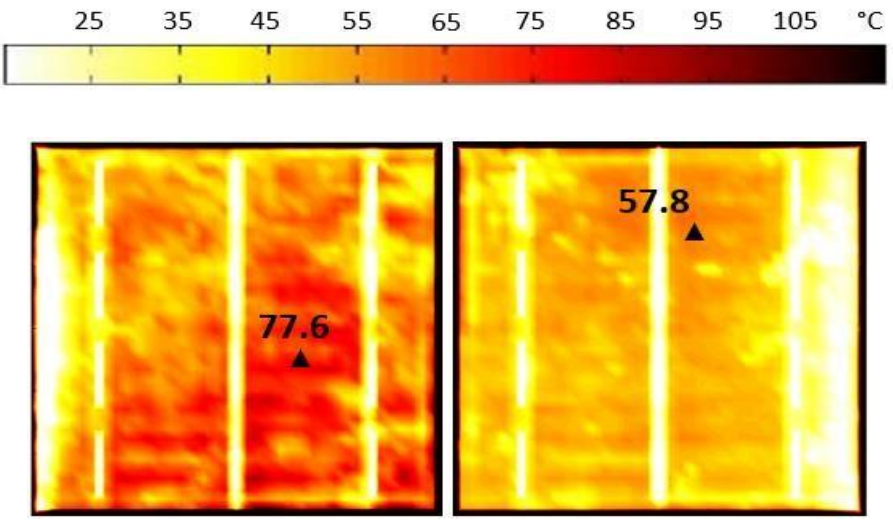

(a) *(b)*

Figure 25. Thermal images of the examined PV cells showing shaded regions under standard test conditions (STC). (a) Case 7, (b) Case 8 [102].

3.3.5 Minicrack Case

PV cell condition assessment requires careful consideration of minicracks, which, unlike major cracks, cause minimal power loss and are often classified as acceptable, as highlighted in the red dashed circles in Figure 26. These small defects are present during PV manufacturing, which require exact detection methods to identify defective cells for proper rejection purposes.

The CNN model was tested on two PV cells with minicracks, Case 9 and Case 10, as shown in Figures 26 (a) and 26(b), respectively. The system correctly classified both samples as healthy since it achieved 99.5% acceptance for Case 9 and 99.9% acceptance for Case 10, which demonstrates its ability to detect minicracks like performance-damaged severe defects. The CNN demonstrated high accuracy which confirms its ability to enforce strict quality standards without discarding valuable cells.

The prediction needed verification through thermal testing which followed (STC) using a PV simulator at 1000 W/m² irradiance and 25°C cell temperature corresponding to shaded area testing protocols. The thermal imaging results in Figures 27(a) and 27(b), showed that both cells had uniform heat distribution and maintained their standard 25°C surface temperature without any hot spots. The absence of elevated temperatures in this test proves that minicracks do not create thermal issues or power loss problems which matches the CNN predictions and demonstrates its value for PV manufacturing quality control.

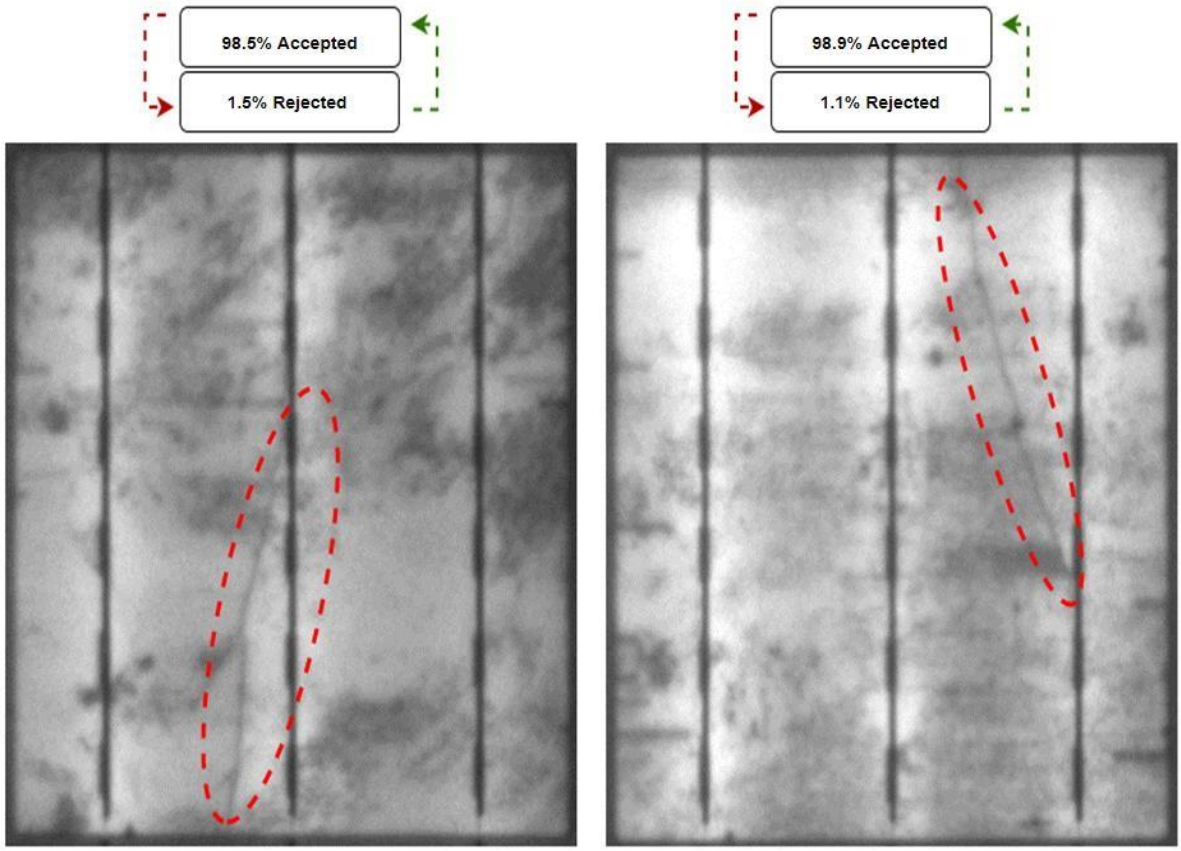

(a) *(b)*

Figure 26. Examined PV cells with no major cracking. (a) Case 9, (b) Case 10 [102].

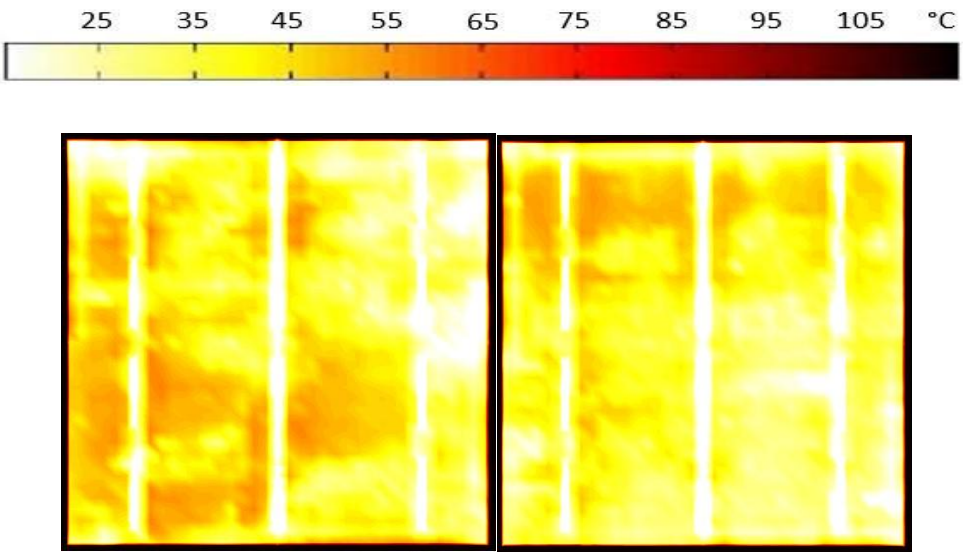

(a) *(b)*

Figure 27. Thermal image of the examined PV cell with minicracks under STC Condition. (a) Case 9, (b) Case 10[102].

3.4 Comparative Analysis.

The effectiveness of the proposed CNN method for PV defect detection was rigorously evaluated by comparing its performance with several established CNN-based crack detection methods widely adopted in the industry, as summarised in Table 8.

Many recent approaches in the field depend on transfer learning methods which apply pretrained networks such as AlexNet, VGG-16, VGG-19, Inception-v3, Inception ResNet50-v2 and ResNet50-v2, with minor modifications to specific datasets. The methods provide success in detecting PV cell cracks through EL images but fail to identify essential defects such as PID and shaded areas. These methods lack validation through thermal testing since thermal testing serves as a critical method to verify how defects affect cell performance.

All these studies failed to discuss methods for PID detection and shaded area identification and thermal testing validation, which limits their approach to complete PV quality control assessments. Moreover, these studies introduced two novel CNN models capable of detecting pre-trained network cracks, but fail to detect PID and shaded areas, which require extensive training datasets and lack thermal imaging verification.

In contrast, the proposed method developed four CNN architectures from scratch through systematic design optimization to achieve better accuracy and reliability results. The architectures reached their peak with the Net4 model that achieved 96.97% validation accuracy for detecting cracks and minicracks, PID and shaded areas through thermal testing on PV assembly units. This comprehensive approach allows for exact PV cell classification, which leads to better manufacturing operations through improved quality control since it detects various defects more accurately than current methods.

Ref.	**Year of Study**	**PV cell cracks detection description**	**Validation**		
			PV cell Cracks	**PID**	**Thermal Test**
[105]	2020	Pre-trained AlexNet-based CNN model: a transfer learning approach for crack detection utilising the pre-trained AlexNet architecture.	✔	x	x

[106]	2021	BAFPN-CNN is designed to achieve multiscale feature fusion through a bidirectional attention feature pyramid network (BAFPN), enabling all pyramid layers to share consistent semantic representations.	✔	x	x
[107]	2021	In this study, pretrained models including VGG-16, VGG-19, Inception-v3, InceptionResNet50-v2, ResNet50-v2, and Xception were individually evaluated prior to their integration through an ensemble learning approach. The ensemble method enhances overall accuracy while minimizing the risk associated with dependence on a single model.	✔	x	x
[108]	2022	PSO Pruner-CNN addresses the pruning challenge of deep convolutional neural networks (DCNNs) by formulating it as a search problem solved using the particle swarm optimization (PSO) algorithm. To enhance the effectiveness of the pruning strategy,	✔	x	x
		the PSO-based automated search process is executed iteratively across multiple rounds.			

[109]	2022	Modified pre-trained AlexNet: the original AlexNet architecture is adapted to extract more detailed feature maps through a novel and efficient multiscale CNN design. Given that low-level convolutions employ small-sized filters, two additional convolutional branches are introduced, each connected in series with 3 × 3 convolutional layers.	✔	x	x
This work	2023	DSMP-CNN: Dual Spin Max-Pooling CNN designed for PV cell crack detection. The development of this architecture enabled the evaluation of multiple network configurations to enhance validation accuracy. By transitioning from mean pooling to max pooling and increasing the number of convolutional layers, the model achieved superior feature extraction and improved overall performance. convolutional layers, and changing the pooling method led to significant improvements in validation accuracy.	✔	✔	✔

Table 8. Comparison of the proposed DSMP-CNN model with several recently developed algorithms for PV cell crack detection. [105], [106], [107], [108], [109].

3.5 Limitations and Future Work.

The proposed CNN method for PV defect detection offers various advantages, but it needs a detailed assessment of its operational limitations. The analysis faces a major limitation

because it depends on a particular dataset which does not represent diverse PV cells such as cells with different busbar configurations and manufacturing defects. The results from this limited dataset may not be applicable to all production environments because it only includes a limited set of cell configurations which are not representative of the full range of configurations found in practical settings. Another critical limitation arises from the reliance on EL images captured in controlled indoor settings and within a PV production facility.

It is important to note that while the specific conditions align with the purpose, these conditions do not duplicate the wide range of situations that can happen outdoors due to the lighting conditions, camera capabilities, and imaging systems that are present in outdoor environments. The system requires standardized indoor imaging which creates doubts about its ability to work with different external environments and EL equipment that requires additional testing to prove its adaptability.

To solve these problems, several approaches will be recommended while creating base structures for future system development. The evaluation's representativeness and model generalisability improve when the dataset includes multiple PV cell types and different busbar designs and manufacturing approaches. Additionally, the system needs testing with EL images from different environmental conditions and multiple detection tools to prove its operational stability in various scenarios.

The CNN's performance and reliability would gain more evidence through comparative studies that evaluate its performances against various crack detection systems operating on different datasets. Partnering with industry collaborators or research organizations to access a broad range of PV samples and imaging conditions would enhance the relevance of the findings to real-world applications. The system's operational reliability can be verified through sensitivity

analysis tests that implement controlled adjustments to lighting conditions and camera settings. By tackling these issues, future research can significantly expand the CNN's applicability and trustworthiness for detecting defects in a wide range of PV cells and imaging environments.

- **Limited Dataset Diversity:** The evaluation depends on a particular dataset which might not capture the complete range of busbar configurations and manufacturing techniques
- **Indoor Imaging Constraints:** The system depends on controlled EL images taken indoors which restricts its ability to function properly when used outdoors or with different imaging devices.
- **Generalisability Concerns:** The system lacks evidence to prove its effectiveness for different PV cell types and real-world applications which limits its potential use.

The experimental results obtained at the solar cell level demonstrate that the proposed CNN architecture provides improved defect classification accuracy and robust feature extraction capability. However, practical photovoltaic inspection scenarios often require defect detection at the module scale, where spatial variability and defect propagation patterns introduce additional complexity. To address this limitation, the following chapter extends the developed methodology to module-level analysis, incorporating advanced image segmentation and decision-making strategies to evaluate model scalability and real-world applicability.

4. Crack Detection for Module Level

4.1 Introduction

Extending the cell-level defect detection framework presented in Chapter 3, this chapter investigates the application of convolutional neural network methodologies for photovoltaic defect identification at the module level. The focus shifts from individual cell analysis to the assessment of defect propagation and spatial variability across complete PV modules. The proposed approach integrates image segmentation techniques and refined CNN architectures to enable reliable classification under diverse electroluminescence imaging conditions. This chapter further evaluates the robustness of the developed models through validation accuracy analysis, confusion matrix assessment, and comparative performance evaluation. The findings contribute to understanding the scalability of deep learning-based inspection systems for practical PV quality assurance applications.

4.2 Materials and Methods

4.2.1 EL Imaging

As discussed in Chapter 3, EL imaging is a non-destructive technique that enables the detection of PV cell defects not visible to the naked eye. Building on this principle, the present study employed a Brightspot automation imager to capture EL images [111]. The system was equipped with a 6k × 4k resolution digital camera and an 18–55 mm focal length lens, which allowed for the acquisition of high-resolution images with enhanced clarity and contrast. The PV module was connected to a power supply to generate the required forward

bias current during imaging. An example of the captured EL image is presented in **Figure28 (a)**, while the main components of the Brightspot EL imaging setup are shown in**28(b).**

(a)

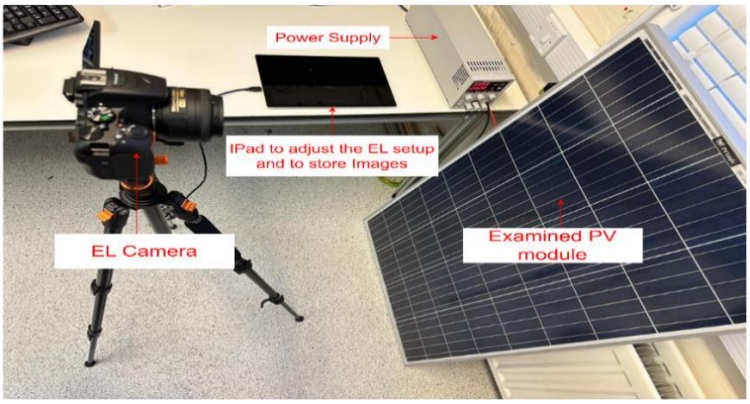

(b)

Figure 28. (a) EL imaging setup, (b) EL imaging components [*110].*

4.2.2 Image Segmentation

As part of computer vision, segmentation of images refers to assigning labels to different regions within images according to the content they represent.[112] The semantic

segmentation process extends this process by assigning a class label to every pixel in the image, which means that the system can be able to predict what each pixel is classified into [113], [114]. This task is accomplished by applying supervised or unsupervised learning approaches that extract distinctive features from the image and then classify every pixel based on those features. For example, such algorithms can identify specific objects in an image and subsequently assign the pixels to the category of the object to which they belong.

The act of labelling an image at the pixel level can be mathematically represented as a set of random variables $\{x0, \dots, xn\}$, where n corresponds to the total pixel count of the image. Each variable xi ∈ L is mapped to one of m possible discrete labels contained in the set L = {1, …, m}. A CNN then defines a probability distribution $Q(X \mid \theta, I)$ across the random variables X, where θ denotes the learnable network parameters. Typically, this distribution is expressed as a product of independent marginals, written $as\ Q(X \mid \theta, I) = \prod i\ qi(xi \mid \theta, I)$ (R). Each marginal represents a SoftMax probability. The term $qi(xi \mid \theta, I)$ is parameterised by a subset of weights θi, which are iteratively learned by the CNN during training [115]. The optimisation of θ is achieved by minimising a loss function that measures the deviation between predicted pixel labels and the ground-truth labels. This relationship is formally expressed in equation (1) [115].

$$q_i(x_i|\theta, I) = z\_^{1}{}_i \exp f_i(x_i; \theta, I) \quad (3)$$

Where $zi = \sum l \in L\ exp(fi(xi;\ \theta, I))$ represents the partition function of pixel i. The function fi represents the numerical score of the neural network.

In this work, the Images of the photovoltaic modules were divided into individual PV cell pixels, and each pixel was classified according to specific conditions, namely healthy cells, minicracks,

major breakdowns, PID and shaded regions, as shown in Figure 29(a). The first category corresponds to healthy pixels, denoted by label 1, which represent all PV cell regions without any form of defect. The second category, labelled as 2, includes pixels that display minicracks within the cells.

The third category consists of pixels showing severe cracks or complete breakdowns, which can significantly diminish the electrical output of the module, and these are marked with label 3 [116]. The fourth category is associated with PID, labelled as 4. PID is one of the primary mechanisms responsible for module deterioration and arises due to high voltages generated between the encapsulation layer and the glass surface, which is grounded either through the module frame or its supporting structure [117].

The final category represents shaded pixels, assigned the label 5 in the colour scheme. Shading disrupts the uniform distribution of current in the busbars, creating stress on the cells and leading to localised heating, which in turn reduces power generation efficiency [118].

Following this labelling process, the pixels were analysed to calculate the proportion of each defect condition across the entire module to evaluate the overall state of the PV cells. During this analysis, small spots were observed on the images, as illustrated in **Figure 29(b)**. These marks appeared due to limitations in the camera's calibration and resolution. They are not indicators of actual defects and therefore can be disregarded when assessing the operational health of the cells.

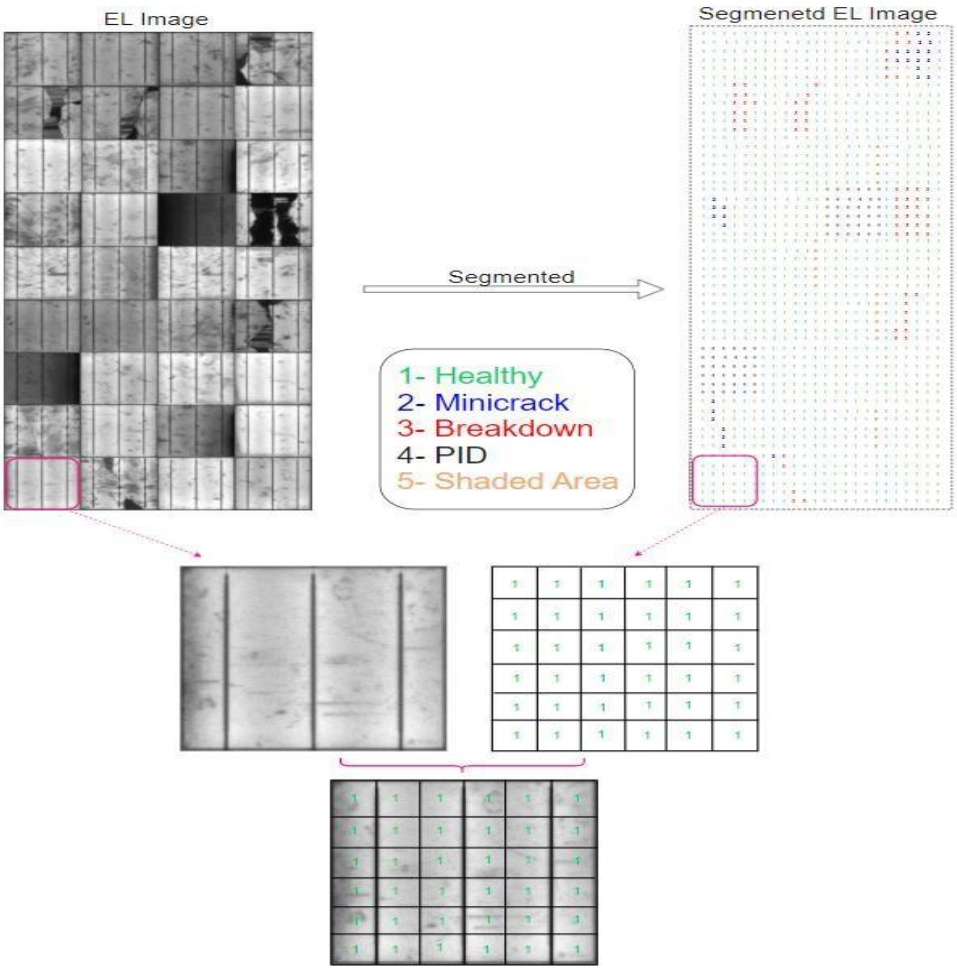

(a)

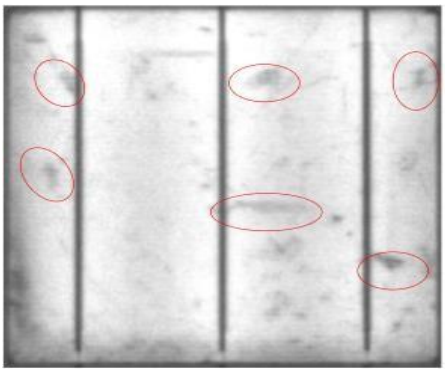

(b)

Figure 29. (a) Segmentation process applied to the PV module EL image; (b) appearance of minor blackspot defects visible in the PV cell's EL image [110].

4.2.3 CNN Architecture

The next step after completing the segmentation stage is to design a CNN architecture that can efficiently handle the training task as well as achieve a high level of validation accuracy. To accomplish this, different layers are incorporated into the CNN framework, as shown in Figure 30. The first layer is the convolutional layer, which consists of filters that are learned during the training process and are smaller in dimension than the input image, this layer is later combined with an activation map.

The subsequent layer is batch normalisation, whose primary role is to maintain consistency, prevent overfitting, and accelerate the computation of the network. The Rectified Linear Unit (ReLU) follows as the activation layer, functioning by setting all negative values to zero. Pooling is another key component, which extracts values from image regions defined by kernels.

There are two approaches to pooling: max pooling, which selects the highest value from the region, and mean pooling, which calculates the average. Since no single method works universally, the decision between the two is made during the training phase. A fully connected layer is also included in the network, where weight matrices are used to transform input vectors into outputs through linear operations, ensuring complete connections between inputs and outputs. At the output stage, the CNN employs the SoftMax function as the activation function, generating probability distributions for multi-class classification problems. The final stage of the network is the classification layer, which applies the decision rules for labelling.

As shown in the Table 7, several CNN architectures have been developed and tested from scratch, each utilizing a different combination of layers. The first architecture (Arch 1) was

constructed with two convolutional layers and mean pooling, which resulted in a validation accuracy of 81.5% after training for 20 epochs at a learning rate of 0.0001. The second architecture (Arch 2) also utilised two convolutional layers, each with 32 filters, placed between normalization and ReLU layers. However, the model employed max pooling instead of mean pooling to achieve a validation accuracy of 87.5%, which was superior to Arch 1. The third architecture (Arch 3) used three convolutional layers with 32 filters and combined max and mean pooling to achieve a validation accuracy of 93.75%. Arch 3's dual pooling strategies produced better results than all previous versions.

Throughout this process, the network designs (Arch 1–4) were repeatedly constructed and evaluated until the fourth architecture was developed, achieving a peak validation accuracy of 98.07%. A detailed representation of Arch 4 is shown in Figure 30, and its parameters are summarised in Table 10. Arch 4 was selected as the final model because it was composed of two double convolutional layers combined with double max pooling, which significantly improved the network's ability to learn complex patterns.

This architecture outperformed all other tested configurations, and further modifications did not yield better results. The reason is that the added depth provided by the double convolutional layers and double max pooling enabled more accurate feature extraction. Altering the components of this configuration reduced the network's depth and complexity, which in turn decreased its validation accuracy.

.

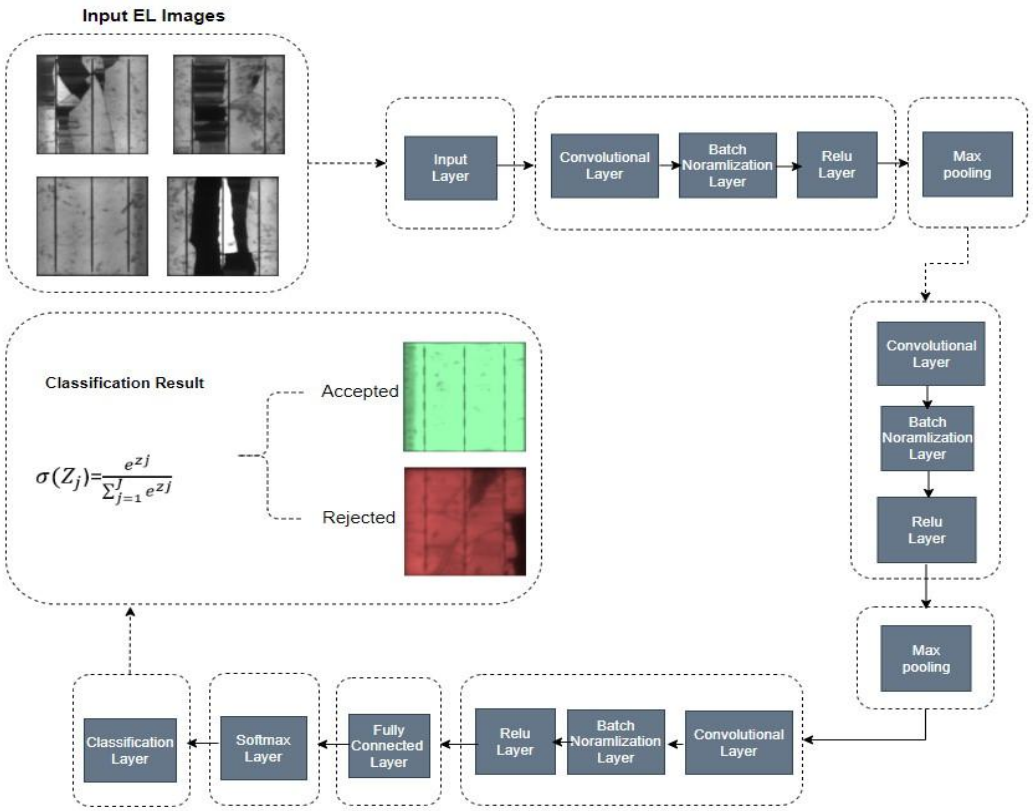

Figure 30. Architecture of the CNN model referred to as Arch 4 [110].

Architecture Name	**Description**	**Validation accuracy**
Arch 1	Comprises two convolutional layers, each with 32 filters, connected to a normalisation layer and a ReLU activation layer through mean pooling, with an initial input size of 227 × 227 × 3 pixels.	81.5%
Arch 2	Consists of two convolutional layers with 32 filters, linked to a normalization layer and a ReLU activation layer via max pooling,	87.5%

	using an initial input size of 227 × 227 × 3 pixels.	
Arch 3	With an initial input dimension of 227 × 227 × 3 pixels, this convolutional block comprises three layers of 32 filters, each connected to a normalization layer and a ReLU activation layer through combined max and mean pooling operations.	93.75%
Arch 4	Composed of three convolutional layers, each with 32 filters and an initial input size of 227 × 227 × 3 pixels, connected to a normalization layer and a ReLU activation layer through dual max-pooling operations.	98.07%

Table 9. Summary of the various CNN architectures developed and evaluated in this study [110].

4.2.4 Validation accuracy of the Architectures

In developing a CNN architecture for PV cell inspection, adjusting parameters such as the number of epochs, learning rate, and validation accuracy was a major challenge [119]. To overcome this challenge, we applied a learning rate of 0.01 and 10 epochs to the first CNN network, gradually increasing the learning rate to 0.0001 and the number of epochs to 20, resulting in the maximum validation accuracy for Arch 1 of 81.5%. By replicating the mean pooling of Arch 1 with the maximum pooling of Arch 2, the validation accuracy for Arch 2 was improved to 87.5%. Adding three convolution layers with max-mean and max-max pooling for Arch 3 and Arch 4, respectively, improved the accuracy to 93.75% and 98.07%, respectively,

with 20 epochs and a learning rate of 0.01. Figure 31 compares the validation accuracy of Arch 1 to 4.

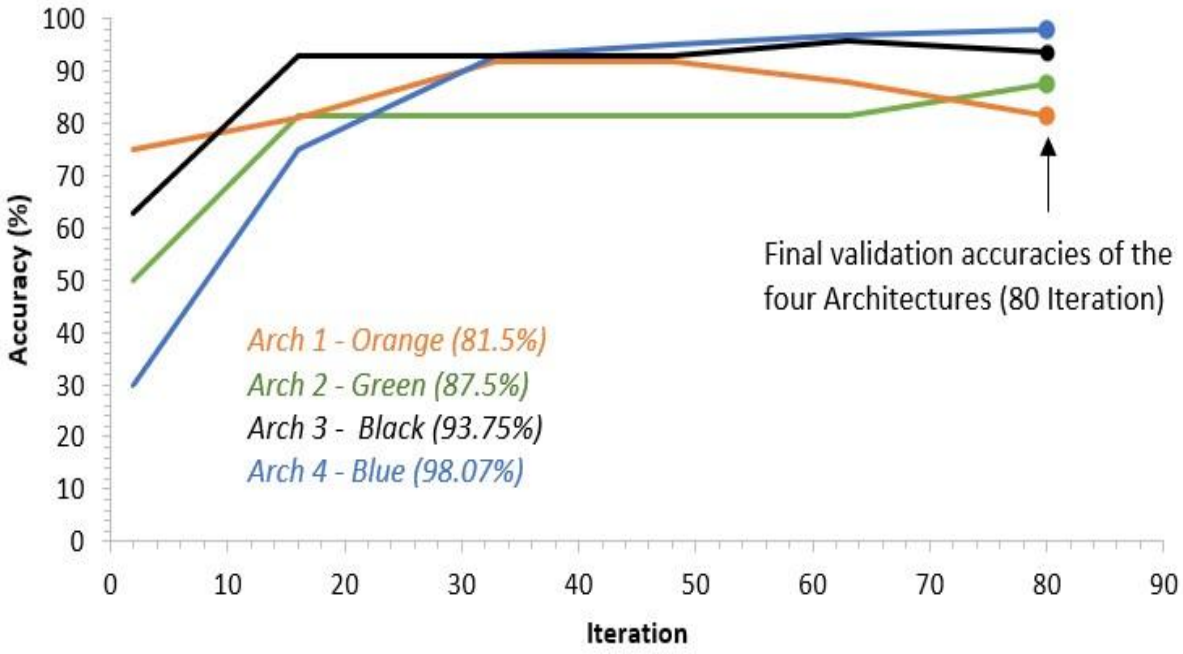

Figure 31. Validation accuracy results for the four CNN architectures evaluated in this study [110].

Parameter	**Value**	**Parameter**	**Value**
Convolutional layers	32 Filters	Epochs	20
Filter size	3,3	Image input Size	227x227x3 Pixels
Mini batch size	16	Learn rate drop factor	0.1
Validation frequency	16	Initial Learn Rate	0.0001
Solver	Sgdm	random rotation (Degree)	-90, 90

Table 10. summary of the input parameters used for CNN architectures Arch 1 through Arch 4 [110].

4.2.5 Decision Making Criterion

The effectiveness of the algorithm relies strongly on the decision-making capability of the CNN. To ensure reliable evaluation, the system is required to process two levels of outputs: the PV module as a whole and the individual PV cells that make up the module. Since each PV module is constructed from multiple cells, the CNN first identifies and analyses the characteristics of the cells within the module to provide an accurate estimate of the module's overall efficiency.

This process offers insight into the performance of the panel and supports optimisation of its operation. Each PV cell is therefore assessed individually, and a decision is made regarding whether it meets the acceptance standard or should be rejected. The results of this process appear in Figure 32 which shows green cells that passed the quality threshold and red cells that failed to meet the established quality threshold.

Once the analysis at the cell level has been carried out, the next stage is to formulate a prediction at the module level, since a module is essentially composed of many PV cells. CNN aggregates individual outcomes to determine module classification. The module fails to pass inspection when PV cells exceeding 20% of the total cells do not meet acceptance standards. Figure 32 shows the detailed quality assessment framework used in this study. This decision making approach relies on aggregating data from each PV cell and comparing the results against predefined quality benchmarks, after which the final module status is determined.

As part of the framework, existing knowledge about the operation of PV systems has been integrated. According to studies, approximately 14% of cells with severe defects such as breakdowns, shading effects, or PID can have a 10% reduction in power output [118], [120],

[121]. Minicracks, on the other hand, have a minimal performance impact when compared to shading defects and PIDs, since shaded areas reduce module performance by about twice as much as minicracks [41], [122], [123]. The rejection criteria follow quality standards established by manufacturers or operators. The model demonstrates flexibility, as PV assembly lines utilize different acceptance parameters, enabling the model to be applied in various industrial settings and to multiple PV assembly lines.

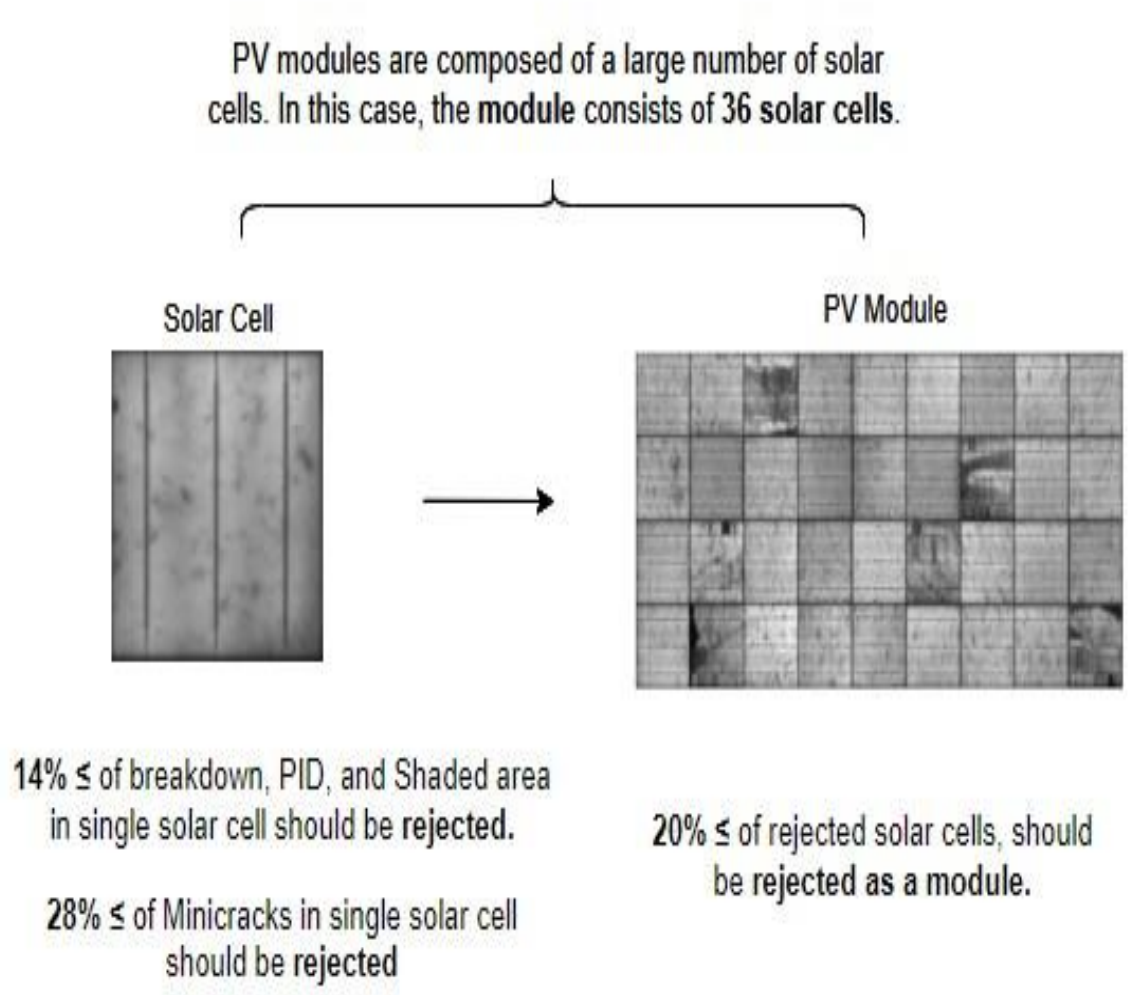

Figure 32. Standard quality criteria [110].

4.3 Results

The assessment of the CNN network in this study can be broken down into two distinct sections, considering its dual-component structure. Specifically, the first component of validation is conducted at the level of individual cells, while the second component focuses on the module level, as the predicted output of the cells directly impacts the overall status of the modules. Through this approach, CNN networks can be validated and their operational performance assessed while the interactions between their individual elements are studied.

4.3.1 Cell Level Prediction

During the inspection stage, each PV cell was analysed individually by the trained CNN. The analysis involved examining all pixels of the cell and classifying them as either accepted or rejected. This step ensured that each cell satisfied the required quality standards, as illustrated in Figure 32.

Four different cells with Varying conditions were evaluated. As presented in Figure 33, the first example was a healthy cell without visible defects. The CNN inspected each pixel independently to check for irregularities, and the final prediction confirmed that the cell was accepted. According to the applied quality standard, cells with less than 14 percent defective pixels are considered healthy, and therefore the cell was displayed as green. In the second case, the CNN determined that the cell was defective because it contained shaded regions. Since more than 14 percent of the pixels showed defects, the cell was rejected and displayed as red.

The third cell presented multiple defects, and the CNN predicted it as rejected since many of its pixels were classified as defective, leading to the cell being illustrated as red. A fourth cell exhibited a minicrack and in this instance the CNN concluded that the cell was healthy. This outcome was based on the fact that the standard tolerance for minicracks was set at 28 percent, which is considerably higher than the standard used for other defects. As the percentage of defective pixels in this case was only 17 percent, the cell was labelled healthy and shown in green.

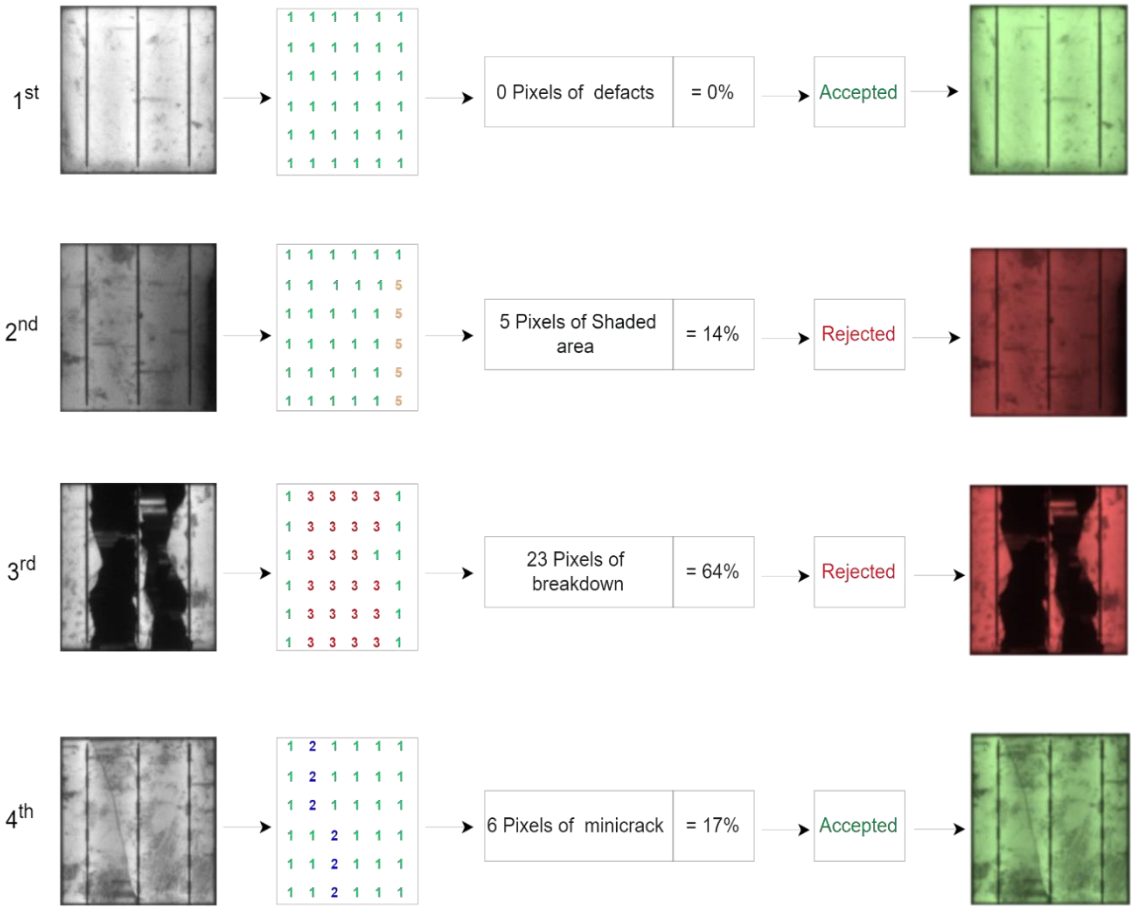

Figure 33. Cell level prediction (Mix of accepted and rejected cases) [110].

4.3.2 Module Level Prediction

This part of the study evaluates the predictive strength of the CNN at the module level by first analysing the PV cells one by one and then applying the results to determine the module's final status. The decision is based on the predefined quality standards illustrated in Figure 32. Such a method ensures that the CNN's performance is measured against recognised benchmarks and also highlights how defects arising from individual cells can influence the overall condition of a module. Inspecting cells separately provides a clearer picture of potential issues that might not be visible when only the module output is considered.

To perform this assessment, a PV module was tested using the CNN. As illustrated in Figure 34**,** the module consisted of 36 cells that were each inspected individually. Out of these, 6 cells were identified as defective, which corresponds to 17 percent of the module. Since this proportion is below the 20 percent rejection threshold, the module was classified as healthy. This outcome shows that the CNN successfully detected defective cells and differentiated them from cells considered healthy, which in turn enabled an accurate evaluation of the module's overall condition. The final classification confirmed that the module met with the required quality level.

To provide further evaluation, the performance of a second PV module was also analysed, as shown in Figure 35. In this case, the CNN determined that 10 out of 36 cells were defective, representing 28 percent of the module. Because this percentage exceeds the standard quality limit of 20 percent, the module was classified as rejected. As a result, once the defect level surpasses a certain threshold, the PV module's expected performance cannot be guaranteed, making it unsuitable for use.

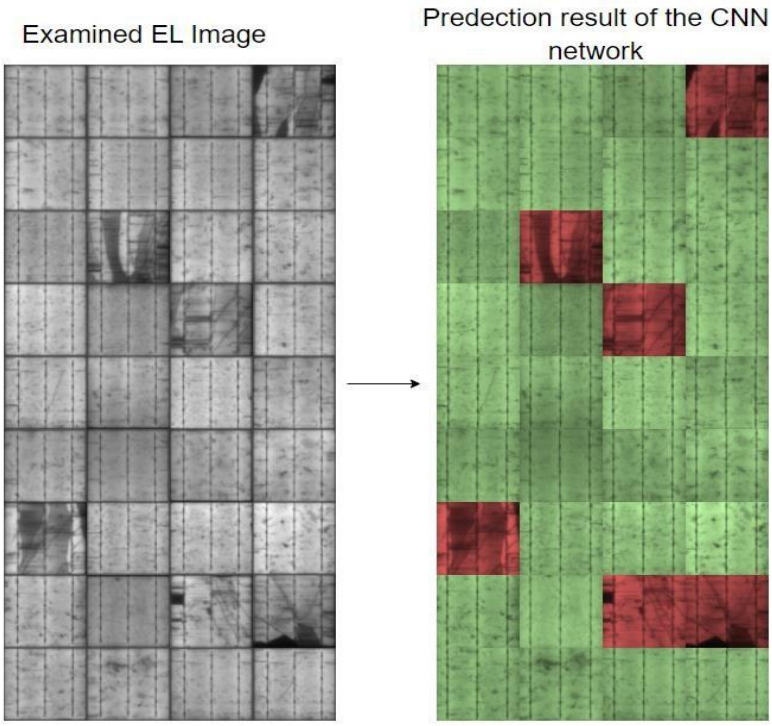

Figure 34. Module level prediction (accepted case*) [110].*

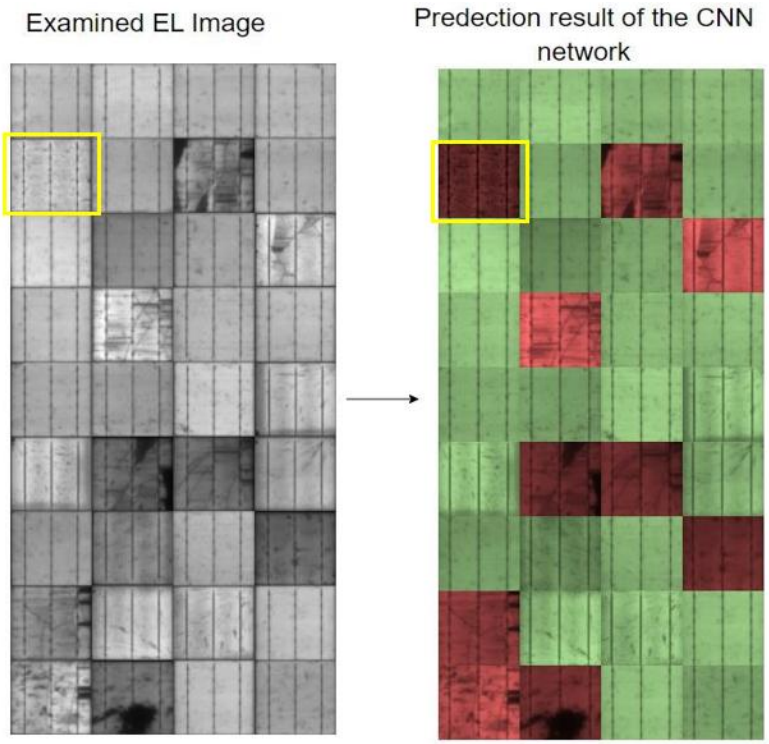

Figure 35. Module level prediction (rejected case) [110].

4.3.3 Diverse EL imaging angles

In standard practice EL imaging is performed by positioning the camera perpendicular to the PV module. However, in real situations this orientation is not always possible. Modules mounted on tilted rooftops or space limitations in a laboratory can prevent perpendicular positioning. Under such circumstances, the camera should be positioned as close to perpendicular as possible, and the EL images need to be corrected accordingly to maintain accuracy.

To investigate this, three EL images were captured from the same PV module at different angles, as shown in Figure 36. The first case, presented in Figure 36(a), represents the conventional configuration, where the EL camera is aligned perpendicularly to the PV module.

In this setup, the CNN produced predictions consistent with normal conditions since no changes were made to the configuration. In the second case, shown in Figure 36(b), the PV module exhibited a slight contrast toward the right while the same EL camera configuration was used. The system still produced results identical to the conventional setup.

A third evaluation was performed with the EL camera angled toward the left of the PV module under the same imaging conditions, as illustrated in Figure 36(c). Even in this scenario, the CNN generated the same prediction as in the perpendicular arrangement. The results therefore indicate that the EL imaging process delivers consistent outputs regardless of orientation, and it This demonstrates that the EL camera can capture light accurately from different directions and reliably detecting module orientation without introducing deviations. The consistency of the predictions across all three cases confirms the robustness of the approach.

When the CNN was tested under these three different angles, it consistently produced the same prediction, as shown in Figure 36(c), highlighting its ability to function effectively even when the perpendicular condition is not met. This underscores the strength of the proposed CNN tool in maintaining reliable performance regardless of the input angle. The quality of the examined PV module further validates the network's ability to provide accurate defect detection.

In addition, the proposed tool has an advantage when dealing with PV cells manufactured with different busbar (BB) technologies. Many of today's cells employ configurations such as 3BB, 4BB, or 5BB. The tool demonstrated its ability to evaluate cells using all these designs and accurately identify defects regardless of the BB arrangement. Furthermore, it is not limited to standard busbar designs but can also assess other types of BB technologies that may be introduced in modern PV manufacturing.

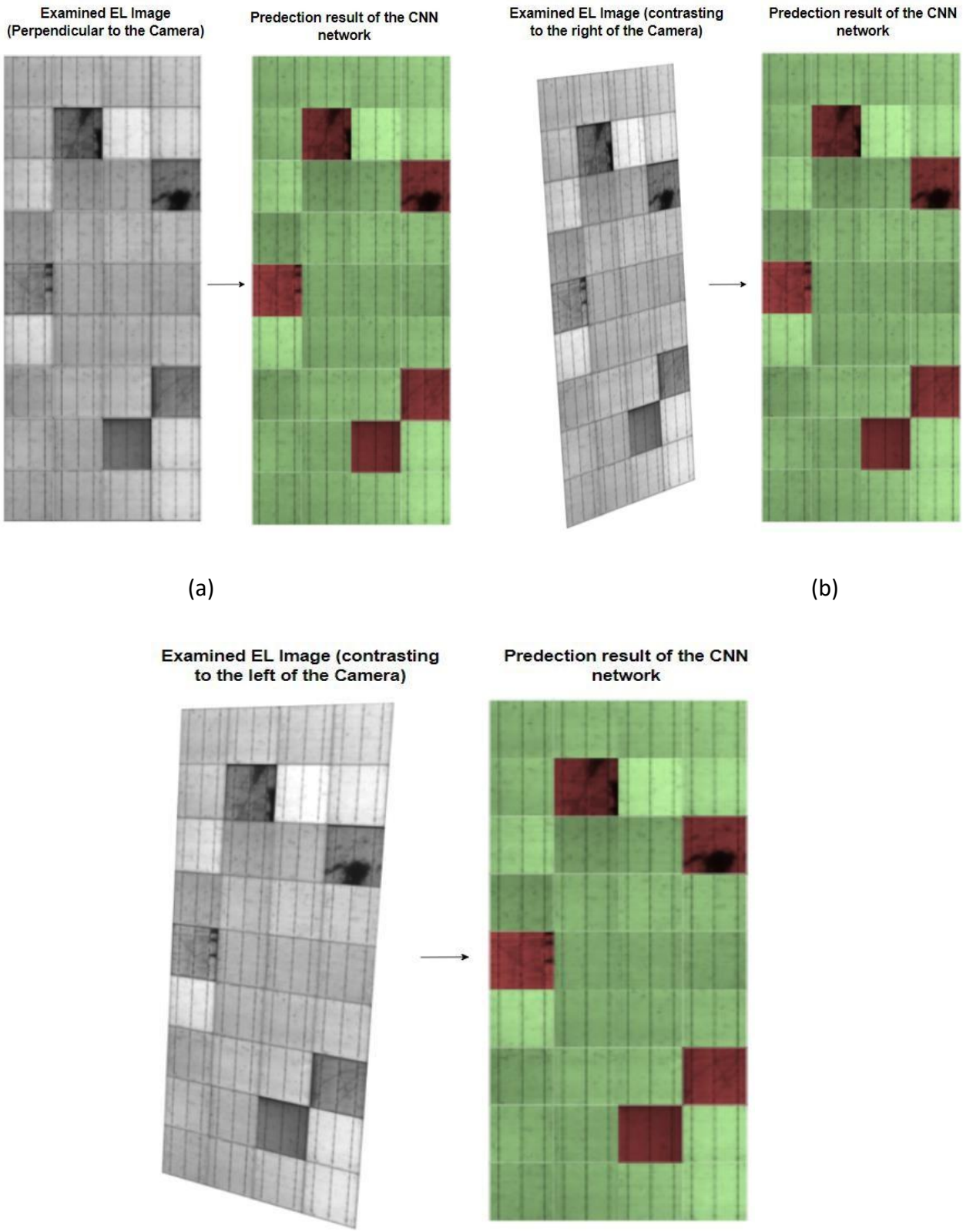

Figure 36. Prediction of PV module condition based on varying imaging angles. (a) Perpendicular to the camera, (b) Contrasting to the right of camera, (c) Contrasting to the left of camera [110].

4.4 Case Study

The proposed CNN is designed to evaluate large PV systems quickly, with minimal manual effort, and with a high level of precision. To test this capability, a case study was carried out on a PV system. The objective of the case study was not only to confirm the accuracy of the CNN but also to test its effectiveness in detecting possible faults across the system. At the same time, the study aimed to explore how the network could support maintenance planning and system optimisation.

As shown in Figure 37, the PV string analysed in this case study was composed of nine polycrystalline silicon modules connected in series. The key electrical parameters of this string are presented in the Table 11.

Figure 37. Examined PV system on the site [110].

Parameter	Value
Power at maximum power point ($\boldsymbol{P_{MPP}}$)	1950 W
Current at maximum power point ($\boldsymbol{I_{MPP}}$)	7.55 A
Voltage at maximum power point ($\boldsymbol{V_{MPP}}$)	258.3 V
Short circuit current ($\boldsymbol{I_{SC}}$)	8.05 A
Open circuit voltage ($\boldsymbol{V_{OC}}$)	331.2 V

Table 11. Electrical characteristics of the second examined PV string measured under standard test conditions [110].

The EL images of the PV modules were first captured, as shown in Figure 38 (a), and then processed by the system for classification according to the quality standards described in Figure 5. The CNN system used the analysis to identify healthy cells through green markings and defective cells through red markings, as shown in Figure 38 (b). Due to the defects found in the PV system, the CNN predicted that all nine modules in the string would need to be rejected since they had PID-related defects.

The proposed tool demonstrates strong potential to serve as an effective solution for large PV power plant installations. The CNN based classification system achieves high precision in detecting defective cells in PV panels. Moreover, the system offers substantial financial benefits by minimising human inspection costs and maintenance needs. The system functions

as an early detection system, detecting potential defects before they become significant issues, thereby reducing the total expenses for operating and maintaining extensive PV systems.

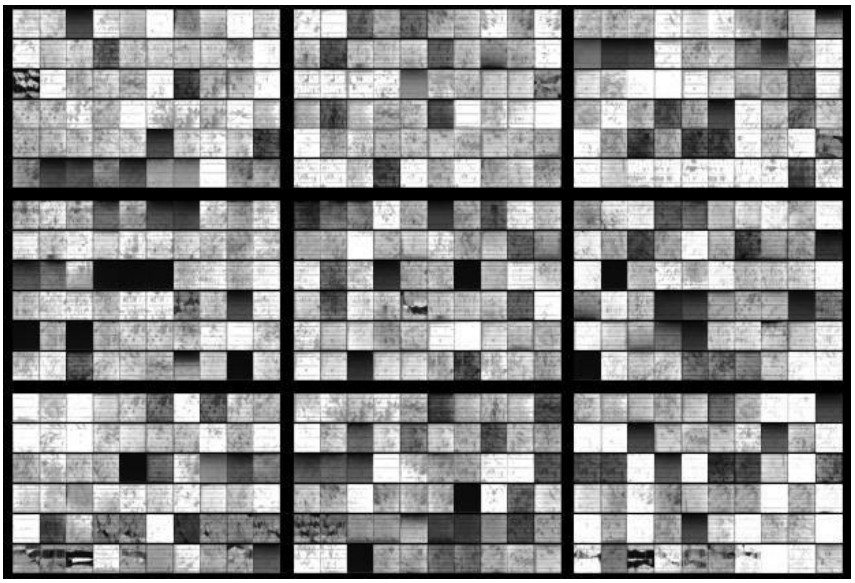

(a)

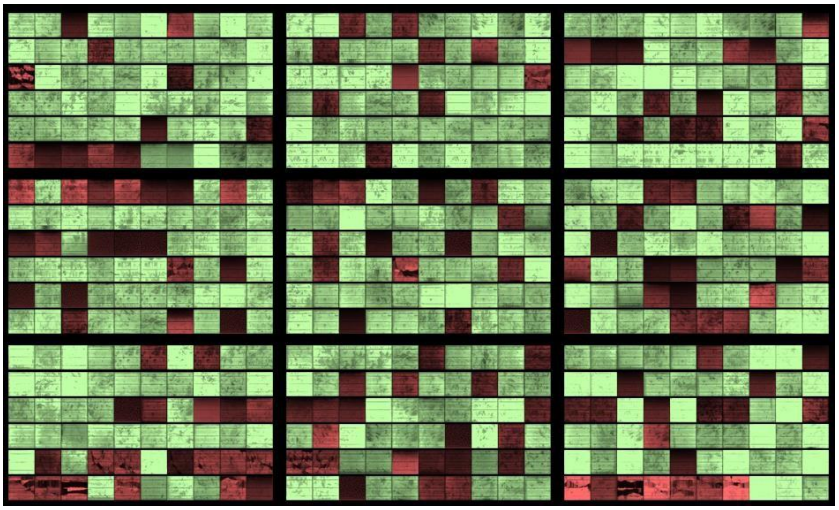

(b)

Figure 38. (a) EL images of the PV modules; (b) corresponding predicted results generated by the CNN model [110].

4.5 Confusion Matrix

Another important parameter for evaluating the system is its ability to correctly or incorrectly classify the dataset, which can be examined through a confusion matrix. The confusion matrix for this case study is presented in Table 12. The dataset consisted of 540 PV cells, out of which 385 were labelled as healthy and 155 were identified as defective. Using this distribution, both the accuracy and precision of the model were calculated according to equations (4) and (5).

In terms of accuracy, the model was able to correctly identify 95.5% of PV cells based on their health status. The precision of the test reached 96.6%, indicating that 96.6% of cells classified as defective were indeed defective. This study proved that the model was both accurate and precise in predicting the conditions of PV cells, as indicated by the study's results.

		Actual No Cracks	**Actual Cracks**
Predicted Value	Predicted No Cracks	374	11
	Predicted Cracks	13	142

Table 12. Confusion matrix of the developed CNN model for the case study (Arch 4) [110].

$$Accuracy = \frac{TP+TN}{TP+TN+FP+FN} = \frac{374+142}{374+142+13+11} = 95.5\% \quad [4]$$

$$Precision = \frac{TP}{TP+FP} = \frac{374}{374+13} = 96.6\% \quad [5]$$

4.6 Loss Function

The CNN's loss function is essential since it measures the difference between the predicted outputs and the actual ground truth values [124]. By tuning key parameters during training, the CNN's performance and prediction capability are improved by minimising its loss function.

The training process relies on continuous minimisation of the loss function to improve model accuracy with each optimisation step.

There are two curves in the Figure 39, which represent the training of Arch 4. The red line represents training loss, and the blue line represents validation loss. The model shows a steady decrease in prediction errors because of the downward trend and the two curves become progressively closer to each other. At the beginning of training, the loss values were relatively high, but with successive iterations, the loss declined and eventually reached zero. This indicates effective learning by the CNN and a notable improvement in accuracy, resulting from the reduction in both error and loss.

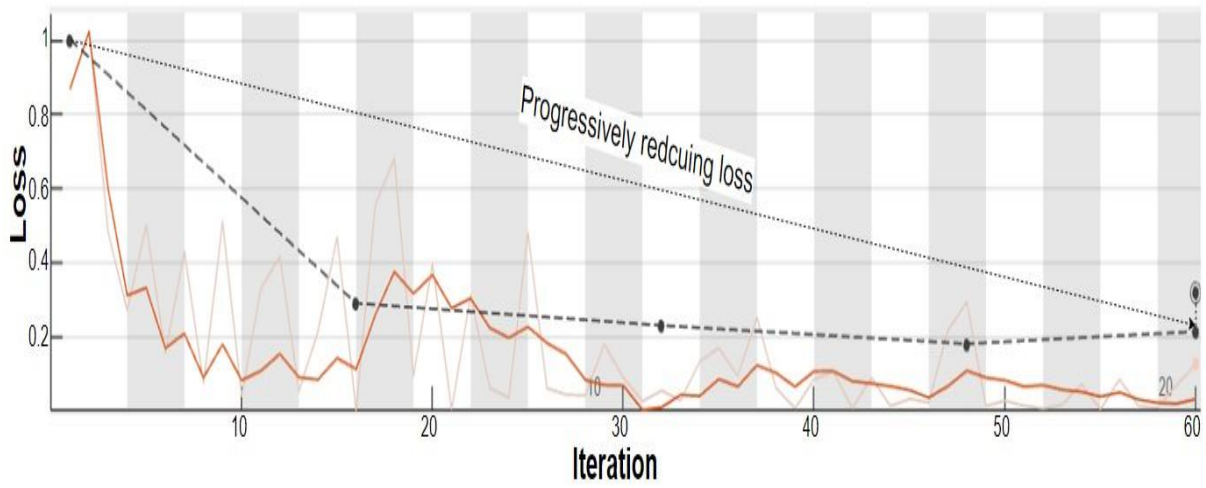

Figure 39. Arch 4 CNN network learning Loss vs learning iterations (epochs) [110]).

4.7 Sensitivity analysis

The following section discusses the model's sensitivity to two key parameters, which are the proportion of data used for training and validation, as well as the number of training epochs

used in the model [125]. Sensitivity analysis is conducted to evaluate how adjustments to these parameters influence the overall performance of the system.

Different ratios of training to validation data were tested, with configurations of 50% training and 50% validation, 55% training and 45% validation, 60% training and 40% validation, 65% training and 35% validation, 70% training and 30% validation, 75% training and 25% validation, and finally 80% training and 20% validation. Accuracy was measured for each of these settings. The findings showed that the 80% training and 20% validation split produced the highest accuracy. This ratio provided an effective balance between having sufficient training data and validation data. Altering the split in either direction reduced accuracy, which highlights the data split ratio as a key determinant of system optimisation.

A sensitivity analysis was also conducted to evaluate the effect of training epochs on the prediction accuracy. Six epoch counts were tested: 5, 10, 15, 20, 25, and 30, as shown in Figure 40, and accuracy was calculated for each configuration. The results showed that training for 20 epochs resulted in the highest accuracy. The model was unable to achieve full convergence due to the limited number of epochs, which resulted in decreased accuracy. However, additional epochs beyond a certain point started to decrease performance slightly. The results indicate that selecting the correct number of training epochs is crucial for achieving optimal model performance.

Table 11 provides confusion matrices to support these observations. The matrices present a comprehensive evaluation of system classification results across various data divisions and training epoch numbers, which helps to understand how parameter variations affect the model's prediction performance.

	Epoch 5	Epoch 10	Epoch 15	Epoch 20	Epoch 25	Epoch 30
Ratio 50:50	76.03%	76.93%	77.18%	78.89%	78.10%	77.63%
Ratio 55:45	78.43%	79.90%	80.50%	82.23%	81.66%	81.01%
Ratio 60:40	83.33%	84.19%	85.53%	87.52%	86.47%	85.96%
Ratio 65:35	89.77%	90.96%	92.22%	93.33%	93.02%	92.86%
Ratio 70:30	95.24%	96.64%	97.13%	98.07%	97.86%	97.55%
Ratio 75:25	93.37%	94.83%	95.21%	96..43%	96.11%	95.79%
Ratio 80:20	91.43%	92.09%	93.21	94.04%	93.88%	93.55%

Table 13. Sensitivity analysis of two key parameters: the data split ratio and the number of training epochs) [110].

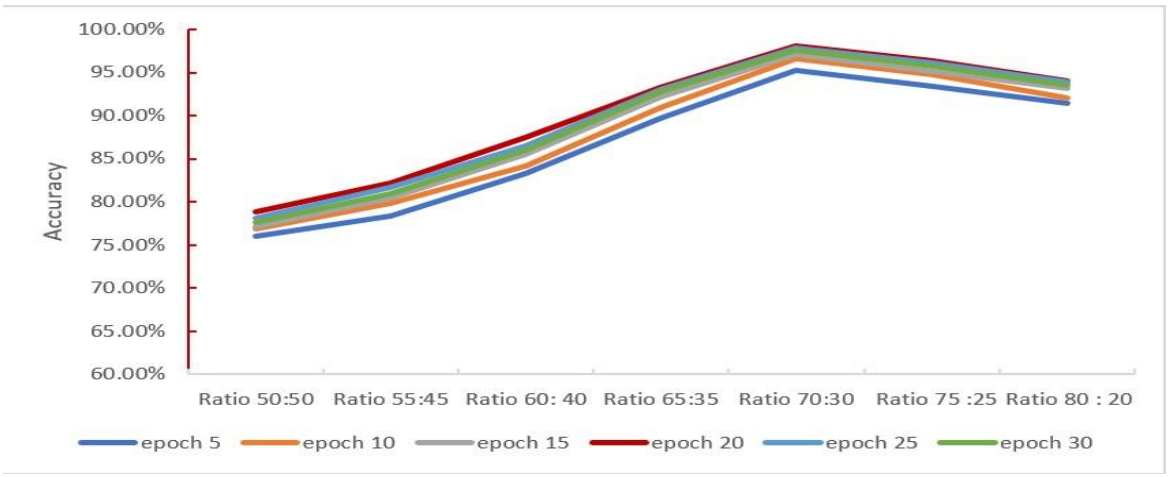

Figure 40. Accuracy sensitivity analysis illustrating the relationship between training epochs and data split ratios [110].

4.8 Comparative Analysis

To evaluate the practicality of the proposed approach, its performance was compared with several automated PV defect detection methods currently applied in the industry [126], [127], [128], [129]. A summary of this comparison is presented in Table 14. Several recent automated techniques rely on CNN architectures [126], [128], [129]. However, these methods share a common limitation in that they can only analyse defects at the cell level and not at the module level, which distinguishes the current work. Another shortcoming is that their classification at the cell level is restricted to cracks alone, regardless of their extent. Consequently, these methods are not capable of identifying other critical issues such as PID or shading.

Pre-trained CNN models through transfer learning provide an alternative solution to designing new architectures for these approaches. The detection of PV defects uses existing CNN frameworks, which work without any modifications to their basic architecture. One example is a recent study that applied a pre-trained AlexNet to inspect defects at the module level [127]. While the method proved to be successful in many aspects, it relied on standard PV images instead of EL images to detect defects, which makes it difficult to detect minicracks and PIDs.

Compared to previous studies, the CNN network developed in this study differs in that it provides automated inspection at both the cell and module levels. For modules, the process is based on analysing the health of individual cells and then determining the acceptance or rejection of the module according to the proportion of healthy cells. This system can detect multiple types of defects, including cracks, PIDs, and shading defects, which is far beyond what current methods can detect. As a result, the proposed tool can serve two major purposes.

First, it can be applied at the cell level on PV assembly lines to evaluate newly manufactured cells. A second advantage of this system is that it enables users to inspect large PV installations at the module level, thereby reducing human interaction and accelerating the process while maintaining the same level of accuracy.

This study presents a novel inspection system that enables real-time simultaneous assessment of PV cells and modules. In addition, the system has the ability to provide inspections from multiple viewing angles since EL images obtained from left and right tilted angle modules produce exact predictions regardless of the angle. This robustness arises from the CNN's ability to detect features regardless of their orientation. The system offers a cost-efficient and effective solution for defect detection and system monitoring in large PV installations.

[105]	2020	AlexNet-CNN: A transfer learning-based approach that utilises the pre-trained AlexNet architecture for detecting cracks in PV cells.	x	✔	✔	X	X
[97]	2019	Light CNN: A compact CNN architecture developed from scratch, consisting of four convolutional layers and employing an L2-based weight regularization scheme.	✔	x	✔	X	X

[128]	2022	Gradient-Guided Architecture: A lightweight CNN design integrating gradient-guided filter tuning with two convolutional layers and two fully connected layers to enhance feature learning efficiency.	✔	x	✔	x	X
This work	2023	In this study, A CNN architecture was developed from scratch using four different architectures and by varying the number of convolution layers and changing the pooling level to double maximum pooling, we achieved the highest validation accuracy.	✔	✔	✔	✔	✔

Table 14. Comparison of the proposed network with several recently developed algorithms for PV cell crack detection. [126], [127], [128], [129].

While the module-level analysis confirms the effectiveness of the proposed CNN-based defect detection framework, further validation is required to assess its performance under large-scale operational conditions. Photovoltaic installations deployed across diverse environments present additional challenges related to degradation mechanisms, imaging variability, and long-term

reliability assessment. Therefore, the next chapter investigates the application of the developed methodology to extensive electroluminescence datasets obtained from multiple field installations,

Chapter 5 Large-Scale Electroluminescence Analysis of PV Cells for Defect Detection and Degradation Studies

5.1 Introduction

To assess the practical applicability and scalability of the proposed defect detection methodology, this chapter presents a large-scale electroluminescence-based analysis of photovoltaic cells deployed across multiple installation sites. Building upon the model development and validation outcomes presented in Chapters 3 and 4, this chapter examines defect classification performance in real-world operational environments. The study explores degradation patterns, residual performance trends, and comparative defect characteristics using extensive EL image datasets. The analysis provides insights into long-term PV system reliability and supports the integration of artificial intelligence-driven inspection frameworks into industrial photovoltaic monitoring and maintenance strategies.

5.2 Methodology

5.2.1 EL Imaging

The underlying principles of EL imaging were presented in Chapter 2 and further applied in Chapter 3. In this chapter, the technique is extended to a large-scale dataset, with the focus placed on the specific imaging setup and testing conditions used for this study.

Digital EL cameras were used to obtain high-resolution images of the modules. The cameras employed in the field had varying specifications, with resolutions ranging from 2k × 2k to 8k ×

8k pixels and focal lengths between 18 mm and 55 mm. These configurations ensured sharp imaging with a wide dynamic range of colours and contrasts, both of which are essential for detecting subtle defects. The high-resolution capacity, combined with a wide field of view, made it possible to capture intricate details and provide a complete overview of the module condition.

To induce electroluminescence, each PV module was connected to a power supply to generate a forward-biased current. In this study, the current was applied at the short-circuit condition of the arrays, which is a standard EL testing practice. This setup allowed defects to be revealed clearly in the captured images, forming the basis for subsequent automated analysis.

5.2.2 PV Installations Locations (Dataset Source)

The dataset employed in this study represents a comprehensive selection of 167 ground mounted PV installations distributed across a wide range of geographic regions, as shown on the map in Figure 41. Data were collected from several EL inspection providers, and the sites were carefully selected to capture diverse climatic and operational conditions. This broad coverage was intended to examine how local environmental factors influence the performance and durability of PV modules. The installations highlighted on the map reflect these varied operating environments.

In total, 85,000 PV modules were inspected, each with operational experience between 2 and 9 years in the field. This large-scale inspection effort provided a dataset that is both extensive and detailed, enabling a thorough assessment of the condition of PV systems. Among these modules, 41,000 contained 72 cells, while the remainder were built with 60 cells, resulting in a combined total of 5,592,000 cells analysed in this work.

EL imaging was used to identify minicracks and other hidden defects that may compromise performance and all images were captured at night to eliminate interference from ambient light. Initial analysis of the images revealed several categories of defects, which will be further classified and investigated in later sections. This classification considers not only the defect types and crack patterns but also their possible links to module age, environmental exposure, and mechanical stresses observed in the field.

The EL dataset was collected from two main sources: 32 PV systems were inspected by the University of York, and the remaining installations were examined by Above Surveying Limited. Although the systems varied in operational age, all imaging was conducted within a single year to maintain consistency in the dataset.

Due to the high costs of large-scale field testing, IV curves were not recorded for every one of the 85,000 modules. Instead, IV curve measurements were taken selectively from modules showing pronounced defects in the EL images. Consequently, the emphasis of this paper is on the diagnostic capability of EL imaging rather than a full quantification of power losses across the entire sample Of the 167 installations assessed, 25 had been in operation for nine years, while the others had operated between 2 and 8 years. For some newer installations, however, determining exact operational age proved difficult because grid connection occurred months or even more than a year after physical installation. For example, certain sites were built five years ago but only connected to the grid between 9 months and 1.5 years later. This variability complicated precise ageing assessments, and therefore the analysis relies mainly on the EL images themselves as the foundation for defect detection and degradation evaluation.

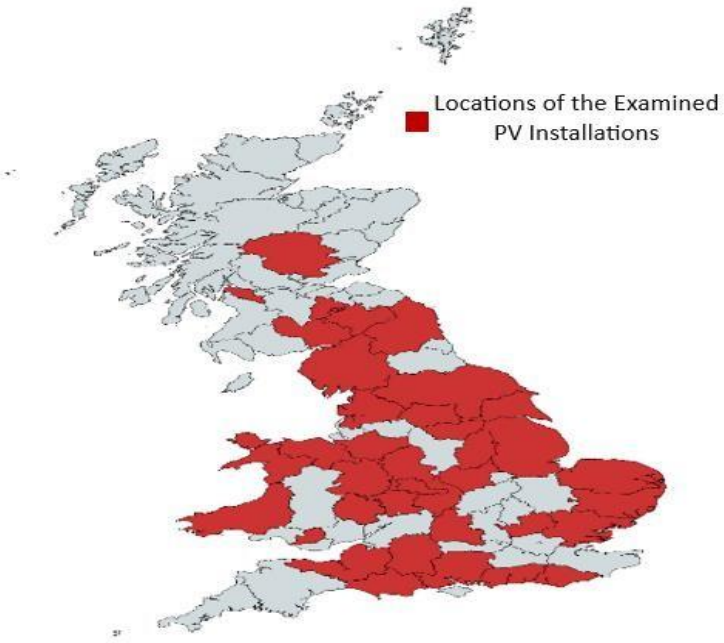

Figure 41. Geographical distribution map illustrating the PV sites analysed across different regions of the UK.

5.2.3 Classification of PV Modules Defects

The classification of PV module defects, including line cracks, soldering anomalies, complex cracks, edge ribbon cracks and PID, has been previously discussed in detail in Section 2.3 and shown in Figure 4.

In this section, the same classification framework is revisited and applied to the experimental results obtained in this study to evaluate how these defect types influence the performance and reliability of the tested PV modules.

Beyond this classification, the dataset of 5,592,000 cells offers an opportunity to study crack patterns observed in the field and the degradation mechanisms they reveal. The breadth of the dataset allows for correlations between specific defect types and variables such as environmental exposure, installation practices, and material ageing. Furthermore, the analysis

explores the frequency and distribution of these defects, contributing toward the development of a predictive model of module lifespan. Such a model would strengthen our understanding of PV durability, inform improvements in module design and production, and help create more resilient PV systems. By highlighting the importance of early detection and systematic classification, this work underscores the role of EL imaging as a powerful tool for quality assurance and long-term maintenance in PV energy applications.

5.2.4 Automating the PV Defects Classification

A major challenge in analysing the extensive EL datasets obtained from PV installations is the need to classify crack types on a cell-by-cell basis. To overcome this, the methodology previously developed in ([102]) was applied to automate the inspection process, as illustrated in Figure 42, enabling the classification of each crack type across the dataset. Automating this process makes it possible to evaluate millions of cells efficiently; however, it does introduce an estimated error rate of about 2 percent.

The algorithm produces this margin of error because it fails to identify overlapping defect features correctly and since the training data does not contain all the different types of defects that exist in real-world applications. The model becomes better at detecting specific defects when the training data contains more examples of those defects but shows reduced accuracy when identifying fewer common defects. As a result, less common defects may be underrepresented in the final defect distribution, which can influence the overall defect profile of the PV modules under analysis.

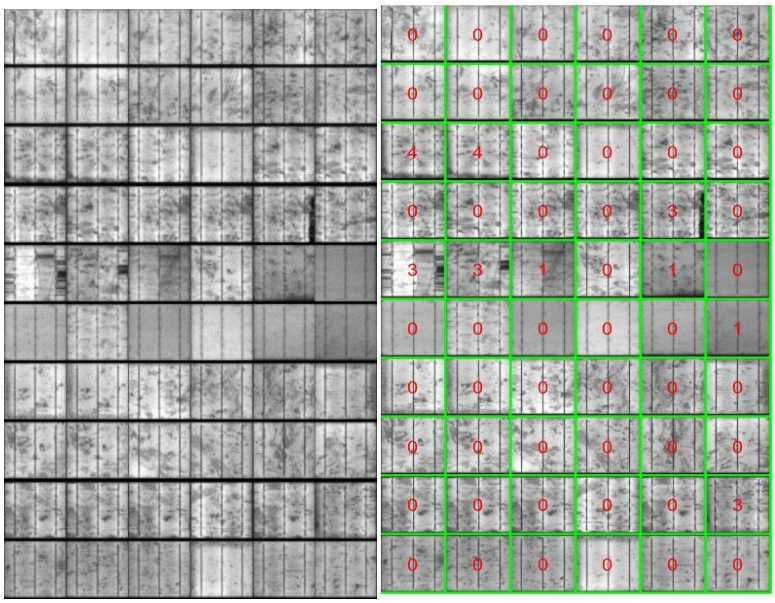

Figure 42. images captured before and after the application of automated crack processing. A designation of 0 indicates a healthy cell, while numerals 1 through 5 correspond to the specific crack types defined in Figure 3 representing line cracks, soldering anomalies, complex cracks, edge ribbon cracks and PID, respectively [33].

The accuracy of defect identification depends strongly on the quality of the EL images captured. Variations in lighting, shadows, or reflections can reduce image clarity and contribute to misclassifications. Even when imaging protocols are standardised, small inconsistencies can influence the results. Furthermore, for reliable classification, the system must be able to generalise across a wide range of PV modules and installation types. Differences in module design and manufacturing processes may create patterns not represented in the training dataset, which can result in classification errors.

In selecting the most suitable diagnostic method, the primary requirement was the ability to reveal subtle internal defects that remain hidden from traditional approaches such as visual inspection or infrared thermography. EL testing conducted under nocturnal conditions was adopted for this reason, as it generates high-resolution images that expose the internal structure of the cells without introducing additional stresses. This approach is particularly

effective for identifying minicracks and other disruptions in the silicon lattice, which are essential indicators of the long-term reliability of PV modules.

A comparative assessment of various inspection methods is summarised in Table 15, which highlights the advantages of EL testing for detecting minicracks and other sub-surface defects. This sensitivity is critical for anticipating possible failure modes of PV modules when exposed to real-world operational stresses. Unlike EL imaging, infrared thermography, although inexpensive and non-destructive, has limited sensitivity to small minicracks that do not significantly affect heat distribution. Similarly, electrical testing focuses on current flow and power output but provides little information about the underlying physical structure of the cells, meaning that non-conductive but structurally important defects remain undetected.

Visual inspection remains the least expensive and simplest method, but it cannot uncover hidden internal defects and is unsuitable for comprehensive monitoring or predictive maintenance. By comparison, EL imaging, although requiring specialised equipment and darkened conditions, offers a balanced solution. It delivers detailed structural information, enables the detection of critical defects, and can be implemented in operational settings without interrupting module functionality.

Method	**Sensitivity to minicracks**	**Non-Destructive**	**Cost Effectiveness**	**Applicability in operational settings**
Electroluminescence	Very High	No	Moderate	High

Infrared Thermography	Moderate	Yes	Low	Moderate
Visual Inspection	Low	Yes	High	Moderate
Electrical testing	Low	No	Moderate	High

Table 15. Comparison of different inspection techniques for PV modules testing.

5.3 Results

5.3.1 Comparative Analysis of the PV Defects

A summary of the defect distribution across PV modules is provided in Table 16, which compares all inspected installations with those commissioned after January 1, 2022. The table presents both the frequency and percentage of each defect type, allowing for a clear comparison between older and newer installations. Several noteworthy patterns emerge from this analysis.

For the full dataset, line cracks are the most prevalent, representing 28.97 percent of total defects. They are followed by complex cracks, which account for 19.06 percent. Soldering anomalies contribute 13.96 percent, while edge ribbon cracks, though less frequent, still make up 7.89 percent of the observed defects. PID defects are the least common, constituting only 6.47 percent in earlier installations.

The distribution changes significantly for systems installed after 2022. In these newer installations, edge ribbon cracks rise sharply to 28.23 percent, making them the most dominant defect type. At the same time, the share of line cracks decreases to 19.59 percent, and complex cracks fall to 10.51 percent. This marked increase in edge ribbon cracks suggests possible links to evolving manufacturing practices or installation

	All PV Installations Data		**New Installed PV System Daya (post-2022)**	
Defect Type	**Number of PV Cells**	**Percentage**	**Number of PV Cells**	**Percentage**
Normal Cell	1322092	23.64	616722	28.30
Line Cracks	1620320	28.97	426932	19.59
Soldering Anomalies	780212	13.96	128624	5.90
Complex Cracks	1066155	19.06	229082	10.51
Edge Ribbon Cracks	441221	7.89	615289	28.23
PID	362000	6.47	162551	7.46
Sum	5592000	100	2179200	100

Table 16. Comparison of Defect Profiles for All PV Installations and New PV Systems (Post-2022).

The comparison of defect distributions is illustrated in Figure 43, which provides a visual representation of the trends between all installations and those commissioned after 2022. In Figure 43 (a), the percentage distribution of defects highlights clear shifts in the prevalence of defect types. The most striking change is the increase in edge ribbon cracks, which rose from 7.89 percent in all installations to 28.23 percent in post-2022 systems. This sharp rise points

toward the possibility that recent manufacturing or installation practices are introducing new mechanical stresses, ultimately compromising the structural stability and efficiency of PV modules.

At the same time, line cracks declined from 28.97 percent in the overall dataset to 19.59 percent in newer installations. This reduction may be associated with improved fabrication methods or enhanced handling procedures that help mitigate such defects. Complex cracks display a similar downward trend, decreasing from 19.06 percent to 10.51 percent, which could reflect gains in the resilience of more recently deployed PV modules.

In Figure 43 (b), the frequency distribution of defects is compared across the same two categories. The results show that while the occurrence of certain defects has diminished in newer modules, edge ribbon cracks have emerged as a far more prominent issue.

In order to determine whether the variations in defect distributions observed between the complete set of installations and those deployed after 2022 are meaningful, a chi-squared test was applied to the defect frequency data presented in Figure 43 (b). The analysis produced a chi-squared statistic of 701,436.18 with a corresponding p-value below 0.001. These results confirm that the differences in defect distributions across the two groups are highly significant from a statistical perspective. The relative influence of each defect type on the overall chi squared outcome is detailed in Table 17.

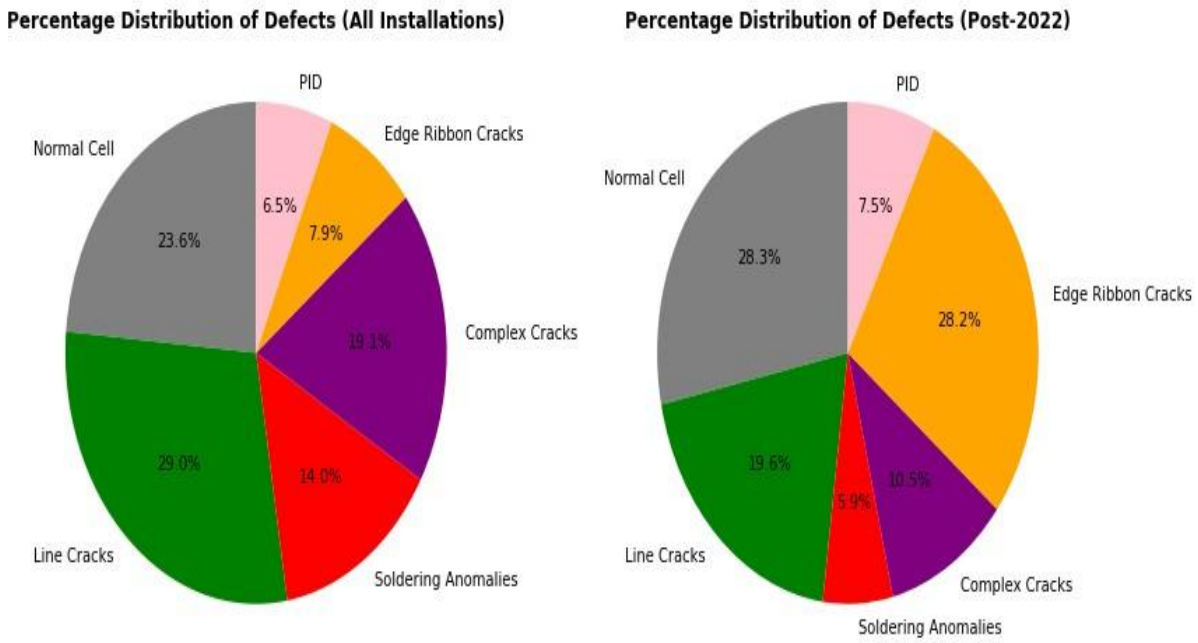

(a)

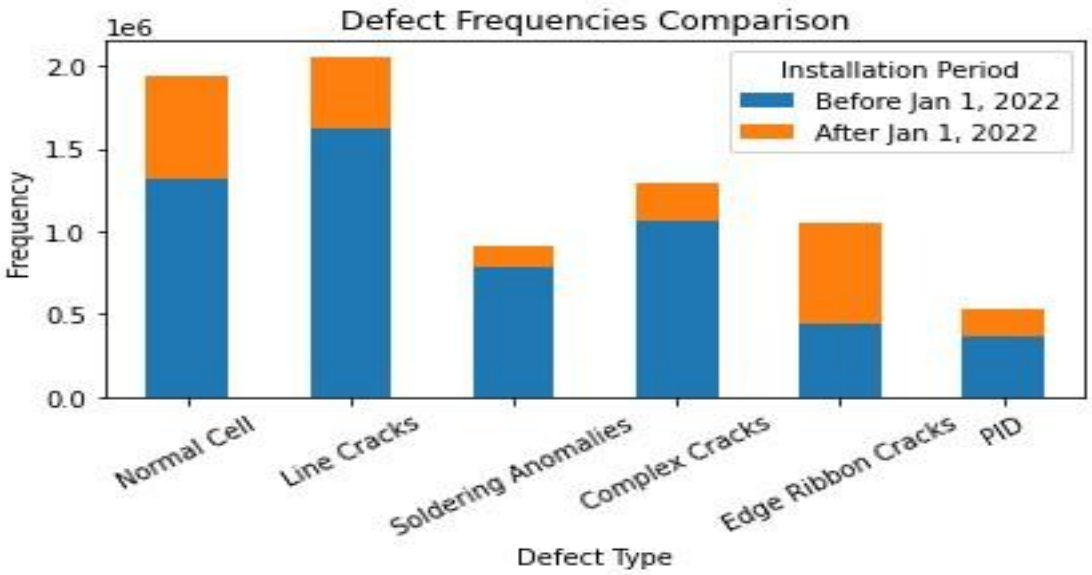

(b)

Figure 43. (a) Percentage distribution of defect types across all PV installations (left) and post-2022 installations (right). The pie charts illustrate the variation in defect proportions before and after 2022, with a noticeable rise in edge ribbon cracks among newer installations. (b) Comparison of defect frequencies between all installations and those installed after 2022. The stacked bar chart highlights shift in defect distribution, including an increase in edge ribbon cracks and a reduction in line cracks in recent systems. The Python code used to generate this figure is provided in Appendix A {33}.

In order to determine whether the variations in defect distributions observed between the complete set of installations and those deployed after 2022 are meaningful, a chi-squared test was applied to the defect frequency data presented in Figure 43 (b). The analysis produced a chi-squared statistic of 701,436.18 with a corresponding p-value below 0.001. These results confirm that the differences in defect distributions across the two groups are highly significant from a statistical perspective. The relative influence of each defect type on the overall chi squared outcome is detailed in Table 17.

Defect Type	**Before Jan 1, 2022**	**After Jan 1, 2022**
Normal Cell	3,823.87	9,812.36
Line Cracks	14,700.09	37,721.59
Soldering Anomalies	24,365.37	62,523.47
Complex Cracks	19,302.48	49,531.68
Edge Ribbon Cracks	133,872.02	343,526.21
PID	632.92	1,624.13

Table 17. *Chi-Squared Contributions for Each Defect Type Before and After January 1, 2022, 4[33].*

As presented in Table 17, edge ribbon cracks accounted for the largest share of the chi squared statistic, with contributions of 133,872.02 prior to 2022 and 343,526.21 in post-2022 installations. This indicates that the sharp increase in this defect type after 2022 is the primary driver of the observed differences in defect distributions. Such a pronounced surge suggests

that recent changes in module fabrication or installation methods may be linked to the rise in edge ribbon cracks, highlighting the importance of further investigation.

Other defects also made notable contributions to the chi-squared outcome. For instance, line cracks contributed 14,700.09 before 2022 and 37,721.59 after 2022. Although their frequency decreased in newer modules, they remain a prominent defect type, influencing the overall distribution. Soldering anomalies and complex cracks also made substantial contributions, confirming that their variations across time have influenced the statistical differences between the two groups.

The contributions associated with normal cells (defect-free cells) were smaller in magnitude but still important. These figures reflect a positive development, as the proportion of defect free cells increased from 23.64 percent in earlier modules to 28.30 percent in post-2022 installations. This improvement, while encouraging, still contributes to the overall change in defect profiles observed.

Taken together, the chi-squared analysis shows that the shifts in defect types are not the result of random variation but are instead linked to genuine changes in manufacturing quality, material characteristics, or installation techniques. The dramatic increase in edge ribbon cracks, observed in both Table 16 and Figure 43(a), is especially concerning. These defects originate at the boundary between the PV cell and its ribbon interconnect, often caused by mechanical stress during handling, transportation or installation. Their sudden rise in frequency could be symptomatic of newer installation practices, higher production pressures, or relaxed quality control protocols.

The implications of this trend are significant. Edge ribbon cracks can expand over time, reducing module efficiency, increasing maintenance needs and leading to premature system

failures. Addressing this issue will require improvements in both production and installation processes. Enhancing material durability, refining handling procedures, and strengthening training for installers will be essential steps to mitigate these failures.

While edge ribbon cracks have emerged as a growing problem in recent years, the data also reveal areas of improvement. Line cracks and complex cracks have declined, and soldering anomalies along with PID defects appear less frequently, suggesting that certain aspects of module design and production have benefited from recent advances. The growing proportion of defect-free cells further supports an overall improvement in quality, even as new challenges emerge.

Moving forward, manufacturers and installers must pay close attention to the increasing prevalence of edge ribbon cracks. Enforcing stricter quality assurance in production and providing more comprehensive installation training are necessary to reduce the mechanical stresses that give rise to these defects. Therefore ongoing monitoring and further research into defect trends will be critical for sustaining improvements and ensuring the long-term reliability of PV systems.

5.3.2 In-Depth Examination of PV Defects and their Impact on Module Power Performance

The assessment of module performance was extended by comparing two diagnostic approaches, as shown in Figure 44. In Figure 44 (a), the results of EL imaging are displayed, while Figure 44(b) illustrates the corresponding power-voltage (P-V) behaviour of the same modules. The P-V curves were obtained in the field using a Seaward PV200 device, which has a reported power curve tracking error margin of ±0.3 percent. Although outdoor IV testing

generally carries higher uncertainty than indoor laboratory setups (typically between 2.5 and 3.5 percent), the ±0.3 percent value was used here to remain consistent with the instrument specifications. Due to logistical constraints, only a subset of modules was subjected to IV measurements rather than the entire dataset of 85,000 modules.

For this comparison, one site was chosen, and IV data were collected under high irradiance conditions of 812 W/m² with an ambient temperature of 20.6 °C. These conditions represent typical operating environments for PV modules. It is important to note that while IV and P-V testing was conducted under such irradiance levels, the EL imaging was performed at night to minimise interference from ambient light and to capture high-quality defect images.

The baseline electrical parameters of the modules under test are provided in Table 18, based on manufacturer nameplate values. These modules were rated at a maximum output of 220 W, which, while modest compared with present-day technologies, reflects the characteristics of the systems deployed during the period covered by the dataset.

EL imaging served as the central diagnostic method in this analysis and effectively identified the defect categories present. Modules labelled PV#1 through PV#5 exhibited various fault types including line cracks, complex cracks, edge ribbon cracks, and soldering anomalies. The visualisation of these issues through EL imaging aligned closely with their reduced electrical performance. For example, PV#1 showed a power loss of 6.3 percent, while PV#4 experienced a slightly higher loss at 7.2 percent, both of which corresponded to the severity of the defects observed.

In contrast, modules PV#6 through PV#10 displayed substantial losses associated with PID.

PV#8 was particularly affected, registering a severe drop of 44.1 percent in power output. The P-V profiles of these modules, illustrated in Figure 44(b), deviate sharply from the expected performance curve, highlighting the destructive impact of PID on energy yield.

Taken together, the findings in Figure 44 demonstrate the strong relationship between defects detected via EL imaging and reductions in electrical output. The contrast between modules affected by cracks or soldering issues and those dominated by PID reveals the varied but equally damaging effects of different defect mechanisms. These results underline the necessity of precise diagnostic tools, as even relatively minor cracks can diminish performance while PID can devastate module efficiency. The evidence reinforces the case for integrating advanced imaging and monitoring techniques into PV quality assurance frameworks to safeguard module reliability and sustain energy production over time.

	Short circuit current (A)	**Current at Maximum Power Point (A)**	**Open Circuit Voltage (V)**	**Voltage at Maximum Power Point (V)**	**Maximum Output Power (W)**
Value	8.12	7.4	36.5	29.8	220

Table 18. Electrical Parameters of the Examined PV Modules Under Standard Test Conditions (Nameplate: TESPV 202W Poly-Si).

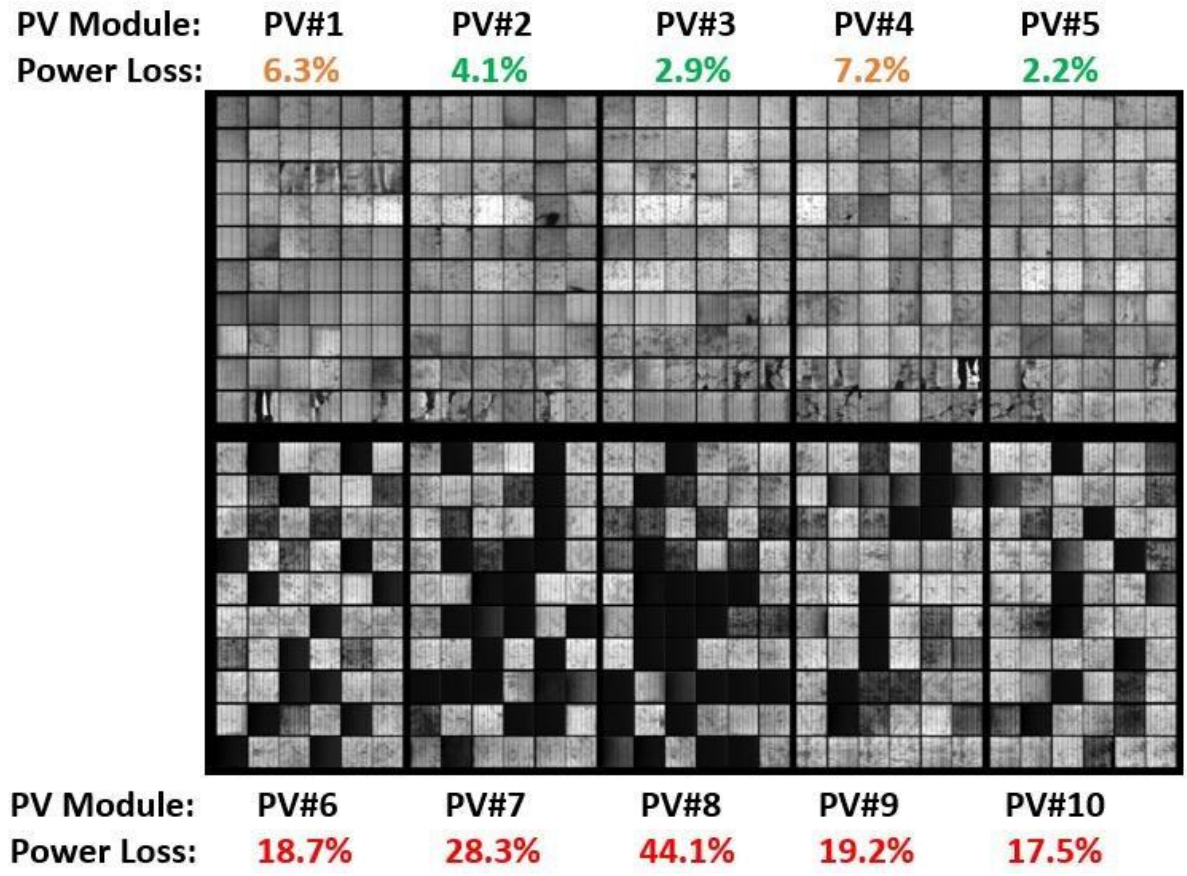

(a)

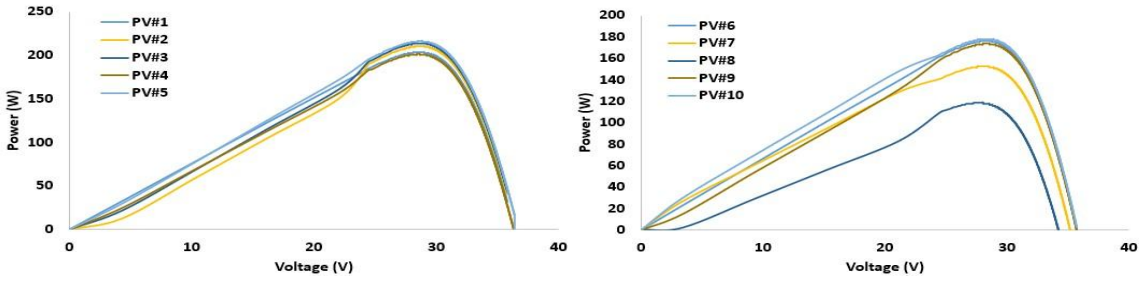

(b)

Figure 44. Impact of PV defects on the electrical performance of PV modules: (a) EL images from a representative sample of ten PV modules; (b) corresponding power–voltage (P–V) characteristics measured under test conditions of 812 W/m² irradiance and an ambient temperature of 20.6 °C. The results illustrate performance variations associated with the identified defects [33].

Figure 45 presents the relationship between the number of defective cells affected either by cracks or PID and the corresponding percentage power loss across ten PV modules. The blue scatter points represent the measured data, while the red line illustrates the fitted linear

regression model that captures this relationship. The general trend indicates that power loss rises as the number of defective cells increases. For instance, modules with fewer than ten defective cells, such as Module 1 with eight defective cells and a 6.3 percent power loss, show comparatively modest losses. In contrast, modules containing a higher number of defective cells display more severe reductions in performance. Module 8 is particularly noteworthy, with 33 defective cells leading to a pronounced power loss of 44.1 percent, which aligns with the steep upward slope of the regression line.

The regression analysis demonstrates a strong correlation between defective cell count and module power loss, as shown by the close alignment of many scatter points with the fitted line. The slope of the model suggests that each additional defective cell contributes incrementally to power loss by a measurable percentage.

While most data follow this linear trend, one outlier at the higher end of the graph may reflect additional influences such as defect clustering or severity that extend beyond the scope of this analysis. Even so, the overall relationship confirms that cracks and PID exert a cumulative impact on PV performance. These findings highlight the value of early defect detection and remediation as essential strategies for safeguarding the long-term efficiency of PV installations.

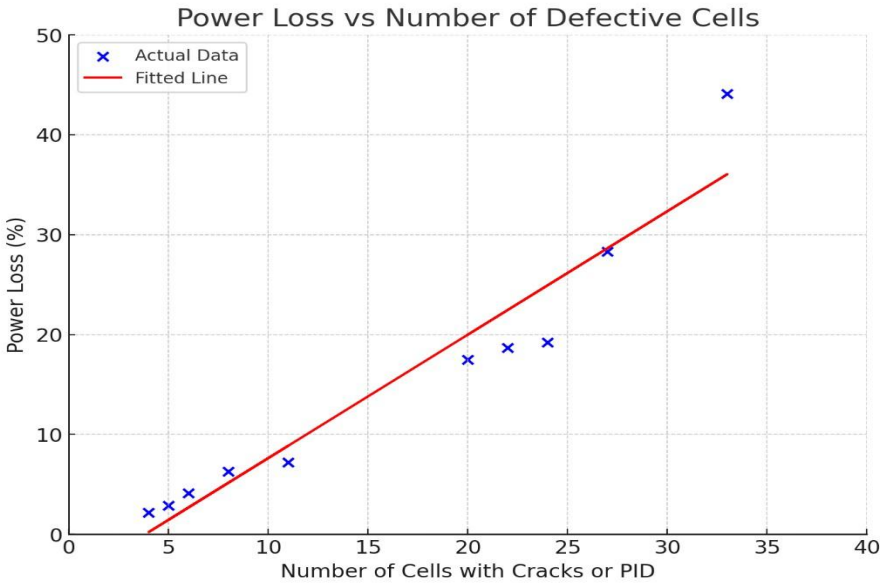

Figure 45. Correlation between the number of defective cells affected by cracks by PID and the corresponding power loss (%) across ten PV modules. The fitted red regression line illustrates the direct relationship between defect count and power loss, demonstrating that power output decreases progressively as the number of defective cells increase [33].

5.3.3 Degradation Rate and Residual Performance Trends in PV Systems

The degradation behaviour of PV systems across time is shown in **Figure 46 (a)** and provides valuable evidence of their long-term reliability. The blue data points represent the mean yearly degradation rates, which show a gradual upward trend while remaining consistently below 1 percent per year, consistent with established industry benchmarks. The red regression line demonstrates a steady increase, with the rate approaching about 0.9 percent annually by 2023. These results highlight the slow and progressive nature of PV module degradation, confirming that despite ageing effects, the systems continue to deliver stable performance over extended periods.

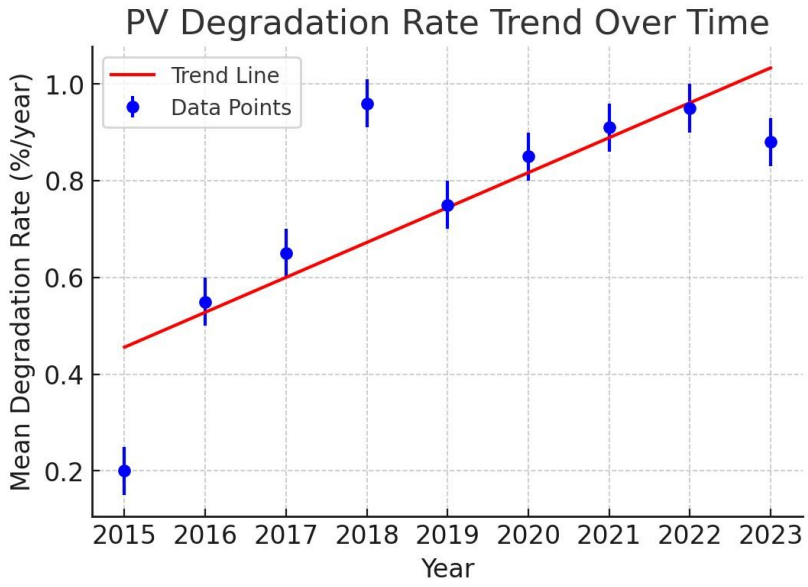

(a)

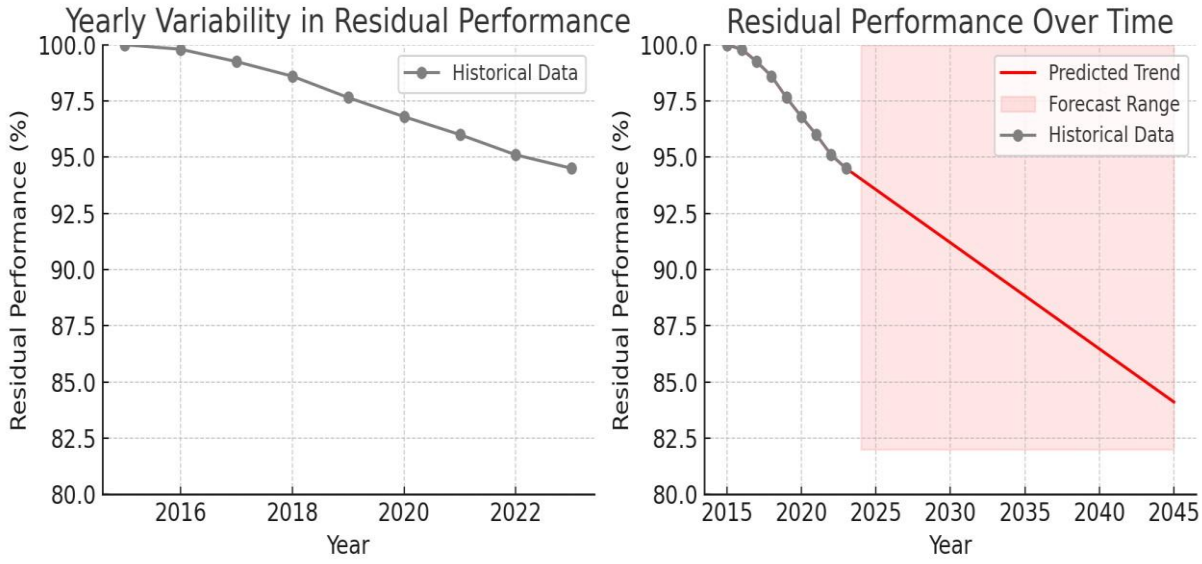

(b)

Figure 46. (a) Mean PV degradation rate between 2015 and 2023, illustrating annual degradation trends across all systems, which consistently remain below 1% per year. The fitted regression line indicates a gradual upward trend, while newer installations exhibit higher variability due to environmental and operational factors. (b) Yearly variation in residual performance and long-term projections. The left panel depicts residual performance from 2015 to 2023, showing a gradual decline across all systems, whereas the right panel extends the projection to 2045. The analysis suggests that PV module performance is expected to remain above 80% of the original nameplate rating after 25 years of operation, consistent with standard industry warranties. The code used to generate this figure is provided in Appendix B [33].

An important outcome from the analysis is the variability observed in degradation rates across different PV systems, represented by the error bars in Figure 46 (a). Although fluctuations are evident throughout the years, the degree of variability in 2022 is not substantially higher than in preceding years. Such variations are likely due to differences in installation quality, exposure to distinct environmental conditions, and diverse operational histories. For example, systems located in harsher climates or subject to greater mechanical stresses tend to show larger deviations in degradation behaviour. This highlights the need for close monitoring of PV performance, particularly in the early years after commissioning, to account for site-specific influences on module ageing.

The overall trend indicates that as systems age, their vulnerability to degradation gradually increases. Nevertheless, the average annual rate of degradation remains below 1 percent per year, consistent with established industry expectations. This finding suggests that even with incremental increases, PV modules continue to deliver reliable performance over extended lifespans. Such results provide reassurance regarding the long-term operational viability of PV technology, provided that regular maintenance is observed.

Figure 46 (b**)** further contextualises these findings by presenting both historical and forecasted residual performance. The left panel displays measured performance from 2015 through 2023, where residual output decreased steadily from 100 percent in 2015 to about 94.5 percent by 2023. This decline illustrates the cumulative effect of small but persistent annual losses inherent to PV degradation. The right panel extends the trend to 2045, with the regression model (red line) projecting a continued, but gradual, decline in residual performance. By 2045, average performance is expected to remain near 82 percent of the

initial nameplate rating, which corresponds closely with standard industry warranties that guarantee 80 percent output after 25 years. The shaded red confidence interval represents potential variability in future degradation, though the overall pattern remains within acceptable boundaries.

These projections imply that even after 25 years, most PV systems are expected to maintain more than 80 percent of their original rated capacity. This level of performance ensures not only continued energy production but also economic feasibility throughout the system lifetime. The gradual decline emphasises the inherent durability of PV modules, provided they are installed under sound practices and benefit from ongoing maintenance. The predictability of this degradation also enhances investor confidence, as performance can be forecast within industry-accepted margins.

It should be acknowledged that regional factors, such as thermal cycling, humidity levels, and maintenance routines, influence the precise degradation behaviour of individual systems. Installations in extreme climates may show somewhat higher rates, whereas those in milder environments with regular servicing may retain performance for longer. Despite these differences, the combined dataset demonstrates that PV installations, on average, deliver strong and reliable performance across diverse conditions.

To further validate the reliability of the observed degradation trend presented in Figure 46, a leave-one-out (LOO) cross-validation approach was considered. This validation technique evaluates the robustness of the regression model by iteratively excluding one annual data point from the dataset and re-estimating the degradation trend using the remaining observations. The resulting trend consistency confirms that the gradual increase in degradation rate is not driven by any single year-specific anomaly but rather reflects a

systematic ageing behaviour of photovoltaic systems. The LOO analysis therefore strengthens confidence in the projected residual performance patterns and supports the conclusion that PV degradation progresses in a predictable and statistically stable manner over time.

Together, the evidence from Figures 46 (a) and (b) offers valuable insight into the longevity of PV technology. Although degradation is unavoidable, it progresses slowly, with annual rates well below 1 percent, which is favourable compared with industry norms. The residual performance projections further support the conclusion that PV modules remain robust energy producers' decades after commissioning. These findings reinforce the value of investing in PV power, showing that with proactive monitoring and preventative maintenance, PV systems can sustain their performance, reliability, and economic return far beyond their initial deployment.

Chapter 6 Discussion and Future Work

6.1 Overview

This chapter brings together the key findings from the previous research chapters and situates them within the wider field of PV defect detection and degradation analysis. Chapters 3, 4, and 5 demonstrated a logical progression in the application of CNNs to EL imaging datasets. The work began with the classification of PV cell defects at the individual cell level, extended to the evaluation of entire modules, and culminated in the large-scale inspection of over 85,000 PV modules comprising more than 5.5 million cells. Together, these studies confirm that EL imaging supported by CNN architectures can provide a scalable, accurate, and robust framework for defect detection across different levels of PV analysis. This chapter integrates those findings, highlighting their strengths, addressing limitations, discussing their industrial and academic implications, and outlining potential directions for further research.

6.2 Comparison Across Scales: Cell, Module, and System-Level

One of the most important contributions of this thesis is the demonstration that CNN-based EL analysis can be applied successfully across three scales of PV inspection: the cell level, the module level, and large scale datasets. At the cell level, as presented in Chapter 3, four CNN architectures were designed to distinguish between healthy and defective PV cells. The most advanced configuration, referred to as Arch 4, achieved a validation accuracy of 98.07 percent. This level of performance confirmed that CNN can successfully detect subtle defects such as

minicracks, soldering anomalies and PID. The findings at this scale showed that CNN can serve as reliable tools for quality assurance on production lines where the early identification of small-scale defects is critical.

At the module level, described in Chapter 4, the methodology was extended to incorporate the collective assessment of individual cells within a module. A classification criterion was established that modules were rejected if more than 20 percent of their cells were defective. This approach made it possible to assess overall module quality while accounting for the distribution of defects among cells. The ability to scale CNN classification from cells to full modules demonstrated the adaptability of the method and provided a framework for operational monitoring at PV installations.

At the system level, Chapter 5 introduced the analysis of more than 85,000 PV modules from 167 installations, equivalent to a dataset of 5,592,000 cells. This large-scale analysis allowed for statistical modelling of defect trends across time and location, and revealed emerging issues such as the significant increase in edge ribbon cracks in installations after 2022. The study also examined the correlation between defect prevalence and module power loss, and projected long-term performance degradation up to the year 2045. These results represent one of the most comprehensive field-based analyses of PV degradation to date, bridging the gap between laboratory testing and large-scale operational insights.

6.3 Strengths of the Proposed Methodology

The proposed framework offers several strengths that contribute to both academic research and industrial practice. One major strength is its high level of automation. Traditional EL image inspection relies heavily on human operators, which is both time-intensive and subject to

variability in interpretation. By contrast, the CNN models developed in this thesis significantly reduce human involvement, enabling millions of cells to be classified with minimal manual intervention. The estimated error rate of only 2 percent demonstrates that the system is not only efficient but also reliable.

Another key strength is the sensitivity of EL imaging when paired with CNN classification. Unlike infrared thermography or standard visual inspection, EL imaging reveals minicracks and other latent defects that would otherwise go undetected. This enhanced sensitivity makes EL imaging particularly valuable for predictive maintenance, as it can identify vulnerabilities in modules before they manifest as major performance losses.

The methodology is also highly versatile. It has been demonstrated to work across different PV module designs, including both 60-cell and 72-cell formats, as well as busbar technologies such as 3BB, 4BB, and 5BB. This adaptability ensures that the approach remains applicable across diverse manufacturing practices and installation conditions.

Perhaps most importantly, the research demonstrated predictive capabilities by establishing a clear relationship between defect frequency and module performance. Regression models showed that each additional defective cell contributes to measurable power loss, providing a practical means of forecasting module performance from defect data. In addition, the degradation forecasting presented in Chapter 5 revealed that even after 25 years, modules are expected to retain more than 80 percent of their original capacity. These findings not only support the economic viability of PV systems but also reinforce confidence in PV energy as a long-term investment.

6.4 Limitations and Sources of Uncertainty

While the methodology presented in this thesis demonstrates considerable potential, it is important to recognise its limitations and the sources of uncertainty inherent in the approach. One limitation lies in the small but notable misclassification rate of around 2 percent. Misclassifications tend to occur in cases where defect features overlap visually, making it difficult for the algorithm to distinguish between them. Rare defect categories are also more difficult to detect accurately, as they are underrepresented in the training data. This limitation underscores the importance of expanding datasets to include a broader range of defect types.

Another source of uncertainty is the reliance on image quality. Even though EL images were captured at night to reduce interference from ambient light, minor variations in imaging conditions such as reflections, shadows, or differences in camera calibration can affect classification accuracy. While these factors were mitigated through standardisation protocols, they cannot be eliminated entirely.

A further limitation is the incomplete availability of IV curve data. Due to practical and financial constraints, IV measurements were only carried out on a subset of modules, particularly those that exhibited clear defects in their EL images. As a result, this thesis focuses more on defect detection than on a comprehensive quantification of power losses across all 85,000 modules.

Finally, regional variability must be considered. Environmental conditions such as temperature fluctuations, humidity and wind loading differ across geographic locations and can influence degradation rates. Although the large dataset allowed for generalised trends to be established, it is important to acknowledge that localised conditions can lead to deviations from the averages reported in this work.

6.5 Implications for the PV Industry

The findings of this thesis have significant implications for both the manufacturing and operational aspects of the PV industry. In manufacturing, CNN-based EL inspection can be incorporated directly into assembly lines, providing automated and reliable defect detection.

This could greatly reduce the number of defective modules leaving the factory, thereby lowering warranty claims and improving customer satisfaction.

For operational PV plants, the methodology provides a powerful diagnostic tool for ongoing system monitoring. EL imaging paired with CNN classification allows operators to detect defects at an early stage, before they lead to substantial power loss. This capability enables the implementation of predictive maintenance strategies, which can reduce downtime, lower maintenance costs and extend the operational lifespan of PV systems.

The research also has important economic implications by demonstrating that PV modules can maintain over 80 percent of their capacity after 25 years reassures investors that PV installations will remain profitable over their lifetime. Furthermore, the identification of emerging defects, such as the rise of edge ribbon cracks in post-2022 installations, provides critical feedback for manufacturers. This insight can inform improvements in design, materials, and installation practices, ultimately leading to more durable PV products.

Finally, the work presented here could inform future **standards and policies** by providing clear evidence of the types of defects that most affect long-term performance, this research supports the development of new industry guidelines regarding defect acceptance thresholds.

6.6 Contribution to Knowledge

This thesis makes several distinct contributions to the field of PV diagnostics. First, it demonstrates the scalability of CNN-aided EL imaging across three levels of individual cells, complete modules and large scale datasets. Second, it integrates EL imaging with long-term degradation forecasting, providing a unique perspective on PV performance over a projected 30-year timescale. Third, it reveals the emergence of edge ribbon cracks as a dominant defect in newer installations, filling an important gap in the literature and offering timely insights for industry. Finally, it contributes one of the largest EL imaging datasets ever analysed, comprising 85,000 modules and 5.6 million cells, which establishes a foundation for future research and industrial applications. So these contributions advance both theoretical understanding and practical applications in PV quality assurance and predictive maintenance.

6.7 Achievement of Research Objectives

This research was guided by a set of defined objectives aimed at advancing photovoltaic defect detection methodologies through deep learning-based image analysis. The first objective focused on identifying key limitations in existing PV inspection approaches and establishing the research motivation. This objective was addressed through the comprehensive literature review presented in Chapter 2.

The second objective involved the development and optimisation of convolutional neural network architectures for crack detection at the solar cell level. This was successfully achieved in Chapter 3, where the proposed CNN configurations demonstrated improved classification accuracy and enhanced feature extraction performance using electroluminescence imaging datasets.

The third objective aimed to evaluate the scalability of the developed defect detection framework at the photovoltaic module level. Chapter 4 presented the extension of the methodology to module-scale analysis, incorporating refined decision-making strategies and comparative performance evaluation.

The fourth objective focused on validating the proposed approach under large-scale operational conditions. This was addressed in Chapter 5 through extensive electroluminescence analysis across multiple PV installations, providing insights into degradation behaviour, defect trends, and practical implementation considerations.

Overall, the research objectives have been systematically achieved, demonstrating the effectiveness of deep learning-driven inspection methodologies for enhancing photovoltaic quality assurance and reliability assessment.

6.8 Future Directions

There are several promising directions for extending this work. One direction is the integration of EL imaging with drone-based inspection, which could greatly accelerate the monitoring of utility-scale PV installations. Another is the combination of EL with complementary diagnostic techniques, such as infrared thermography, IV tracing or electroluminescence video, to provide a more comprehensive picture of module health. Transfer learning could also be employed to enhance the detection of rare defects by leveraging pre-trained CNN.

In addition, the development of real-time monitoring systems that integrate diagnostic algorithms directly into PV installations would enable continuous performance tracking and

immediate fault detection. Finally, applying the methodology to larger, international datasets would allow for validation under a wide range of operating conditions, helping to establish global benchmarks for PV performance and reliability.

6.9 Reflection Against Existing Literature

Placing the findings of this thesis in the context of the broader literature highlights both the alignment and the novelty of the work. Previous studies have reported PV degradation rates typically ranging between 0.5 and 1.0 percent per year, with some variability depending on geographic location and module technology. The results from this thesis, showing an average annual degradation rate below 1 percent and a projection of approximately 0.9 percent per year by 2023, are consistent with these established values. However, the added contribution here lies in the scale of the dataset, which surpasses most existing studies and therefore provides greater statistical confidence in the observed trends.

Defect categorisation within PV modules has also been widely examined. Studies employing EL imaging have typically identified line cracks as a dominant defect type a finding corroborated by this thesis in installations prior to 2022[33]. However, the present analysis is among the first to show that edge ribbon cracks have recently emerged as a major defect type, rising to more than 28 percent of total defects in newer installations. This divergence from earlier literature points to possible changes in manufacturing or installation practices, and it establishes a new line of inquiry for both researchers and industry practitioners.

The use of CNN for EL image analysis has been explored in prior work, often achieving classification accuracies above 90 percent [91]. The results reported here, with validation accuracy reaching 98.07 percent at the cell level, reinforce the capability of CNNs while also

demonstrating their scalability to module and system-wide analysis [102]. This contrasts with many existing approaches that only focus laboratory datasets or smaller sample sizes. By applying CNN classification to more than 85,000 modules, this thesis expands the literature and demonstrates the feasibility of deploying such methods in installation diagnostics.

Finally, the integration of defect detection with long-term degradation forecasting represents a unique contribution, while prior studies have often treated defect detection and degradation modelling as separate areas of research, this thesis combines the two, linking micro-level defect data with macro-level performance projections extending to 2045. This integration provides a more understanding of PV system reliability and making connection the gap between immediate defect identification and long-term operational forecasting.

6.9 Conclusion

This chapter has synthesised the findings from the previous three research chapters, demonstrating how CNN inspections EL analysis can provide robust defect detection and degradation assessment across multiple scales. The methodology is characterised by its automation, sensitivity, versatility and predictive capacity, although it is subject to limitations relating to misclassifications, image quality, and incomplete IV data. The implications for the PV industry are wide-ranging, encompassing quality assurance, predictive maintenance, economic viability, and policy development. The novel contributions of this thesis include the scalability of CNN backed EL analysis, integration with long-term degradation forecasts, identification of emerging defect types and the assembly of one of the largest EL datasets available to date. Looking forward, future work should focus on enhancing scalability, integrating multiple diagnostic methods, and expanding the approach to international

datasets. So, these findings provide a foundation for improving PV quality assurance and ensuring the long-term sustainability of PV energy systems.

Appendix A.

```
import pandas as pd import

scipy.stats as stats import

matplotlib.pyplot as plt

# Data: Defect frequencies for PV installations before and after Jan 1, 2022 data_counts

= {

   'Defect Type': ['Normal Cell', 'Line Cracks', 'Soldering Anomalies', 'Complex Cracks', 'Edge Ribbon Cracks', 'PID'],

   'Before Jan 1, 2022': [1322092, 1620320, 780212, 1066155, 441221, 362000],

'After Jan 1, 2022': [616722, 426932, 128624, 229082, 615289, 162551]

}

# Create a DataFrame df =

pd.DataFrame(data_counts)

# Set the 'Defect Type' as the index (optional, for better readability) df.set_index('Defect

Type', inplace=True)

# Display the table print(df)

# Create a contingency table from the data contingency_table =

df.values  # Converts the DataFrame to a 2D array

# Perform the Chi-square test chi2, p_value, dof, expected =

stats.chi2_contingency(contingency_table)

# Display the results print(f"Chi-square

statistic: {chi2}") print(f"p-value:

{p_value}") print(f"Degrees of

freedom: {dof}") print (f"Expected

frequencies:\n{expected}") # Calculate
```

```
the differences (actual - expected)

expected_df =

pd.DataFrame(expected

columns=df.columns, index=df.index)

differences = df - expected_df print

("Differences between actual and

expected frequencies:")

print(differences)

# Calculate the contribution of each cell to the Chi-square statistic

chi_square_contributions = (df - expected_df) ** 2 / expected_df

print ("Chi-square contributions from each cell:") print

((chi_square_contributions / 1000).round(0))

# Plot a stacked bar chart with adjusted figure size and rotated x-axis labels

plt.figure(figsize=(15, 6))  # Set figure size df.plot(kind='bar', stacked=True)

# Customize the plot plt.title('Defect Frequencies Comparison')

plt.xlabel('Defect Type') plt.ylabel('Frequency')

# Rotate x-axis labels by 30 degrees for better readability

plt.xticks(rotation=30) # Add legend and adjust layout

plt.legend(title='Installation Period') plt.tight_layout()

plt.show()
```

Appendix B.

```
import numpy as np import

matplotlib.pyplot as plt

# Define the years and residual performance years = np.arange(2015, 2024)  # Years from 2015 to

2023 for historical data historical_performance = np.array([100, 99.5, 98.7, 97.9, 96.5, 94.8, 92.7, 90.3,

86.0])  # Historical data

# Predicted years and new predicted performance for gradual degradation predicted_years = np.arange(2024, 2046)

# Years from 2024 to 2045 initial_performance = historical_performance[-1]  # Start from 86% in 2023

predicted_performance = initial_performance - 0.3 * (predicted_years - 2023)  # Example: 0.3% degradation per year

# Ensure the residual performance doesn't go below 80% by 25 years (reaching around 82% for realism)

predicted_performance = np.maximum(predicted_performance, 80)

# Plot the historical performance (left subplot) plt.figure(figsize=(10, 4))

plt.subplot(1, 2, 1) plt.plot(years, historical_performance, 'o-', color='gray',

label='Historical Data') plt.xlabel('Year') plt.ylabel('Residual Performance (%)')

plt.title('Yearly Variability in Residual Performance') plt.ylim([80, 100])

plt.grid(True) plt.legend()

# Plot the predicted performance (right subplot) plt.subplot(1, 2, 2)

plt.plot(np.concatenate((years, predicted_years)),

np.concatenate((historical_performance, predicted_performance)),

    'r-', label='Predicted Trend') plt.fill_between(predicted_years, 80, 100, color='red',

alpha=0.1, label='Forecast Range') plt.plot(years, historical_performance, 'o-',

color='gray', label='Historical Data') plt.xlabel('Year')

plt.ylabel('Residual Performance (%)')

plt.title('Residual Performance Over

Time') plt.ylim([75, 105]) plt.grid(True)

plt.legend() # Show the plots

plt.tight_layout() plt.show()
```

References

[1] A. Rehman, Z. Batool, Q. U. Ain, and H. Ma, "The renewable energy challenge in developing economies: An investigation of environmental taxation, financial development, and political stability," *Nat Resour Forum*, vol. 49, no. 1, pp. 699–724, Feb. 2025, doi: 10.1111/14778947.12418.

[2] S. Saurabh, A. Kumar, and R. Kumar, "Techno Economic Analysis of Grid Connected Photovoltaic Systems With Battery Energy Storage: A Comprehensive Review," *Energy Storage*, vol. 7, no. 1, p. e70119, Feb. 2025, doi: 10.1002/EST2.70119.

[3] M. S. Hossain, A. Wadi Al-Fatlawi, L. Kumar, Y. R. Fang, and M. E. H. Assad, "Solar PV highpenetration scenario: an overview of the global PV power status and future growth," *Energy Systems*, pp. 1–57, Sep. 2024, doi: 10.1007/S12667-024-00692-6/METRICS.

[4] A. Mahdi *et al.*, "A Review of Photovoltaic Module Failure and Degradation Mechanisms: Causes and Detection Techniques," *Solar 2024, Vol. 4, Pages 43-82*, vol. 4, no. 1, pp. 43–82, Jan. 2024, doi: 10.3390/SOLAR4010003.

[5] E. Tarigan, "Identification of early operational defects in photovoltaic modules: A case study of a 24.9 MWp solar PV system in Sumatra, Indonesia," *Unconventional Resources*, vol. 6, p. 100156, Apr. 2025, doi: 10.1016/J.UNCRES.2025.100156.

[6] B. Adothu *et al.*, "Comprehensive review on performance, reliability, and roadmap of c-Si PV modules in desert climates: A proposal for improved testing standard," *Progress in Photovoltaics: Research and Applications*, vol. 32, no. 8, pp. 495–527, Aug. 2024, doi: 10.1002/PIP.3827.

[7] A. Mahdi *et al.*, "A Review of Photovoltaic Module Failure and Degradation Mechanisms: Causes and Detection Techniques," *Solar 2024, Vol. 4, Pages 43-82*, vol. 4, no. 1, pp. 43–82, Jan. 2024, doi: 10.3390/SOLAR4010003.

[8] G. E. Mustafa Abro, A. Ali, S. Ali Memon, T. Din Memon, and F. Khan, "Strategies and Challenges for Unmanned Aerial Vehicle-Based Continuous Inspection and Predictive Maintenance of Solar Modules," *IEEE Access*, vol. 12, pp. 176615–176629, 2024, doi: 10.1109/ACCESS.2024.3505754.

[9] C. Bu *et al.*, "CNN-based defect detection and classification of PV cells by infrared thermography method," *Nondestructive Testing and Evaluation*, vol. 40, no. 5, pp. 1752–1769, May 2025, doi: 10.1080/10589759.2024.2357240.

[10] R. del Prado Santamaría, M. Dhimish, G. A. dos Reis Benatto, T. Kari, P. B. Poulsen, and S. V. Spataru, "From Indoor to Daylight Electroluminescence Imaging for PV Module Diagnostics: A Comprehensive Review of Techniques, Challenges, and AI-Driven Advancements," *Micromachines 2025, Vol. 16, Page 437*, vol. 16, no. 4, p. 437, Apr. 2025, doi: 10.3390/MI16040437.

[11] T. Dimitriou, N. Skandalos, and D. Karamanis, "Progress in Improving Photovoltaics Longevity," *Applied Sciences (Switzerland)*, vol. 14, no. 22, p. 10373, Nov. 2024, doi:

10.3390/APP142210373/S1.

[12] M. Afridi, A. Kumar, F. ibne Mahmood, and G. S. TamizhMani, “Comparative Analysis of Hotspot Stress Endurance in Pristine and Thermal Cycled Prestressed Glass–Glass

Photovoltaic Modules,” *Sustainability 2023, Vol. 15, Page 12131*, vol. 15, no. 16, p. 12131, Aug. 2023, doi: 10.3390/SU151612131.

[13] W. Tao *et al.*, “Thermo-mechanical stress modeling and experimental investigation on microcracks in tilling ribbon photovoltaic modules during lamination and mechanical load test,” *Solar Energy*, vol. 249, pp. 521–531, Jan. 2023, doi: 10.1016/J.SOLENER.2022.11.037.

[14] D. Moazami Goodarzi, J. Lauri, J. Putaala, O. Nousiainen, and T. Fabritius, “Eddy current soldering of solar cell ribbons under a layer of glass,” *Solar Energy Materials and Solar Cells*, vol. 259, p. 112427, Aug. 2023, doi: 10.1016/J.SOLMAT.2023.112427.

[15] G. Badran and M. Dhimish, “Potential Induced Degradation in Photovoltaic Modules: A Review of the Latest Research and Developments,” *Solar 2023, Vol. 3, Pages 322-346*, vol. 3, no. 2, pp. 322–346, Jun. 2023, doi: 10.3390/SOLAR3020019.

[16] C. Reichel *et al.*, “Design aspects in consideration of hotspot phenomena in high-performance photovoltaic modules featuring different silicon solar cell architectures,” *Solar Energy Materials and Solar Cells*, vol. 276, p. 113058, Oct. 2024, doi: 10.1016/J.SOLMAT.2024.113058.

[17] M. Dhimish and Y. Hu, “Rapid testing on the effect of cracks on solar cells output power performance and thermal operation,” *Sci Rep*, vol. 12, no. 1, pp. 1–11, Dec. 2022, doi: 10.1038/S41598-022-16546-Z;SUBJMETA.

[18] A. Eslami Majd and N. N. Ekere, “Crack initiation and growth in PV module interconnection,” *Solar Energy*, vol. 206, pp. 499–507, Aug. 2020, doi: 10.1016/J.SOLENER.2020.06.036.

[19] L. Feng, J. Zhang, T. S. Kiong, K. Ding, N. Amin, and F. U. Hamelmann, “Estimating Crack Effects on Electrical Characteristics of PV Modules Based on Monitoring Data and I-V Curves,” *IEEE J Photovolt*, vol. 13, no. 4, pp. 558–570, Jul. 2023, doi: 10.1109/JPHOTOV.2023.3275251.

[20] W. Tao *et al.*, “Thermo-mechanical stress modeling and experimental investigation on microcracks in tilling ribbon photovoltaic modules during lamination and mechanical load test,” *Solar Energy*, vol. 249, pp. 521–531, Jan. 2023, doi: 10.1016/J.SOLENER.2022.11.037.

[21] H. Mohammed Niyaz, R. Meena, and R. Gupta, “Impact of cracks on crystalline silicon photovoltaic modules temperature distribution,” *Solar Energy*, vol. 225, pp. 148–161, Sep. 2021, doi: 10.1016/J.SOLENER.2021.07.038.

[22] G. Oreski *et al.*, “Investigation of the crack propensity of co-extruded polypropylene backsheet films for photovoltaic modules,” *Solar Energy Materials and Solar Cells*, vol. 259, p. 112438, Aug. 2023, doi: 10.1016/J.SOLMAT.2023.112438.

[23] M. Dhimish and P. I. Lazaridis, “An empirical investigation on the correlation between solar cell cracks and hotspots,” *Sci Rep*, vol. 11, no. 1, pp. 1–11, Dec. 2021, doi: 10.1038/S41598-02103498-Z;SUBJMETA.

[24] S. Hassan and M. Dhimish, “Review of Current State-of-the-Art Research on Photovoltaic Soiling, Anti-Reflective Coating, and Solar Roads Deployment Supported by a Pilot Experiment on a PV Road,” *Energies 2022, Vol. 15, Page 9620*, vol. 15, no. 24, p. 9620, Dec. 2022, doi: 10.3390/EN15249620.

[25] M. Dhimish, A. Ahmad, and A. M. Tyrrell, “Inequalities in photovoltaics modules reliability: From packaging to PV installation site,” *Renew Energy*, vol. 192, pp. 805–814, Jun. 2022, doi: 10.1016/J.RENENE.2022.04.156.

[26] N. Klasen, F. Heinz, A. De Rose, T. Roessler, A. Kraft, and M. Kamlah, “Root cause analysis of solar cell cracks at shingle joints,” *Solar Energy Materials and Solar Cells*, vol. 238, p. 111590, May 2022, doi: 10.1016/J.SOLMAT.2022.111590.

[27] D. Moazami Goodarzi, J. Lauri, J. Putaala, O. Nousiainen, and T. Fabritius, “Eddy current soldering of solar cell ribbons under a layer of glass,” *Solar Energy Materials and Solar Cells*, vol. 259, p. 112427, Aug. 2023, doi: 10.1016/J.SOLMAT.2023.112427.

[28] K. Lee, S. B. Cho, J. Yi, and H. S. Chang, “Simplified Recovery Process for Resistive Solder Bond (RSB) Hotspots Caused by Poor Soldering of Crystalline Silicon Photovoltaic Modules Using Resin,” *Energies 2022, Vol. 15, Page 4623*, vol. 15, no. 13, p. 4623, Jun. 2022, doi: 10.3390/EN15134623.

[29] W. Tao *et al.*, “Thermo-mechanical stress modeling and experimental investigation on microcracks in tilling ribbon photovoltaic modules during lamination and mechanical load test,” *Solar Energy*, vol. 249, pp. 521–531, Jan. 2023, doi: 10.1016/J.SOLENER.2022.11.037.

[30] O. A. Alimi, E. L. Meyer, and O. I. Olayiwola, “Solar Photovoltaic Modules’ Performance Reliability and Degradation Analysis—A Review,” *Energies 2022, Vol. 15, Page 5964*, vol. 15, no. 16, p. 5964, Aug. 2022, doi: 10.3390/EN15165964.

[31] M. Dhimish and J. Kettle, “Impact of Solar Cell Cracks Caused during Potential-Induced Degradation (PID) Tests,” *IEEE Trans Electron Devices*, vol. 69, no. 2, pp. 604–612, Feb. 2022, doi: 10.1109/TED.2021.3135365.

[32] R. Kumar, V. E. Puranik, and R. Gupta, “Unveiling the Potential of Infrared Thermography in Quantitative Investigation of Potential-Induced Degradation in Crystalline Silicon PV Module,” *Solar Energy Advances*, vol. 4, p. 100049, Jan. 2024, doi: 10.1016/J.SEJA.2023.100049.

[33] S. Hassan and M. Dhimish, “Broad-scale Electroluminescence analysis of 5 million+ photovoltaic cells for defect detection and degradation assessment,” *Renew Energy*, vol. 237, p. 121868, Dec. 2024, doi: 10.1016/J.RENENE.2024.121868.

[34] M. Abdelsattar, A. AbdelMoety, and A. Emad-Eldeen, “ResNet-based image processing approach for precise detection of cracks in photovoltaic panels,” *Sci Rep*, vol. 15, no. 1, pp. 1–22, Dec. 2025, doi: 10.1038/S41598-025-09101-Z;SUBJMETA.

[35] A. Garg, A. Zar, B. V. S. Chauhan, and S. Jain, “Optimizing Renewable Energy with AI: Environmental Monitoring and Predictive Maintenance Strategies,” *Prospects of Artificial Intelligence in the Environment*, pp. 61–96, 2025, doi: 10.1007/978-981-96-6863-2_3.

[36] M. Abdelsattar, A. Abdelmoety, M. A. Ismeil, and A. Emad-Eldeen, “Automated Defect Detection in Solar Cell Images Using Deep Learning Algorithms,” *IEEE Access*, vol. 13, pp. 4136–4157, 2025, doi: 10.1109/ACCESS.2024.3525183.

[37] S. Berretti, J.-B. Thomas, K. Hayat, F. Abdollahi-Mamoudan, C. Ibarra-Castanedo, and X. P. V Maldague, “Non-Destructive Testing and Evaluation of Hybrid and Advanced Structures: A Comprehensive Review of Methods, Applications, and Emerging Trends,” *Sensors 2025, Vol. 25, Page 3635*, vol. 25, no. 12, p. 3635, Jun. 2025, doi: 10.3390/S25123635.

[38] N. Ahn and M. Choi, “Towards Long-Term Stable Perovskite Solar Cells: Degradation Mechanisms and Stabilization Techniques,” *Advanced Science*, vol. 11, no. 4, p. 2306110, Jan. 2024, doi: 10.1002/ADVS.202306110.

[39] S. Deitsch *et al.*, “Automatic classification of defective photovoltaic module cells in electroluminescence images,” *Solar Energy*, vol. 185, pp. 455–468, Jun. 2019, doi: 10.1016/J.SOLENER.2019.02.067.

[40] M. Dhimsih and P. Mather, “Development of Novel Solar Cell Micro Crack Detection Technique,” *IEEE Transactions on Semiconductor Manufacturing*, vol. 32, no. 3, pp. 277–285, Aug. 2019, doi: 10.1109/TSM.2019.2921951.

[41] M. Dhimish, V. Holmes, M. Dales, and B. Mehrdadi, “Effect of micro cracks on photovoltaic output power: case study based on real time long term data measurements,” *Micro Nano Lett*, vol. 12, no. 10, pp. 803–807, Oct. 2017, doi: 10.1049/MNL.2017.0205.

[42] A. M. Hilton, A. D. Cahill, and E. R. Heller, “A comparison of electroluminescence spectra from plan view and cross-sectioned AlGaN/GaN devices,” *IEEE Trans Electron Devices*, vol. 65, no. 1, pp. 59–63, Jan. 2018, doi: 10.1109/TED.2017.2775101.

[43] H. Bakır, “Detection of micro-cracks in PV system using electroluminescence (EL) testing Elektrolüminesans (EL) testi kullanılarak FV sistemindeki mikro çatlakların tespiti,” *Bilim. Derg. / NOHU J. Eng. Sci*, vol. 13, no. 2, pp. 413–418, 2024, doi: 10.28948/ngumuh.1318611.

[44] E. Ozturk, E. Ogliari, M. Sakwa, A. Dolara, N. Blasuttigh, and A. M. Pavan, “Photovoltaic modules fault detection, power output, and parameter estimation: A deep learning approach based on electroluminescence images,” *Energy Convers Manag*, vol. 319, p. 118866, Nov. 2024, doi: 10.1016/J.ENCONMAN.2024.118866.

[45] R. Kumar, V. E. Puranik, and R. Gupta, “Review, challenges, and scope of advancements in outdoor quantitative electroluminescence imaging for solar PV,” *Journal of Renewable and Sustainable Energy*, vol. 17, no. 5, Sep. 2025, doi: 10.1063/5.0273915.

[46] A. Redondo-Plaza, A. Z. Velasco-Bonilla, J. I. Morales-Aragones, Á. L. Zorita-Lamadrid, V. Alonso-Gómez, and L. Hernández-Callejo, “Electroluminescence Imaging Based on FFT Analysis for Outdoor Photovoltaic Module Inspection: A Self-Powered Signal Modulation Approach,” *Applied Sciences 2025, Vol. 15, Page 4606*, vol. 15, no. 9, p. 4606, Apr. 2025, doi: 10.3390/APP15094606.

[47] L. Koester, S. Lindig, A. Louwen, A. Astigarraga, G. Manzolini, and D. Moser, “Review of photovoltaic module degradation, field inspection techniques and techno-economic assessment,” *Renewable and Sustainable Energy Reviews*, vol. 165, p. 112616, Sep. 2022, doi: 10.1016/J.RSER.2022.112616.

[48] J. Zikulnig, W. Muhleisen, M. Simor, V. Gevaerts, and M. De Biasio, “Photoluminescence Imaging for Industrial Quality Control during Manufacturing of Thin-Film Solar Cells,” *Proceedings of IEEE Sensors*, vol. 2022-October, 2022, doi:

10.1109/SENSORS52175.2022.9967278.

[49] R. Bhoopathy, O. Kunz, M. Juhl, T. Trupke, and Z. Hameiri, “Outdoor photoluminescence imaging of photovoltaic modules with sunlight excitation,” *Progress in Photovoltaics: Research and Applications*, vol. 26, no. 1, pp. 69–73, Jan. 2018, doi: 10.1002/PIP.2946.

[50] M. Waqar Akram, G. Li, Y. Jin, and X. Chen, “Failures of Photovoltaic modules and their Detection: A Review,” *Appl Energy*, vol. 313, p. 118822, May 2022, doi: 10.1016/J.APENERGY.2022.118822.

[51] A. Redondo Plaza *et al.*, “Partial Photoluminescence Imaging for Inspection of Photovoltaic Cells: Artificial LED Excitation and Sunlight Excitation,” *Energies 2023, Vol. 16, Page 4531*, vol. 16, no. 11, p. 4531, Jun. 2023, doi: 10.3390/EN16114531.

[52] M. Meribout, V. Kumar Tiwari, J. Pablo Peña Herrera, and A. Najeeb Mahfoudh Awadh Baobaid, “Solar panel inspection techniques and prospects,” *Measurement*, vol. 209, p. 112466, Mar. 2023, doi: 10.1016/J.MEASUREMENT.2023.112466.

[53] O. Nos *et al.*, “Quality control method based on photoluminescence imaging for the performance prediction of c-Si/a-Si:H heterojunction solar cells in industrial production lines,” *Solar Energy Materials and Solar Cells*, vol. 144, pp. 210–220, Jan. 2016, doi: 10.1016/J.SOLMAT.2015.09.009.

[54] S. Starzy´ Starzy´nski *et al.*, “Machine Learning in Solar Plants Inspection Automation,” *Energies 2022, Vol. 15, Page 5966*, vol. 15, no. 16, p. 5966, Aug. 2022, doi: 10.3390/EN15165966.

[55] M. Dhimish, “Thermal impact on the performance ratio of photovoltaic systems: A case study of 8000 photovoltaic installations,” *Case Studies in Thermal Engineering*, vol. 21, p. 100693, Oct. 2020, doi: 10.1016/J.CSITE.2020.100693.

[56] L. Morando, C. T. Recchiuto, J. Calla, P. Scuteri, and A. Sgorbissa, “Thermal and Visual Tracking of Photovoltaic Plants for Autonomous UAV Inspection,” *Drones 2022, Vol. 6, Page 347*, vol. 6, no. 11, p. 347, Nov. 2022, doi: 10.3390/DRONES6110347.

[57] C. Henry, S. Poudel, S. W. Lee, and H. Jeong, “Automatic Detection System of Deteriorated PV Modules Using Drone with Thermal Camera,” *Applied Sciences 2020, Vol. 10, Page 3802*, vol. 10, no. 11, p. 3802, May 2020, doi: 10.3390/APP10113802.

[58] M. Alsafasfeh, I. Abdel-Qader, B. Bazuin, Q. Alsafasfeh, and W. Su, “Unsupervised Fault Detection and Analysis for Large Photovoltaic Systems Using Drones and Machine Vision,” *Energies 2018, Vol. 11, Page 2252*, vol. 11, no. 9, p. 2252, Aug. 2018, doi: 10.3390/EN11092252.

[59] M. Parenti, M. Fossa, and L. Delucchi, “A model for energy predictions and diagnostics of large-scale photovoltaic systems based on electric data and thermal imaging of the PV fields,” *Renewable and Sustainable Energy Reviews*, vol. 206, p. 114858, Dec. 2024, doi: 10.1016/J.RSER.2024.114858.

[60] P. Zhang, L. Zhang, T. Wu, H. Zhang, and X. Sun, “Detection and location of fouling on photovoltaic panels using a drone-mounted infrared thermography system,” *https://doi.org/10.1117/1.JRS.11.016026*, vol. 11, no. 1, p. 016026, Feb. 2017, doi: 10.1117/1.JRS.11.016026.

[61] U. Pruthviraj, Y. Kashyap, E. Baxevanaki, and P. Kosmopoulos, “Solar Photovoltaic Hotspot Inspection Using Unmanned Aerial Vehicle Thermal Images at a Solar Field in South India,” *Remote Sensing 2023, Vol. 15, Page 1914*, vol. 15, no. 7, p. 1914, Apr. 2023, doi: 10.3390/RS15071914.

[62] V. Kirubakaran *et al.*, “Infrared Thermal Images of Solar PV Panels for Fault Identification Using Image Processing Technique,” *International Journal of Photoenergy*, vol. 2022, no. 1, p. 6427076, Jan. 2022, doi: 10.1155/2022/6427076.

[63] Irshad, Z. A. Jaffery, and A. Haque, “Temperature measurement of solar module in outdoor operating conditions using thermal imaging,” *Infrared Phys Technol*, vol. 92, pp. 134–138, Aug. 2018, doi: 10.1016/J.INFRARED.2018.05.017.

[64] A. De Vos and H. Pauwels, “On the thermodynamic limit of photovoltaic energy conversion,” *Applied Physics*, vol. 25, no. 2, pp. 119–125, Jun. 1981, doi: 10.1007/BF00901283.

[65] U. Hijjawi, S. Lakshminarayana, T. Xu, G. Piero Malfense Fierro, and M. Rahman, “A review of automated solar photovoltaic defect detection systems: Approaches, challenges, and future orientations,” *Solar Energy*, vol. 266, p. 112186, Dec. 2023, doi: 10.1016/J.SOLENER.2023.112186.

[66] “Deep learning in defects detection of PV modules: A review,” *Solar Energy Advances*, vol. 5, p. 100090, Jan. 2025, doi: 10.1016/J.SEJA.2025.100090.

[67] M. G. Ragab *et al.*, “A Comprehensive Systematic Review of YOLO for Medical Object Detection (2018 to 2023),” *IEEE Access*, vol. 12, pp. 57815–57836, 2024, doi: 10.1109/ACCESS.2024.3386826.

[68] A. Pravallika, M. F. Hashmi, and A. Gupta, “Deep Learning Frontiers in 3D Object Detection: A Comprehensive Review for Autonomous Driving,” *IEEE Access*, vol. 12, pp. 173936–173980, 2024, doi: 10.1109/ACCESS.2024.3456893.

[69] C. Albuquerque, R. Henriques, and M. Castelli, “Deep learning-based object detection algorithms in medical imaging: Systematic review,” *Heliyon*, vol. 11, no. 1, p. e41137, Jan. 2025, doi: 10.1016/J.HELIYON.2024.E41137.

[70] Y. M. Abbas and H. Alghamdi, “Semantic segmentation and deep CNN learning vision-based crack recognition system for concrete surfaces: development and implementation,” *Signal Image Video Process*, vol. 19, no. 4, pp. 1–15, Apr. 2025, doi: 10.1007/S11760-025-039132/METRICS.

[71] Y. Pei, Y. Huang, Q. Zou, X. Zhang, and S. Wang, “Effects of Image Degradation and Degradation Removal to CNN-Based Image Classification,” *IEEE Trans Pattern Anal Mach Intell*, vol. 43, no. 4, pp. 1239–1253, Apr. 2021, doi: 10.1109/TPAMI.2019.2950923.

[72] H. Cho, Y. Kim, E. Lee, D. Choi, Y. Lee, and W. Rhee, “Basic Enhancement Strategies When Using Bayesian Optimization for Hyperparameter Tuning of Deep Neural Networks,” *IEEE Access*, vol. 8, pp. 52588–52608, 2020, doi: 10.1109/ACCESS.2020.2981072.

[73] A. Fathi and S. F. Masoudi, “Combining CNN and Q-learning for increasing the accuracy of lost gamma source finding,” *Sci Rep*, vol. 12, no. 1, pp. 1–10, Dec. 2022, doi: 10.1038/S41598-02206326-0;SUBJMETA.

[74] Y. Su and X. Jiang, “Prediction of tide level based on variable weight combination of LightGBM and CNN-BiGRU model,” *Sci Rep*, vol. 13, no. 1, pp. 1–13, Dec. 2023, doi: 10.1038/S41598022-26213-Y;SUBJMETA.

[75] I. C. Hwang *et al.*, “Differential diagnosis of common etiologies of left ventricular hypertrophy using a hybrid CNN-LSTM model,” *Sci Rep*, vol. 12, no. 1, pp. 1–12, Dec. 2022, doi: 10.1038/S41598-022-25467-W;SUBJMETA.

[76] B. Shinde, S. Wang, P. Dehghanian, and M. Babakmehr, “Real- time detection of critical generators in power systems: A deep learning HCP approach,” *2020 IEEE Texas Power and Energy Conference, TPEC 2020*, Feb. 2020, doi: 10.1109/TPEC48276.2020.9042552.

[77] R. Stahl, A. Hoffman, D. Mueller-Gritschneder, A. Gerstlauer, and U. Schlichtmann, “DeeperThings: Fully Distributed CNN Inference on Resource-Constrained Edge Devices,” *Int J Parallel Program*, vol. 49, no. 4, pp. 600–624, Aug. 2021, doi: 10.1007/S10766-021-007123/FIGURES/12.

[78] X. Zhao, L. Wang, Y. Zhang, X. Han, M. Deveci, and M. Parmar, “A review of convolutional neural networks in computer vision,” *Artif Intell Rev*, vol. 57, no. 4, pp. 1–43, Apr. 2024, doi: 10.1007/S10462-024-10721-6/FIGURES/33.

[79] G. Habib, I. A. Malik, J. Ahmad, I. Ahmed, and S. Qureshi, “Exploring the Efficacy of Group-Normalization in Deep Learning Models for Alzheimer’s Disease Classification,” Apr. 2024, Accessed: Oct. 24, 2025. [Online]. Available: https://arxiv.org/pdf/2404.00946

[80] P. Sinha, D. Sahu, S. Prakash, T. Yang, R. S. Rathore, and V. K. Pandey, “A high performance hybrid LSTM CNN secure architecture for IoT environments using deep learning,” *Sci Rep*, vol. 15, no. 1, pp. 1–26, Dec. 2025, doi: 10.1038/S41598-025-94500-5;SUBJMETA.

[81] P. P. Rege, M. Yin, S. Parihar, J. Versaggi, and S. Nemawarkar, “An In-Memory-Computing Binary Neural Network Architecture with In-Memory Batch Normalization,” *IEEE Access*, vol. 12, pp. 190889–190896, 2024, doi: 10.1109/ACCESS.2024.3444481.

[82] N. F. Razali, I. S. Isa, S. N. Sulaiman, M. K. Osman, N. K. A. Karim, and S. A. Nordin, “Optimization of ReLU Activation Function for Deep-Learning-based Breast Cancer Classification on Mammogram Images,” *2024 IEEE International Conference on Automatic Control and Intelligent Systems, I2CACIS 2024 - Proceedings*, pp. 267–272, 2024, doi: 10.1109/I2CACIS61270.2024.10649623.

[83] A. Ghazvini, S. N. H. S. Abdullah, and M. Ayob, “Effect of continuous S-shaped rectified linear function on deep convolutional neural network,” *Applied Intelligence*, vol. 55, no. 6, pp. 1–24, Apr. 2025, doi: 10.1007/S10489-025-06399-0/METRICS.

[84] M. Elumalai and T. F. Fernandez, “Operative features of CNN layers characterizing deep learning,” *AIP Conf Proc*, vol. 3075, no. 1, Jul. 2024, doi: 10.1063/5.0217380.

[85] J. Zhao and Z. Wang, “Specialized convolutional transformer networks for estimating battery health via transfer learning,” *Energy Storage Mater*, vol. 71, p. 103668, Aug. 2024, doi: 10.1016/J.ENSM.2024.103668.

[86] T. Bashir, H. Wang, M. Tahir, and Y. Zhang, “Wind and solar power forecasting based on hybrid CNN-ABiLSTM, CNN-transformer-MLP models,” *Renew Energy*, vol. 239, p. 122055, Feb. 2025, doi: 10.1016/J.RENENE.2024.122055.

[87] W. Gamaleldin, O. Attayyib, L. Mohaisen, N. Omer, and R. Ming, “Developing a hybrid model based on Convolutional Neural Network (CNN) and Linear Discriminant Analysis (LDA) for investigating anti-selection risk in insurance,” *J Radiat Res Appl Sci*, vol. 18, no. 2, p. 101368, Jun. 2025, doi: 10.1016/J.JRRAS.2025.101368.

[88] Y. Zeng, Y. Zhang, Z. Xiao, and H. Sui, “A multi-classification deep neural network for cancer type identification from high-dimension, small-sample and imbalanced gene microarray data,” *Sci Rep*, vol. 15, no. 1, pp. 1–19, Dec. 2025, doi: 10.1038/S41598-025-89475-2;SUBJMETA.

[89] H. Munawer Al-Otum, “Classification of anomalies in electroluminescence images of solar PV modules using CNN-based deep learning,” *Solar Energy*, vol. 278, p. 112803, Aug. 2024, doi: 10.1016/J.SOLENER.2024.112803.

[90] F. M. Shakiba, S. M. Azizi, M. Zhou, and A. Abusorrah, “Application of machine learning methods in fault detection and classification of power transmission lines: a survey,” *Artif Intell Rev*, vol. 56, no. 7, pp. 5799–5836, Jul. 2023, doi: 10.1007/S10462-022-10296-0.

[91] S. Hassan and M. Dhimish, “A Survey of CNN-Based Approaches for Crack Detection in Solar PV Modules: Current Trends and Future Directions,” *Solar 2023, Vol. 3, Pages 663-683*, vol. 3, no. 4, pp. 663–683, Dec. 2023, doi: 10.3390/SOLAR3040036.

[92] I. Polymeropoulos, S. Bezyrgiannidis, E. Vrochidou, and G. A. Papakostas, “Enhancing Solar Plant Efficiency: A Review of Vision-Based Monitoring and Fault Detection Techniques,” *Technologies 2024, Vol. 12, Page 175*, vol. 12, no. 10, p. 175, Sep. 2024, doi: 10.3390/TECHNOLOGIES12100175.

[93] A. V. Jonnalagadda, H. A. Hashim, and A. Harris, “Comprehensive and Comparative Analysis between Transfer Learning and Custom Built VGG and CNN-SVM Models for Wildfire Detection,” *6th International Conference on Intelligent Computing in Data Sciences, ICDS 2024*, 2024, doi: 10.1109/ICDS62089.2024.10756303.

[94] Z. Azouz, B. Honarvar Shakibaei Asli, and M. Khan, “Evolution of Crack Analysis in Structures Using Image Processing Technique: A Review,” *Electronics 2023, Vol. 12, Page 3862*, vol. 12, no. 18, p. 3862, Sep. 2023, doi: 10.3390/ELECTRONICS12183862.

[95] M. Iman, H. R. Arabnia, and K. Rasheed, “A Review of Deep Transfer Learning and Recent Advancements,” *Technologies 2023, Vol. 11, Page 40*, vol. 11, no. 2, p. 40, Mar. 2023, doi: 10.3390/TECHNOLOGIES11020040.

[96] M. Hussain, H. Al-Aqrabi, and R. Hill, “PV-CrackNet Architecture for Filter Induced Augmentation and Micro-Cracks Detection within a Photovoltaic Manufacturing Facility,” *Energies 2022, Vol. 15, Page 8667*, vol. 15, no. 22, p. 8667, Nov. 2022, doi: 10.3390/EN15228667.

[97] M. W. Akram *et al.*, “CNN based automatic detection of photovoltaic cell defects in electroluminescence images,” *Energy*, vol. 189, p. 116319, Dec. 2019, doi: 10.1016/J.ENERGY.2019.116319.

[98] S Verma, PD Scholar, H Kumar Taluja, and P Chaudhary, “Automatic Defect Classification of Electro-Luminescence... - Google Scholar,” *Mech. Eng*, 2022, Accessed: Oct. 22, 2025. [Online]. Available: https://scholar.google.com/scholar?hl=en&as_sdt=0%2C5&scioq=Verma%2C+S.%3B+Scholar

%2C+P.D.%3B+Kumar+Taluja%2C+H.%3B+Chaudhary%2C+P.+Automatic+Defect+Classification+of+Electro-
Luminescence+Images+of+Photovoltaic+Modules+Based+on+Deep+Learning+CNN.+Int.+J.+Mech.+Eng.+2022%2C+6%2C+974%E2%80%935823.&q=Automatic+Defect+Classification+of+Electro-
Luminescence+Images+of+Photovoltaic+Modules+Based+on+Deep+Learning+CNN&btnG=

[99] M. R. Rahman, S. Tabassum, E. Haque, M. M. Nishat, F. Faisal, and E. Hossain, "CNN-based Deep Learning Approach for Micro-crack Detection of Solar Panels," *2021 3rd International Conference on Sustainable Technologies for Industry 4.0, STI 2021*, 2021, doi: 10.1109/STI53101.2021.9732592.

[100] L. Liu, Y. Zhu, M. R. Ur Rahman, P. Zhao, and H. Chen, "Surface Defect Detection of Solar Cells Based on Feature Pyramid Network and GA-Faster-RCNN," *Proceedings - 2nd China Symposium on Cognitive Computing and Hybrid Intelligence, CCHI 2019*, pp. 292–297, Sep. 2019, doi: 10.1109/CCHI.2019.8901952.

[101] D. Korkmaz and H. Acikgoz, "An efficient fault classification method in solar photovoltaic modules using transfer learning and multi-scale convolutional neural network," *Eng Appl Artif Intell*, vol. 113, p. 104959, Aug. 2022, doi: 10.1016/J.ENGAPPAI.2022.104959.

[102] S. Hassan and M. Dhimish, "Dual spin max pooling convolutional neural network for solar cell crack detection," *Sci Rep*, vol. 13, no. 1, pp. 1–16, Dec. 2023, doi: 10.1038/S41598-023-381778;SUBJMETA.

[103] P. Mishra and K. Sarawadekar, "Polynomial Learning Rate Policy with Warm Restart for Deep Neural Network," *IEEE Region 10 Annual International Conference, Proceedings/TENCON*, vol. 2019-October, pp. 2087–2092, Oct. 2019, doi: 10.1109/TENCON.2019.8929465.

[104] X. Zhai, F. Qiao, Y. Ma, and H. Lu, "A Novel Fault Diagnosis Method under Dynamic Working Conditions Based on a CNN with an Adaptive Learning Rate," *IEEE Trans Instrum Meas*, vol. 71, 2022, doi: 10.1109/TIM.2022.3177233.

[105] I. Zyout, A. O.-2020 A. in S. and Engineering, and undefined 2020, "Detection of PV solar panel surface defects using transfer learning of the deep convolutional neural networks," *researchgate.netI Zyout, A Oatawneh2020 Advances in Science and Engineering Technology International, 2020•researchgate.net*, Accessed: Oct. 22, 2025. [Online]. Available: https://www.researchgate.net/profile/Imad-Zyout/publication/342225232_Detection_of_PV_Solar_Panel_Surface_Defects_using_Transfer_Learning_of_the_Deep_Convolutional_Neural_Networks/links/5fb822b9299bf104cf64f657/Detection-of-PV-Solar-Panel-Surface-Defects-using-Transfer-Learning-of-the-DeepConvolutional-Neural-Networks.pdf

[106] B. Su, H. Chen, and Z. Zhou, "BAF-Detector: An Efficient CNN-Based Detector for Photovoltaic Cell Defect Detection," *IEEE Transactions on Industrial Electronics*, vol. 69, no. 3, pp. 3161– 3171, Mar. 2022, doi: 10.1109/TIE.2021.3070507.

[107] M. R. Rahman, S. Tabassum, E. Haque, M. M. Nishat, F. Faisal, and E. Hossain, "CNN-based Deep Learning Approach for Micro-crack Detection of Solar Panels," *2021 3rd International Conference on Sustainable Technologies for Industry 4.0, STI 2021*, 2021, doi: 10.1109/STI53101.2021.9732592.

[108] C. Huang, Z. Zhang, and L. Wang, “PSOPruner: PSO-Based Deep Convolutional Neural Network Pruning Method for PV Module Defects Classification,” *IEEE J Photovolt*, vol. 12, no. 6, pp. 1550–1558, Nov. 2022, doi: 10.1109/JPHOTOV.2022.3195099.

[109] M. Dhimish and A. M. Tyrrell, “Power loss and hotspot analysis for photovoltaic modules affected by potential induced degradation,” *Npj Mater Degrad*, vol. 6, no. 1, pp. 1–8, Dec. 2022, doi: 10.1038/S41529-022-00221-9;SUBJMETA.

[110] S. Hassan and M. Dhimish, “Enhancing solar photovoltaic modules quality assurance through convolutional neural network-aided automated defect detection,” *Renew Energy*, vol. 219, p. 119389, Dec. 2023, doi: 10.1016/J.RENENE.2023.119389.

[111] H. Acikgoz, “An automatic detection model for cracks in photovoltaic cells based on electroluminescence imaging using improved YOLOv7,” *Signal Image Video Process*, vol. 18, no. 1, pp. 625–635, Feb. 2024, doi: 10.1007/S11760-023-02724-7/METRICS.

[112] F. Sultana, A. Sufian, and P. Dutta, “Evolution of Image Segmentation using Deep Convolutional Neural Network: A Survey,” *Knowl Based Syst*, vol. 201–202, p. 106062, Aug. 2020, doi: 10.1016/J.KNOSYS.2020.106062.

[113] G. K. Mahani *et al.*, “Bounding Box Based Weakly Supervised Deep Convolutional Neural Network for Medical Image Segmentation Using an Uncertainty Guided and Spatially Constrained Loss,” *Proceedings - International Symposium on Biomedical Imaging*, vol. 2022March, 2022, doi: 10.1109/ISBI52829.2022.9761558.

[114] W. Kim, A. Kanezaki, and M. Tanaka, “Unsupervised Learning of Image Segmentation Based on Differentiable Feature Clustering,” *IEEE Transactions on Image Processing*, vol. 29, pp. 8055–8068, 2020, doi: 10.1109/TIP.2020.3011269.

[115] X. Liu, L. Song, S. Liu, and Y. Zhang, “A Review of Deep-Learning-Based Medical Image Segmentation Methods,” *Sustainability 2021, Vol. 13, Page 1224*, vol. 13, no. 3, p. 1224, Jan. 2021, doi: 10.3390/SU13031224.

[116] M. Aghaei *et al.*, “Review of degradation and failure phenomena in photovoltaic modules,” *Renewable and Sustainable Energy Reviews*, vol. 159, p. 112160, May 2022, doi: 10.1016/J.RSER.2022.112160.

[117] M. Dhimish and A. M. Tyrrell, “Power loss and hotspot analysis for photovoltaic modules affected by potential induced degradation,” *Npj Mater Degrad*, vol. 6, no. 1, pp. 1–8, Dec. 2022, doi: 10.1038/S41529-022-00221-9;SUBJMETA.

[118] M. Dhimish and P. I. Lazaridis, “An empirical investigation on the correlation between solar cell cracks and hotspots,” *Sci Rep*, vol. 11, no. 1, pp. 1–11, Dec. 2021, doi: 10.1038/S41598-02103498-Z;SUBJMETA.

[119] C. Garbin, X. Zhu, and O. Marques, “Dropout vs. batch normalization: an empirical study of their impact to deep learning,” *Multimed Tools Appl*, vol. 79, no. 19–20, pp. 12777–12815, May 2020, doi: 10.1007/S11042-019-08453-9/METRICS.

[120] M. Dhimish, V. Holmes, B. Mehrdadi, and M. Dales, “The impact of cracks on photovoltaic power performance,” *Journal of Science: Advanced Materials and Devices*, vol. 2, no. 2, pp. 199–209, Jun. 2017, doi: 10.1016/J.JSAMD.2017.05.005.

[121] M. Dhimish, V. D'Alessandro, and S. Daliento, "Investigating the Impact of Cracks on Solar Cells Performance: Analysis Based on Nonuniform and Uniform Crack Distributions," *IEEE Trans Industr Inform*, vol. 18, no. 3, pp. 1684–1693, Mar. 2022, doi: 10.1109/TII.2021.3088721.

[122] M. Dhimish, V. H.-J. of S. A. M. and, and undefined 2019, "Solar cells micro crack detection technique using state-of-the-art electroluminescence imaging," *Elsevier*, Accessed: Feb. 05, 2023. [Online]. Available: https://www.sciencedirect.com/science/article/pii/S2468217919302345

[123] M. Dhimish, "Micro cracks distribution and power degradation of polycrystalline solar cells wafer: Observations constructed from the analysis of 4000 samples," *Renew Energy*, vol. 145, pp. 466–477, Jan. 2020, doi: 10.1016/J.RENENE.2019.06.057.

[124] O. Elharrouss *et al.*, "Task-based Loss Functions in Computer Vision: A Comprehensive Review," Apr. 2025, Accessed: Oct. 23, 2025. [Online]. Available: https://arxiv.org/pdf/2504.04242

[125] E. O. Garvin *et al.*, "Machine learning for exoplanet detection in high-contrast spectroscopy - Revealing exoplanets by leveraging hidden molecular signatures in cross-correlated spectra with convolutional neural networks," *Astron Astrophys*, vol. 689, p. A143, Sep. 2024, doi: 10.1051/0004-6361/202449149.

[126] M. W. Akram *et al.*, "CNN based automatic detection of photovoltaic cell defects in electroluminescence images," *Energy*, vol. 189, p. 116319, Dec. 2019, doi: 10.1016/J.ENERGY.2019.116319.

[127] I. Zyout, A. O.-2020 A. in S. and Engineering, and undefined 2020, "Detection of PV solar panel surface defects using transfer learning of the deep convolutional neural networks," *researchgate.netI Zyout, A Oatawneh2020 Advances in Science and Engineering Technology International, 2020•researchgate.net*, Accessed: Oct. 23, 2025. [Online].

[128] M. Hussain, T. Chen, S. Titrenko, P. Su, and M. Mahmud, "A Gradient Guided Architecture Coupled With Filter Fused Representations for Micro-Crack Detection in Photovoltaic Cell Surfaces," *IEEE Access*, vol. 10, pp. 58950–58964, 2022, doi: 10.1109/ACCESS.2022.3178588.

[129] Z. Ying, M. Li, W. Tong, and C. Haiyong, "Automatic Detection of Photovoltaic Module Cells using Multi-Channel Convolutional Neural Network," *Proceedings 2018 Chinese Automation Congress, CAC 2018*, pp. 3571–3576, Jul. 2018, doi: 10.1109/CAC.2018.8623258.